METAL OXIDES MODIFIED CARBON ELECTRODE MATERIALS FOR FLUORIDE AND PARAQUAT REMOVAL FROM WATER BY CAPACITIVE DEIONIZATION

Tusekile Alfredy

A Thesis Submitted in Fulfilment of the Requirements for the Degree of Doctor of Philosophy in Materials Science and Engineering of the Nelson Mandela African Institution of Science and Technology

Arusha, Tanzania

June, 2024

ABSTRACT

Capacitive deionization (CDI) is an emerging water treatment technology with many advantages, including low energy consumption, high efficiency, low cost, green and pollution-free electrode regeneration. However, the electrode material is the main controlling factor for achieving high CDI performance. For a long time, activated carbon (AC) has been a preferred electrode material for CDI due to its availability, ease of preparation, low cost, and tunable textural properties. However, the pristine AC lacks selectivity towards the targeted ions, resulting in unnecessary energy consumption for treating polluted water and decreasing the removal efficiency (RE) of the targeted pollutant. To improve ion selectivity, in this study, composites of AC with metal oxides have been synthesized through a simple and one-step co-precipitation method at ambient temperature (23-27°C) for defluoridation and removing paraquat (PQ) from water. The composite properties were characterized by X-ray diffraction, scanning electron microscopy, Fourier transform infrared spectroscopy, energy-dispersive X-ray spectroscopy, and Brunauer-Emmett-Teller analysis. In competitive fluoride (F^-) removal CDI experiments, AC–$Al_4Fe_{2.5}Ti_4$ composite reduced the F^- concentration from 5.15 to 1.18 mg/L, below the allowable limit of 1.5 mg/L set by the World Health Organization while pristine AC reduced the F^- concentration to 4.5 mg/L. Also, AC–$Al_4Fe_{2.5}Ti_4$ composite demonstrated a high RE of 79% and excellent regeneration performance after continuous electric adsorption–desorption cycles. Furthermore, CDI batch experiments compared the electrosorption of paraquat (PQ) herbicide by the composite electrodes (AC-Al_2O_3: 1:1) and pristine AC. The performance of the composite electrodes showed that PQ RE and electrosorption capacity (EC) depend on aluminium content loading, applied potential, flow rate, and charging time. At 1.2 V, a flow rate of 15 mL/min, and a charging time of 3 h, the composite electrode demonstrated a RE, EC, and energy consumption of 95.5%, 1.27 mg/g, and 0.055 kWh/m^3, respectively, compared to 62%, 0.83 mg/g, and 0.11 kWh/m^3 for the pristine AC. The presence of other ions/pollutants was found to have negligible interference on PQ pesticide removal as the RE of the AC/Al_2O_3-1:1 composite in both artificial and natural water were 95.5 and 87.5% while EC was 1.27 and 1.17 mg/g, respectively. Therefore, the modified AC-metal oxides electrodes are promising and efficient materials for removing inorganic pollutants from water, such as F^- and organic pollutants, including PQ pesticides for CDI technology.

DECLARATION

I, Tusekile Alfredy, do hereby declare to the Senate of the Nelson Mandela African Institution of Science and Technology that this Thesis titled *"Metal Oxides Modified Carbon Electrode Materials for Defluoridation and Paraquat Herbicide Removal from Water by Capacitive Deionization"* is my original work and that it has neither been submitted nor being concurrently submitted for degree award in any other institution.

17/07/2024

Tusekile Alfredy Date

The above declaration is confirmed by:

17/07/2024

Prof. Yusufu Abeid Jande Chande Date

17/07/2024

Dr. Joyce Elisadiki Date

COPYRIGHT

CERTIFICATION

The undersigned certify that they have read and hereby recommend for acceptance by the Senate of the Nelson Mandela African Institution of Science and Technology a Thesis entitled "*Metal Oxides Modified Carbon Electrode Materials for Defluoridation and Paraquat Herbicide Removal from Water by Capacitive Deionization*" in fulfilment of the requirements for the Degree of Doctor of Philosophy in Materials Science and Engineering at Nelson Mandela African Institution of Science and Technology, Arusha Tanzania.

Prof. Yusufu Abeid Jande Chande Date

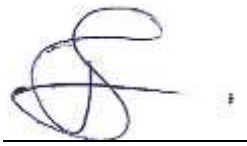

Dr. Joyce Elisadiki Date

ACKNOWLEDGMENTS

Foremost, I thank my almighty GOD, the Most Merciful, for his unwavering protection, guidance, endurance, and spiritual healing since the beginning of my PhD programme.

My heartfelt appreciation goes to the Partnership for Skills in Applied Sciences, Engineering and Technology (PASET) and the African Centre of Excellence for Water Infrastructure and Sustainable Energy Futures (WISE-Futures) for their invaluable financial assistance towards my doctoral studies. Furthermore, I am deeply grateful to my employer, the Nelson Mandela African Institution of Science and Technology (NM-AIST), for granting me a study leave to pursue my PhD program.

I would like to express my immense gratitude towards my supervisors, Prof. Yusufu Abeid Chande Jande and Dr. Joyce Elisadiki, for their invaluable guidance and support throughout my PhD. I feel incredibly fortunate to have had such exceptional advisors and mentors who provided me with their vast knowledge, common sense, and perceptiveness, which were essential for completing my research. Their enthusiasm, inspiration, and ability to explain complex concepts in a simple manner made the investigation enjoyable and engaging for me. Throughout my thesis period, my supervisors offered me encouragement, sound advice, excellent teaching, great company and friendship, and numerous innovative ideas, without which I would have been lost. Learning from their example as both researchers and mentors is a privilege. Their prompt responses to my questions and queries, and their unwavering support, were instrumental in my academic growth and success. I am immensely grateful to my supervisors for their constructive and meticulous support, which undoubtedly contributed to my career growth. They are truly exemplary, and I aspire to follow their lead in my future endeavors.

I sincerely appreciate Professor Cecil Kithongo for his valuable insights, suggestions, and unwavering commitment to assisting students. He is a role model in my academic arena, always willing to offer support and guidance despite his demanding schedule. He is a true mentor and a friend to anyone who desires to excel in academic and research pursuits.

I am extremely thankful for the guidance provided by Prof. Mouad Dahbi, my International Partiner supervisor at the Department of Materials Science, Energy, and Nano-engineering at Mohammed VI Polytechnic University, Ben Guerir, Morocco. It was a great privilege for me

to work in his laboratory, and I sincerely appreciate the support and mentorship he provided throughout my stay in Morocco.

I am deeply grateful to Dr. Ramadhani Bakari for his invaluable support during my PhD journey. He has been a constant source of guidance and assistance, always available to lend a helping hand whenever needed. I am particularly grateful for his critical feedback on my research and his mentorship on the software tools used for sample analysis, which have been of immense help.

I would like to thank Dr. Alfred Said Mateso for generously sharing his expertise and knowledge without any expectation of reciprocity. He is truly a kind-hearted individual.

I would like to convey my sincere gratitude to the CDI research group at NM-AIST, including Mr. Betwel Kipchirchir Tarus, Mr. Omary Sufiani, and Mr. Furaha Ndeki Alphonse, for being instrumental in helping one another to achieve our goals. I am also immensely grateful to my peers, especially Mr. Ishaq Kariim, Mr. Joshua Oyetade, Mr. Hashimu Hamisi, Mr. Wilson Mahene, and Mr. Stanislaus Mtavangu, for their unwavering support, valuable feedback, seamless cooperation, and the cherished camaraderie we shared.

Furthermore, I would like to thank Ms. Irene Tesha and Mr. Idd Hussein, the laboratory technicians at NM-AIST, for their invaluable technical assistance during my laboratory work.

I feel deeply privileged to convey my sincere appreciation to my wonderful husband, Mr. Joseph Gregory Gishinda, for his unwavering patience, support, and exceptional care for me and our children, Glory, and Geovann, during my absence. Additionally, I would like to express my heartfelt thanks to my sisters, Ms. Elizabeth, Neema, Upendo Alfred Mwakibinga, and Eliana Pius, for their steadfast support, which has been instrumental in allowing me to pursue my doctoral studies.

I express my genuine recognition and appreciation for the immense effort and unwavering commitment of my beloved mother, Mr. Grina Sambote, who drove me to strive hard in my studies. She dedicated herself to ensuring that I had the opportunity to receive a quality education. Although she has passed away, her contribution to my academic success will always be remembered.

DEDICATION

I dedicate this work to my lovely husband, Mr. Joseph Gregory, my daughter, Glory, and my son Geovann.

TABLE OF CONTENTS

LIST OF TABLES

LIST OF FIGURES

LIST OF ABBREVIATIONS AND SYMBOLS

AC	Activated carbon
Al_2O_3	Alumimium oxide
ANOVA	Analysis of Variance
As	Arsenic
BBD	Box-Behnken design
Bi	Bismuth
BJH	Barrett-Joyner-Halender
C.V.	Coefficient of variance
CDI	Capacitive deionization
Cl^-	Chlorine ion
CNT	Carbon nano tube
Cr	Chromium
CV	Cyclic voltammetry
EC	Electrosorption capacity
EDLs	Electric double layers
EO	Electro-oxidation
F^-	Fluoride ion
Fe_2O_3	Iron oxide
FTIR	Fourier-transform infrared spectroscopy
HA	Hydroxyapatite
JCPDS	Joint Committee on Powder Diffraction Standards
MO	Metal oxide
NiAl-LMO	Nickel Aluminium-layered metal oxide
NiCoAl-LMO	Nickel, Cobalt, Aluminium-layered metal oxide
NiFeMn-LMO	nickel, iron, manganese layered metal oxide
NO_3^-	Nitrate ion
PANI	Polyaniline
Pb	Lead
PQ	Paraquat herbicide
PZC	Potential of zero charge
RE	Removal efficiency
rGO	Reduced graphene oxide

RO	Reverse osmosis
RSM	Response surface methodology
SEM	Scanning electron microscopy
SO_4^{2-}	Sulphate ion
TEM	Transmission electron microscopy
$Ti(OH)_4$	Titanium hydroxide
TiO_2	Titanium oxide
TOrCs	Trace organic compounds
TWBAC	Tea waste biomass activated carbon electrode
XRD	X-ray diffraction

CHAPTER ONE

INTRODUCTION

1.1 Background of the problem

The rapid expansion of industrial and agricultural activities worldwide has resulted in significant water pollution, while the rising population has caused a shortage of water resources (Dahiya *et al.,* 2020; Toledo-Carrillo *et al.,* 2020). It has been reported that 80% of the wastewater produced globally is discharged into the environment without any treatment (Franco *et al.,* 2022), resulting in high concentration levels of inorganic and organic contaminants like fluoride ions (F^-) (Khatibikamal *et al.,* 2010; Shen *et al.,* 2003; Wan *et al.,* 2021) and paraquat (PQ) herbicides (Leite *et al.,* 2013; Santos *et al.,* 2014). Freshwater resources account for only 3% of the earth's water, with the remaining 97% being seawater unsuitable for human consumption. The pollution and contamination of water resources and freshwater scarcity pose a significant threat to human survival, making the purification of water resources an urgent necessity.

Fluoride is among the monovalent anionic species which has been identified as a prominent inorganic pollutant that impacts human health in the affected areas at the global scale (Grillo *et al.,* 2014; Thompson *et al.,* 2007). Ayoob and Gupta (2006) reported that over 200 million people worldwide had been exposed to drinking water with excess F^- levels. In many regions of the world, including China, India, Thailand, and Tanzania, fluoride pollution in drinking water has been identified as a serious threat to public health. In China fluoride in drinking water is reported to be up to 21.5 mg/L (Ayoob *et al.,* 2008), 0.12–24.17 mg/L in India (Jha *et al.,* 2013), 1.13–7.85 mg/L in Pakistan (Rafique *et al.,* 2015) , 0.01–14.12 mg/L in Thailand (Chuah *et al.,* 2016) and 0.76 –1103 mg/L in Arusha-Tanzania (Mbabaye *et al.,* 2018). The World Health Organization (WHO) recommended F^- concentration of 0.5 – 1.5 mg/L (Fan *et al.,* 2003). Though F^- at the optimum level is vital for the health of the teeth as it prevents decay, excessive exposure to F^- may lead to dental fluorosis, whereby the teeth become mottled, discolored, and pitted during their development. Also, it can lead to skeletal fluorosis at F^- concentrations level between 8 to 20 mg/L and crippling fluorosis if the consumption of fluorides is in excess of about 20 mg/day for 20 years or more. With this regard, defluoridation of drinking water becomes a widespread concern in the water supply industry and to date, it is still a tough issue for decentralized water desalination engineering in many rural areas.

Furthermore, as the population keeps increasing, the use of pesticides becomes a necessary condition in the agriculture industry in the world to ensure food security. However, its use resulted into environmental concerns including water pollutions. The 4.1 million tons of pesticides were used worldwide in 2016, with 1.4% going to Oceania, 2.2% to Africa, 11.8% to Europe, 33.3% to the Americas, and 51.3% to Asia (Pérez-Parada *et al.,* 2018). Nevertheless, only 1% of pesticides that were applied actually reached the intended organisms; the other 99% ended up in soils and water sources (Ali *et al.,* 2019). Amongst various pesticides, paraquat (PQ) (1,1-dimethyl-4,4-dipyridinium dichloride) is one of the most widely used herbicides in agriculture worldwide due to its cost effectiveness, high efficiency, familiarility and availability, labour saving, soil consrvation and non-selectivity in combating broadleaf weeds in the pre-planting of cotton, rice and tobacco crops (Bertrand, 2019; Bromilow, 2004; Nanseu-Njiki *et al.,* 2010; Núñez *et al.,* 2002; Santos *et al.,* 2013; Sieliechi & Thue, 2014). Surface water, groundwater, and wastewater worldwide have shown the presence of PQ in the current years (Grillo *et al.,* 2014; Leite *et al.,* 2013; Ritter, 2002; Santos *et al.,* 2014). The risk of contaminating groundwater and surface water with PQ is enhanced by its higher solubility (620 g/L) (Tomlin, 2009). The PQ residues are regarded as a potent health risk because they are highly persistent (De Souza *et al.,* 2006; Hamadi *et al.,* 2004). Several studies report deaths caused by poisoning via skin exposure or ingestion (Brown *et al.,* 2004). The literature reported that PQ is highly toxic even at low concentrations (Lee *et al.,* 2008; Tang *et al.,* 2020). To Canadian drinking water quality guidelines, the maximum acceptable concentration (MAC) for PQ in drinking water is 0.01 mg/L (Canada, 2011). The World Health Organization set an advisory limit for paraquat in drinking water at 10 µg/L (Thongpitak *et al.,* 2020). While according to the Office of Water of the US Environmental Protection Agency (EPA), the maximum contaminant level of PQ in drinking waters is 0.003 mg /L (Núñez *et al.,* 2002).

Paraquat has been linked with mitochondrial dysfunction and oxidative stress resulting in Parkinson's disease (Cochemé & Murphy, 2008; Costello *et al.,* 2009). According to reports, PQ affects the dysregulated biosynthesis of cholesterol in human brains and impacts the brain's reactive oxygen species (ROS) (Castello *et al.,* 2007; Tatjana *et al.,* 2021). Furthermore, PQ can cause organ damage in the kidneys and lungs (Brown *et al.,* 2004). The PQ is highly toxic when ingested by humans with an oral Lethal Dose (LD_{50}) value of 4 mg kg^{-1}, and it can easily enter the body through the skin (Vickers, 2017). Loha *et al.* (2018) reported that more than 50% of farmers exposed to PQ pesticides in Tanzania had experienced headaches, excessive salivation, nausea, vomiting, and skin or eye irritation. Also, over 40% experienced dizziness, blurred vision, sleeplessness, and breathing difficulties while over 20% reported tremors,

diarrhoea, chest pain, pain when urinating, fever, wheezing, or nosebleed due to the exposure to PQ pesticides. Therefore, PQ contamination in water is one of the global environmental issues which needs instant solution.

Several technologies have been developed for the removal of inorganic and organic pollutants from water, specifically F^- and PQ, respectively, such as adsorption (Aw *et al.,* 2022; Salomón *et al.,* 2021), nanofiltration membranes and reverse osmosis (Ahmad *et al.,* 2008; Mohapatra *et al.,* 2009; Sieliechi & Thue, 2014), photocatalytic degradation (Aungpradit *et al.,* 2007; Mahalakshmi *et al.,* 2007), electrodialysis (Mohapatra *et al.,* 2009), Nalgonda technique (Kumar *et al.,* 2019), coagulation and precipitation (Gong *et al.,* 2012; Khatibikamal *et al.,* 2010; Turner *et al.,* 2005).

Adsorption is the most affordable and effective method for removing inorganic and organic pollutants from water as it can be applied in the large-scale advanced treatment of dispersed water sources (Bai *et al.,* 2019; Sieliechi & Thue, 2014) and achieve high adsorption capacity. However, despite its high adsorption capacity, it suffers from problems in regenerating the exhausted adsorbent (Bai *et al.,* 2019). Regeneration is usually done by treating the spent adsorbents with acid or alkali, which produces a large amount of wastewater. As a result, the regeneration process becomes complicated and leads to secondary water pollution. Additionally, Nanofiltration membranes and reverse osmosis can adsorb more than 98% of F^- from the water (Chakrabortty *et al.,* 2013; Ndiaye *et al.,* 2005); and it is an efficient method for the removal of organic pollutants. However, this method faces challenges such as membrane fouling or degradation, making the membrane processes normally impractical and costly (Boutin *et al.,* 2009; Daneshvar *et al.,* 2007; Lapertot *et al.,* 2007). Therefore, technologies that will overcome the regeneration challenges of adsorbents and fouling are highly needed.

Capacitive deionization (CDI) has become an up-and-coming water treatment technology due to its critical advantages of low energy consumption, high efficiency, low cost, green and pollution-free, and renewable electrodes. In addition, based on the reversible electrochemical process, 46.6 % of the energy used by capacitive deionization can be partially recovered by connecting external loads, reducing the energy consumption and leading to economic cost of the system (Bao *et al.,* 2023). Also, CDI has high water recoveries and low fouling (Saleem & Kim, 2018; Welgemoed & Schutte, 2005).

The typical CDI process cycle consists of two phases: purification and regeneration (Figure 1). During the purification phase, an electric potential (<1.8 V) is applied to the pair of electrodes, which forces charged ions in the electrolyte solution to migrate toward oppositely charged electrodes and held in the electrical double layer (Bao *et al.,* 2023). The adsorbed ions concentrate at the electrodes, thereby reducing their concentrations in the electrolyte. When the electrode becomes saturated, regeneration is achieved by shorting the electrodes or reversing the polarity of the applied cell potential to expel the adsorbed ions into the concentrated stream (Bao *et al.,* 2023; Lee *et al.,* 2006; Leonard *et al.,* 2009; Park *et al.,* 2007).

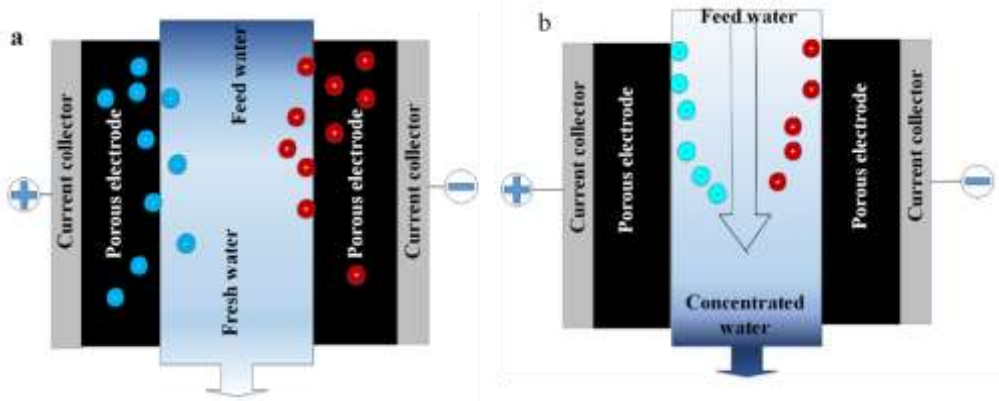

Figure 1: Schematic diagram of a CDI system showing (a) the purification step, (b) the regeneration step

There are several parameters influencing CDI performance such as device design (plate size, plate spacing and operation mode), operational factors (applied voltage, flow rate) and environmental factors (concentration of ions in the solution, target ion properties, temperature of solution and pH value of the solution) (Che *et al.,* 2021; Chen *et al.,* 2019). However, The electrode material is the main controlling factor for CDI performance (Han *et al.,* 2019; Tang *et al.,* 2019).

Conventional carbon electrode materials, such as activated carbon (AC), carbon nanotubes (CNTs), carbon fibers, carbon aerogels, and graphene, have recently received considerable interest for CDI applications, including water defluoridation (Elisadiki *et al.,* 2020; Elisadiki *et al.,* 2019; Tang *et al.,* 2015). However, CNTs and graphene have drawbacks as CDI electrode materials owing to their inadequate porosity, and thus, low surface areas also preparation requires expensive precursors and complex procedures (Bao *et al.,* 2023; Porada *et al.,* 2013; Yang *et al.,* 2013). In contrast, carbon fibers have shown excellent CDI performance (Chen *et al.,* 2014); however, they may be unsuitable as electrode materials because of their high manufacturing costs (Haq *et al.,* 2019). Activated carbon is one of the best and most extensively used electrode materials for CDI applications because of its lower price and stability, high

surface area, and abundance (Huang *et al.,* 2013b). However, its low conductivity, poor wettability, low capacity and high electrical transfer resistance limit its development for practical CDI usage (Bao *et al.,* 2023; Foo & Hameed, 2009). Therefore, several AC modification processes have been employed, including chemical treatment (Wu *et al.,* 2016), surface coating and element doping (Khan *et al.,* 2019), activation (Bao *et al.,* 2023) and compositing with metal oxides (Li *et al.,* 2018; Ryoo *et al.,* 2003) to enhance the CDI performance of AC.

Additionally, for F^- removal, particularly in the presence of other anions (complex solution), AC is insufficiently efficient owing to its low selectivity, low removal capacity, and poor regeneration, thus limiting its applications in CDI (Hameed *et al.,* 2021; Li *et al.,* 2020; Suss *et al.,* 2015; Wu *et al.,* 2016). Moreover, AC electrodes suffer from the co-ion repulsion effect, which constrains the free ions from approaching them and cause the adsorbed ions to easily return to the solution (Xiao & Hatton, 2017). Therefore, surface modification of pristine AC is needed to overcome the aforementioned shortcomings.

Recently, metal oxide nanomaterials and their composites based on iron (Fe), aluminium (Al) titanium (Ti), magnesium (Mg), silicon (Si), zirconium (Zr), cerium (Ce), manganese (Mn), and nickel (Ni) oxides have been developed for the defluoridation process and demonstrated improved F^- removal efficiency (Bai *et al.,* 2019; Li *et al.,* 2019; Wang *et al.,* 2021). The oxide nanoparticles have abundant surface functional groups, making them particularly stable in F^- electrosorption. Hence, metal oxides, such as Al, Fe, and Ti oxides, are chosen for water defluoridation because of their high adsorption capacity, nontoxicity, low water solubility, hydrophilicity, and strong F^- affinity, and desorption potential (Cheng *et al.*, 2019; Mukherjee *et al.,* 2019; Suriyaraj & Selvakumar, 2016; Wu *et al.,* 2016). Therefore, the present study composited AC with Al, Fe and Ti oxides to enhance its F^- removal and selectivity.

Although several studies have examined defluoridation with metal oxide-modified AC as a CDI electrode material, most current research mainly focuses on the performance of AC modified with a single metal oxide for F^- removal from simulated water. For instance, Li *et al.* (2018) studied titanium hydroxide-loaded AC named ($Ti(OH)_4$–AC) for F^- removal from a solution containing F, Cl^-, NO_3^-, and SO_4^{2-}. The electrode's maximum electrosorption capacity (EC) was 115.2 mg/g at an applied voltage of 1.2 V from a solution with an initial F^- concentration of 50 mg/L. The synthesized $Ti(OH)_4$–AC presented good electrosorption selectivity of F^-, unaffected by the competitive anions in the feed solution. Similarly, Min *et al*. (2020) investigated the electrosorption performance of a bismuth/reduced graphene oxide

nanocomposite (Bi/rGO) to selectively remove F^- and Cl^-. Their results demonstrated that the material had strong ion selectivity and regeneration ability, as revealed by the F^- and Cl^- removal capacities insignificantly decreasing after ten cycles. The maximal F^- electrosorption capacity was 0.48 mmol/g, approximately four times lower than Cl^-, indicating that Bi/rGO favours Cl^- selection over F^-. In addition, Wu *et al.* (2016) synthesized titanium oxide (TiO_2)-loaded AC and used it as a potential material for F^- removal from simulated water. The developed TiO_2-loaded AC electrode achieved a maximum F^- removal capacity of 157.8 μmol/g at an applied potential of 1.5 V. Various studies reported that the composite of metal oxide materials inherit the advantages of each parent metal oxide and exhibits evident synergistic effects for efficient F^- removal as demonstrated by a bimetallic oxide composite outperforming the monometallic components in terms of adsorption efficiency (Fu *et al.,* 2019; Nyangi *et al.,* 2021).

Despite the promising results of CDI for defluoridation, the majority of the studies are based on laboratory research on synthetic water. Synthetic water has a simple composition compared to real water, which is characterized by a complex mixture of non-target treatment objects such as organic and inorganic substances and impurity ions. The presence of these components in natural water can adversely affect CDI performance and hinder its practical application. Therefore, the gap exists on the performance of AC electrodes composited with trimetallic oxides for both synthetic and natural water defluoridation by CDI. In this study, CDI electrode materials were synthesized by compositing AC with trimetallic oxides (Al, Fe, and Ti oxides) at different mass ratios of Al, Fe, and Ti oxides by a simple one-step co-precipitation method at a temperature range of 23 – 27°C, and their F^- removal from simulated and actual water was investigated.

In real-life scenarios, wastewater and natural water contain various ionic species and organic pollutants, including pharmaceuticals, phenolic compounds, humic substances, dyes, and pesticides. These pollutants can lead to significant environmental problems globally and compete against each other during the CDI process for removal, leading to different selectivity and electrosorption capacities (Achilleos & Hatton, 2016; Su & Hatton, 2017; Xiao & Hatton, 2017). However, most studies focused only on using CDI technology to remove inorganic (ionic) species. Presently, researchers integrated CDI technology with other methods to effectively treat wastewater containing various pollutants. The integration aims to ensure the continuous functionality of CDI systems when applied in practical scenarios. For instance, Chen *et al*. (2023) integrated CDI and electro-oxidation (CDI-EO) methodologies to create a

hybrid system capable of simultaneously removing organic pollutants (acid orange) and heavy metal ($Cu^{2+)}$ ions from wastewater. Liang *et al.* (2019) also combined ultrafiltration with CDI to simultaneously remove inorganic salts and organic contaminants from wastewater.

Drawing from the aforementioned studies, it is evident that integrating CDI technology with other technologies is essential to create a novel system capable of effectively removing organic contaminants. Although the integrated strategy based on CDI resolves the issue of the synergistic removal of organic pollutants and other ions in wastewater, the facilities and operations are complex at the commercialization scale, and the maintenance and operation cost is expensive (Bao *et al.,* 2023). To overcome the abovementioned challenges of the integrated system, few studies investigated the usefulness of CDI system alone for the removal of organic pollutants and have shown promising performance. For example, in their investigation, Senoussi and Bouhidel (2018b) used granular AC as a CDI electrode material to remove textile dyes from industrial wastewater. At a flow rate of 10 mL/min and a voltage of 2 V, the highest achieved values were 98% for RE and 1.75 mg/g for EC.

Lester (2019) conducted research involving the utilization of AC as an electrode material for the removal of salts and trace organic pollutants like pentoxifylline, carbamazepine, estrone, and bisphenol A from water with CDI. The sequence of removal efficiency for the trace organic contaminants is as follows: bisphenol A > estrone > carbamazepine > pentoxifylline. The authors reported the RE exceeding 90% for bisphenol A. Based on that, there is an expectation that the same approach of using CDI could be applied for the removal of the cationic PQ herbicide from water.

Therefore, this study investigated the suitability of commercial AC and AC composited with the oxides of Al, Fe and Ti as CDI electrode materials for removing PQ from synthetic and real water for the first time. In addition, the influence of various CDI operational factors, such as mass loading of the metal oxides on the AC surface, applied voltage, the flow rate of the solution, treatment/charging time and cycle stability of AC for PQ removal were examined in batch mode experiments.

1.2 Statement of the problem

Carbon-based materials, specifically activated carbons (AC), are among the best and most extensively used electrode materials for CDI applications owing to their lower price and stability, high surface area, and abundance (Huang *et al.,* 2013a). Several studies have

investigated the capability of AC from different precursors, including biomasses as CDI electrode materials for water the removal of various water contaminants including F^- (Elisadiki *et al.*, 2019; Gaikwad & Balomajumder, 2017b, 2018). However, AC electrode materials presented low selectivity, low removal capacity, and poor regeneration for the removal of various contaminants such as F^-. Additionally, most of the available studies focused on CDI performance for removing inorganic pollutants including F^- from water. However, the removal of organic pollutants such as pesticides and pharmaceuticals, which pose serious environmental problems worldwide and require serious attention, is left behind. Thus, to improve the CDI performance with AC, modification of AC is required. Therefore, this study modified AC with Al, Fe, and Ti oxides as CDI electrode materials for F^- and PQ herbicides removal from synthetic and natural water. Furthermore, the study investigated on the suitability of CDI for the removal of organic contaminants specifically PQ pesticide.

1.3 Rationale of the study

The world's growing population has led to a shortage of clean water resources due to the expansion of industrial and agricultural activities that have caused significant water pollution worldwide. As a result, there is a need to explore alternative methods to ensure access to clean and safe water for human survival and to meet the increasing demand. While many water purification technologies exist, most are energy-intensive and rely on fossil fuels, making them costly for low-income societies and those without access to the national grid. To address these issues, a green and chemical-free CDI unit with low-cost electrode materials prepared at ambient temperature (AC-modified metal oxides) offers cost-effective and energy-efficient water defluoridation and paraquat pesticide removal technology. Additionally, Since CDI has the advantage of consuming relatively low energy compared to other conventional technologies, CDI unit can utilize renewable energy sources like solar and wind, making it accessible even to rural households and communities not connected to the national grid. This makes CDI technology a promising water purification method as the world continues transitioning away from fossil fuels as a primary energy source.

1.4 Objectives of the study

1.4.1 General objective

To investigate the suitability of AC composited with Al, Fe, and Ti oxides as a CDI electrode material for water defluoridation and PQ pesticide removal from simulated and natural water.

1.4.2 Specific objectives

(i) To develop and characterize the composites of AC with Al, Fe and Ti oxides,

(ii) To evaluate the performance of pristine AC and the composites of AC with Al, Fe and Ti oxides CDI electrodes for the F^- removal from both simulated and natural water.

(iii) To investigate the suitability of the CDI method for the removal of PQ herbicides from water using pristine AC as electrode materials.

(iv) To evaluate the performance of the composites of AC with Al, Fe and Ti oxides as CDI electrodes for the PQ herbicide removal from both synthetic and natural water.

1.5 Research questions

(i) What are the characteristics of pristine AC and the composites of AC with Al, Fe and Ti oxides that make them effective CDI electrode materials for defluoridation and PQ removal?

(ii) To what extent do AC composites with Al, Fe and Ti oxides enhance the F^- removal capacity with CDI?

(iii) To what extent do CDI technology suitable for removing PQ pesticides from water?

(iv) To what extent have the composites of AC with Al, Fe and Ti oxides enhanced the removal of PQ pesticides from water?

1.6 Significance of the study

Utilizing cost-effective, eco-friendly, efficient, and sustainable CDI electrode materials can facilitate the application of CDI systems on a commercial scale for water treatment. In this study, AC composited with metal oxides (MO) was synthesized using a simple and one-step co-precipitation method at ambient temperature and evaluated as CDI electrode materials for defluoridation of natural water and removal of PQ pesticides from water. The findings of this study will contribute to the existing body of knowledge in the field of water defluoridation and pesticide removal using AC composited with MO and promote the application of CDI systems for water purification purposes. Additionally, this work will contribute to attaining target 6.1 of Sustainable Development Goal (SDG) number 6 on Universal Access to Safe and Affordable

Drinking Water and directly links to target 3.9 of SDG number 3 on a significant reduction in the number of deaths and illnesses from water and soil pollution and contamination.

1.7 Delineation of the study

This study aimed to improve pristine AC performance by modifying it with MO for natural water defluridation and paraquat pesticides removal with CDI technology. This study discusses the synthesis methods, characterization of materials and performance of the developed CDI electrodes in terms of removal efficiencies and electrosorption capacities towards PQ and F^- removal. This dissertation is organized into five Chapters. Chapter one includes background information, the purpose of the study, objectives, research questions, and the significance of the study. Chapter two presents the literature review in which different electrode materials studied for water defluoridation, their electrosorption capacities and F^- removal efficiencies, and the parameters that influence CDI performance during defluoridation are discussed. Furthermore, chapter two also presented different electrode materials that have been investigated for the removal of organic pollutants with CDI. Chapter three (materials and methods) presented the synthesis of activated carbon composited with MO, different techniques used in characterizing the developed materials, preparation of CDI electrodes and CDI experiments. Chapter four presents the results and discussion where the characteristics of the prepared composites, the effect of mass loading of the metal oxides on the AC surfaces, interaction effects of the independent variable on removal efficiency, as well as the CDI operating conditions including applied potential, charging time, flowrate towards PQ and F^- removal are discussed. Finally, the conclusion and recommendations are presented in Chapter five. The study thought to enhance the performance of commercial AC by compositing with MO using a simple preparation method to develop an affordable CDI system capable of removing F^- and PQ pesticides from natural water samples. However, the cost benefit analysis of the prepared CDI electrode materials and its selectivity to other non-targeted contaminants in the collected natural water samples after CDI testing were not investigated, which represents a limitation of the study and leaves a gap for future studies of this nature. The scope of this study spanned towards developing efficient materials for water defluoridation and pesticide removal. The efficiency of the AC modified with metal oxides towards fluoride and paraquat removal from natural water demonstrated the future promise of the material to be used on a commercial scale. Therefore, since this work was primarily based on a lab-scale CDI system, further research is necessary to investigate the performance of the developed materials in real field applications.

CHAPTER TWO

LITERATURE REVIEW

2.1 Introduction

The global clean and safe water crisis is a growing concern that poses significant challenges to human health, economic development, and environmental sustainability. With increasing population growth, urbanization, and industrialization, water demand escalates rapidly, resulting in over-extraction of groundwater, pollution of water sources, and degradation of water quality. Many communities worldwide lack access to clean and safe water, leading to waterborne diseases, sanitation issues, and economic disparities. Developing efficient, sustainable, green and cost-effective water purification technologies to treat the contaminated water sources and make it appropriate for various daily use such as drinking, household activities, agriculture and for different industrial applications could be among the alternatives solution to ensure water accessibility. Several water purification technologies are commercially available for water and wastewater treatments. Still, most of them demonstrated various limitations, such as high energy consumption during the purification process and the introduction of secondary water pollution. This calls for developing cost-effective, green and energy- efficient water purification technologies. Capacitive deionization is a promising water treatment technology due to its critical advantages of low energy consumption, high efficiency, low cost, green and pollution-free, and renewable electrodes. However, finding effective and less expensive CDI electrode materials for treating wastewater with high electrosorption capacity is still challenging. Therefore, research on the synthesis of efficient, cost-effective electrode materials for removing different water pollutants such F^- and PQ pesticides is highly needed. This Chapter highlighted the performance of the existing CDI electrode materials used for defluoridation and pointed out important parameters affecting CDI performance on the F^- removal from water. Furthermore, the Chapter also presented the performance of different electrode materials that have been investigated for removing various organic pollutants with CDI.

2.2 Performance of various CDI electrode materials for defluoridation

2.2.1 Carbon-based materials

Carbon-based electrode materials have been studied extensively for F^- removal, as shown in Table 1, because carbon has a good affinity with F^- (Karthikeyan & Elango, 2008). Carbon-

based materials derived from biomass have been studied and show good defluoridation ability. For instance, Dong *et al.* (2021) successfully synthesized biochar from lignocellulosic waste for defluoridation with the highest removal efficiency of 91.98% and electrosorption capacity of 1.28 mg/g at 1.2 V. The improved CDI performance for F^- removal was ascribed to the electrostatic force generated when the potential was applied, and the effect of the electric double layer (EDL) formed. Also, the developed biochar was revealed to have a negative zeta potential, implying that the synthesized materials do not favor the electrosorption of negative ions, including F^- because the electrode surface of the developed biochar was negatively polarized. Thus, it is important to understand the nature of the electrode materials' surface by determining the potential of zero charges or zeta potential to improve CDI performance. Gaikwad and Balomajumder (2017b) investigated the feasibility of AC derived from tea waste biomass (TWBAC) for defluoridation and hexavalent chromium removal simultaneously via CDI. The obtained highest EC of the prepared tea waste biomass activated carbon electrode (TWBAC) towards F^- was 0.74 mg/g (85.20%) and 2.49 (28.52%) at 10 mg/L and 100 mg/L F^- initial concentration, respectively, at a cell potential of 1.2 V. The results showed that the prepared TWBAC is more favorable for chromium (Cr^-) adsorption over F^- in the mixed feed solution (Fig. 2) due to the difference in hydrated radius and valence as the hydrated radius of F^- is smaller than that of Cr (VI); also the electrosorption selectivity of multivalent anions is higher than that of monovalent (Li *et al.,* 2016).

Furthermore, similar behavior was observed when commercial AC was used as CDI electrode material for the simultaneous removal of F^- and Cr^- (Gaikwad & Balomajumder, 2017a). The maximum F^- and Cr^- removal efficiency of AC was 94.20 and 97.1%, respectively, for the initial F^- concentration of 10 mg/L binary feed solution of F^- and Cr^-, pump flow rate 16 mL/min and applied potential of 1.2 V. Their results demonstrated the effect of Cr^- in the mixed solution towards electrosorption selectivity of F^-.

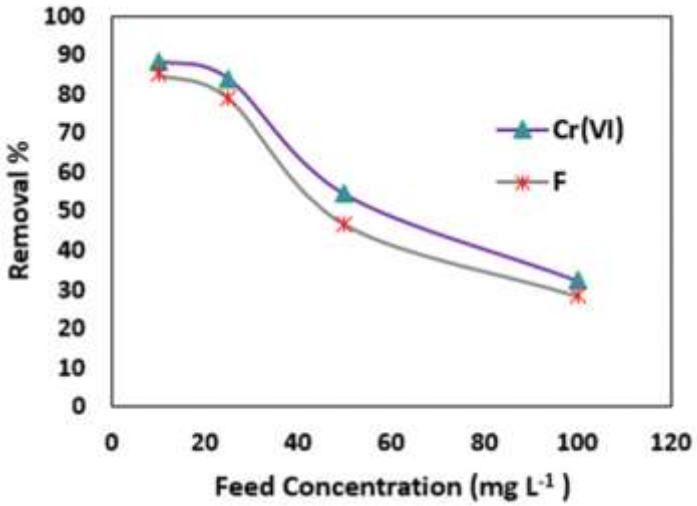

Figure 2: Comparison of the electrosorption capacity of F^- and Cr (VI) (Gaikwad & Balomajumder, 2017b)

Also, Elisadiki *et al.* (2019) studied the AC derived from jackfruit peel for the removal of F^- from natural water. Their results showed that the developed materials successfully brought down F^- concentration from 3.11 to 1.18 mg/L from natural water in the presence of natural organic substances and other ions. The highest electrosorption capacity was reported to be 0.13 mg/g, achieved at the charging potential of 2.0 V and flow rate of 5 mL/min. Moreover, Wu *et al.* (2021) synthesized a Polyaniline-CNT (PANI-CNT) composite electrode for defluoridation with CDI. The highest removal capacity of PAN-CNT was reported to be 0.52 mmol/ g at pH 7 and voltage of 1.6 V, which was approximately 1.5 times more than that of CNTs. Wu *et al.* (2021) emphasized that the improved electrosorption capacity was due to incorporating PANI into CNTs.

From all these studies, as summarized in Table 1, it has been observed that the selectivity of the carbon-based materials for defluoridation is still low. Thus, there is a need to focus more on the development of new CDI electrode materials with high selectivity, which are environmentally friendly, cheap and efficient to improve the F^- electrosorption selectivity. Since the selectivity of the electrode materials for F^- removal is an important feature as some of the electrode materials could evidence good efficiency in bench tests but fail under real conditions at water treatment plant due to the reduction of the electrosorption capacity caused by electrodes' active sites occupation by other co-ions present in treated water. Moreover, from Table 1, one can see that the majority of the studies were conducted with synthetic water; thus, there is a need to investigate the performance of the synthesized materials in both simulated and natural water defluoridation studies to evaluate the effect of natural matters that present in water affecting the performance of CDI electrodes towards F^- selectivity and come up with a

clear solution on how to deal with that effect to promote the practical applications of CDI system in real water settings.

Table 1: Carbon-based electrode materials for defluoridation with their maximum removal efficiency and electrosorption capacity

Electrode material	Water source	IFC (mg/L)	Voltage (V)	Flowrate (mL/min)	Removal (%)	EC (mg/g)	References
Biochar	Synthetic water	20	1.2	15	91.98	1.28	Dong *et al.* (2021)
Commercial AC	Synthetic water	10	1.2	16	94.20	0.82	Gaikwad & Balomajumder (2017a)
TWBAC	Synthetic water	10	1.2	-	85.20	0.74	Gaikwad & Balomajumder (2017b)
PANI-CNT	Synthetic water	38	1.6	5	-	9.88	Gaikwad & Balomajumder (2021)
Commercial AC	Synthetic water	-	1.5	-	98.49	-	Kushwaha *et al.* (2020)
Micropore-dominant AC	Synthetic water	50	1.6	10	-	16.8	Li *et al.* (2017)
JFAC	Natural water	3.11	2.0	5	63	0.13	Elisadiki *et al.* (2019)

AC = Activated carbon, EC = Electrosorption capacity, IFC= Initial F^- concentration

2.2.2 Metal oxides and their composite

Single, two or more metal oxides, as summarized in Table 2, especially those prepared in nanoscale, have been reported to have great potential for removing F^- from drinking water and showed remarkable adsorption capacities. This is due to their unique features, including the large specific surface area of the metal oxides nanoparticles, which is favorable for F^- adsorption (Kumar *et al.,* 2011; Li *et al.,* 2014; Maliyekkal *et al.,* 2006; Prasad *et al.,* 2014; Raul *et al.,* 2012), fast adsorption kinetics rate, the presence of functional groups at the metal oxides nanomaterials surfaces (Khandare & Mukherjee, 2019), good desorption potential, limited solubility in water, and non-toxicity in nature (Loganathan *et al.,* 2013; Tomar *et al.,* 2013).

Bai *et al.* (2019) studied the potential of NiAl-layered metal oxide (NiAl-LMO) as CDI electrode materials for the selectivity of F^- from drinking water. The obtained maximum electrosorption capacity of NiAl-LMO towards F^- was 49.28 mg/g, which was higher than the electrosorption capacity and selectivity of other anions present in solution chlorine (Cl^-) and sulphate (SO_4^{-2}) ions.

Likewise, Wang *et al.* (2021) successfully synthesized and characterized nickel, iron, and manganese layered metal oxide (NiFeMn-LMO) electrodes for defluoridation applications. The maximum defluoridation capacity of the developed electrode material reported was 16.7 mg/g at 500 mg/L initial F^- feed concentration. Wang *et al.* (2021) emphasized that the good defluoridation performance of NiFeMn-LMO electrodes for F^- selectivity depicted was due to the synergistic effect of the ternary metals.

Li *et al.* (2019) studied the electrosorption performance of nickel, cobalt and aluminium (NiCoAl)-layered metal oxide (NiCoAl-LMO) nanosheets and reduced graphene oxide (rGO) composites (NiCoAl-LMO/rGO) which were prepared by one-step urea precipitation method. The prepared electrodes achieved an electrosorption capacity of 24.5 mg/g, with the initial NaF concentration of 500 mg/L at 1.4 V applied voltage and maximum cycle stability of 40.

These studies demonstrated that metal oxide nanomaterials and their composites have good potential for the selectivity of fluoride removal from water. The improved F^- electrosorption selectivity depicted was attributed to the electrostatic interaction between the charging surface and fluoride synergistic when the potential is applied and the exchange of surface hydroxyl groups with F^- (Habuda-Stanic *et al.*, 2014; 2019; Mukherjee *et al.*, 2019). However, few studies in the literature investigated the potential of metal oxides for defluoridation. Additionally, it is important to note that all the studies in Table 2 have focused on F^- removal from synthetic water samples. Therefore, it is crucial to conduct further research to assess the applicability of the developed metal oxide CDI electrode materials in real water samples, which may contain various other contaminants that could affect the materials' performance.

Table 2: Comparison of the F^- maximum removal efficiency and electrosorption capacity of different metal oxides and their composites

Electrode material	Water source	IFC (mg/L)	Voltage (V)	Flowrate (mL/min)	Removal (%)	EC (mg/g)	References
NiAl-LMO	Simulated water	5	1.0	-	73.5	49.28	Bai *et al.* (2019)
NiFeMn-LMO	Simulated water	9.5	1.4	-	-	16.7	Wang *et al.* (2021)
NiCoAl-LMO/rGO	Simulated water	9.5	1.4	-	-	24.5	Li *et al.* (2019)

AC = Activated carbon, EC= Electrosorption capacity, IFC = Initial F^- concentration

2.2.3 Carbon-based materials and metal oxides/hydroxides composites

Different carbon-based materials have been modified with metal oxides or hydroxides to form a composite to improve their properties, especially for the selectivity of the targeted pollutants

present in water, including F^-, as summarized in Table 3, for enhancing the CDI performance. For instance, Li *et al.* (2018) investigated the performance of AC modified with titanium hydroxide ($Ti(OH)_4$) for the removal of F^- from the solution of different kinds of anions. The maximum adsorption capacity of the electrode made from $Ti(OH)_4$-loaded AC was 115.2 mg/g at 1.2 V applied voltage with F^- initial concentration of 50 mg/L for the investigation of the adsorption selectivity of the electrode on F^-, a mixed solution containing Cl^-, NO_3^- and SO_4^{2-} was prepared. The experimental results revealed that the competitive anions present in the feed solution did not affect the adsorption selectivity of F^-.

Min *et al.* (2020) also investigated the electrosorption performance of bismuth/reduced graphene oxide nanocomposite (Bi/rGO) for the selective removal of F^- and Cl^-. The findings revealed that the material exhibited a good selectivity toward the ions and better regeneration, as after 10 cycles, there was no significant change in removal capacity for both Cl^- and F^-. The obtained maximum electrosorption capacity of F^- of 0.48 mmol/g was approximately 4 times lower than that of Cl^- which implies that Bi/rGO favors the selectivity of Cl^- than F^-. Furthermore, Park *et al.* (2020) studied the potential of reduced graphene oxide/hydroxyapatite composite (rGO/HA) prepared by the hydrothermal method for the selectivity of F^- from aqueous solution via the CDI. Park *et al.* (2020) compared the pristine AC and rGO/HA performance. They found that the defluoridation performance of the rGO/HA electrode was superior compared to that of the pristine AC electrode. The highest F^- removal capacity of rGO/HA and AC was found to be 0.2 and 0.041 mmol/g, respectively, in the mixed feed solution of F^-, Cl^-, and NO_3^-. They found that the F^- removal capacity of rGO/HA was not affected by the existence of Cl^- and NO_3^- in the feed solution. Also, the rGO/HA exhibited good cycle stability and reusability as even after 50 cycles no significant loss of electrode capacity was observed. The good performance of rGO/HA towards F^- removal was explained by the high affinity of HA in the rGO/HA electrode to the selectivity of F^-.

Also, Wu *et al.* (2016) modified AC with titanium oxide (TiO_2) to form (Ti-AC) composite and employed it as potential material for the electrosorption of F^- from water. The synthesized Ti-AC electrodes achieved a maximum F^- removal capacity of 157.8 μmol/g at an applied potential of 1.5 V. The good removal capacity observed was attributed to the external electric field applied to the cell and the chemical bonding between F^- and TiO_2.

From these studies, the results evidenced that the composite of carbon materials with metal oxide and hydroxide possesses high electrosorption capacity and excellent selectivity for F^- removal from water, which is attributed to both electrostatic driving force induced by the

potential applied on the electrode surfaces and the exchange of surface hydroxyl groups with F^- (Habuda-Stanic *et al.,* 2014; 2019; Mukherjee *et al.,* 2019). However, the available literature focused on the efficiency of carbon materials loaded with single metal oxides for CDI defluoridation. Thus, more studies are needed to investigate the synergistic effect of bimetallic and trimetallic oxides loaded with carbon materials as electrode materials for defluoridation to enhance the performance of the CDI system. Furthermore, while the existing studies have primarily examined the performance of materials in synthetic water, there is a need for further investigation using real water samples. Real water scenarios can consist of different contaminants that may interfere with F^- removal and potentially decrease the EC and RE of the materials. Therefore, future research should consider conducting experiments using real water samples to understand better the practical applicability of these materials for F^- removal in real-world scenarios.

Table 3: Comparison of the F maximum removal efficiency and electrosorption capacity of different composites of carbon materials and metal oxides and hydroxides

Electrode material	Water source	IFC (mg/L)	Voltage (V)	Flowrate (miL/min)	Removal (%)	EC (mg/g)	References
$Ti(OH)_4$ -AC	Simulated water	50	1.2	-	-	115.2	Li *et al.* (2018)
TiO_2-loaded AC	Simulated water	10	1.5	25	-	2.99	Wu *et al.* (2016)
Bi/rGO	Simulated water	420	1.2	-	-	9.12	Min *et al.* (2020)
rGO/HA	Simulated water	42	1.2	8	-	3.79	Park *et al.* (2021)

AC = Activated carbon, EC= Electrosorption capacity. IFC = Initial F^- concentration

2.2.4 MXenes

MXenes are a class of two-dimensional inorganic compounds that consist of atomically thin layers of transition metal carbides, nitrides, or carbonitrides. They were first reported in 2011 and have since gained significant attention in materials science. MXenes accept various hydrophilic terminations and can be classified based on their structures, such as multi-layer MXene (ML-MXene) or few-layer MXene (FL-MXene). These materials are produced by selectively etching out the A element from a MAX phase or other layered precursor, where M is an early transition metal, A is an element from group 13 or 14 of the periodic table, X is C and/or N, and n = 1–4. MXenes exhibit good conductivity and volumetric capacitance, making them suitable for various applications such as water purification (Huang *et al.,* 2019; X. Huang *et al.,* 2019; Liu *et al.,* 2020; Srimuk *et al.,* 2016; Ying *et al.,* 2015), energy storage (Anasori

et al., 2017; Zhang & Nicolosi, 2019), environmental remediation (Zou *et al.*, 2016), and sensors (Szuplewska *et al.*, 2020; Zhu *et al.*, 2017). The application of MXenes as CDI electrode material for removing various pollutants present in water, including F^-, has been studied. The MXenes evidenced significant sorption selectivity and efficient reduction capability for various targeted pollutants present in water due to their fascinating characteristics such as excellent selectivity towards specific pollutants, high surface area and presence of different functional groups (-O and -OH), as well as reduction capabilities towards numerous pollutants (Huang *et al.*, 2019; Ihsanullah, 2020; Szuplewska *et al.*, 2020; Zou *et al.*, 2016).

For instance, 2D Ni/MAX (Ti_3AlC_2) nanocomposite was employed as CDI electrode materials for defluoridation and removal of lead (Pb) and Arsenic (As (III)) ions (Bharath *et al.*, 2021). Ni/MAX (Ti_3AlC_2) nanocomposite demonstrated good selectivity of F^- from water with a maximum removal capacity of 68 mg/g at the applied potential of 1.4 V, initial F^- concentration of 100 mg/L, the flow rate of 5 mL/min and charging time of 150 min. The good electrosorption capacity obtained was attributed to the electrostatic force of attraction induced by the voltage applied and the presence of functional groups on the Ni/MAX (Ti_3AlC_2) surface. As per our review, limited studies investigated the potential of MXenes for defluoridation with CDI. Many studies focused on applying MXenes to remove heavy metals and organic contaminants, such as dyes, from water through adsorption and membrane processes. This is a call for the research community to study the practicability of MXenes for the removal of F^- from water with CDI due to their hydrophilicity, high electrical conductivity, selective surface chemistry and tunable surface that are the required properties of the CDI electrode materials (Ihsanullah, 2020; Oren, 2008) and therefore, can be promising material in future water purification, particularly F^- removal.

2.3 Parameters affecting the defluoridation process with capacitive deionization

Although electrode material property is the main controlling factor in any CDI system, its effectiveness can be controlled by several other CDI operating parameters. As a result, optimizing these factors is crucial for achieving efficient and effective CDI performance in water treatment applications. This section summarizes some of the key parameters such as flow rate, initial concentration, charging time, applied voltage, and type of electrolyte (Aldalbahi *et al.*, 2018; Gabelich *et al.*, 2002; Han *et al.*, 2014; Mossad & Zou, 2012) that have a contribution to the effectiveness of developed CDI electrode materials for defluoridation.

2.3.1 Applied voltage

The applied potential is among the significant parameters to consider in the electrosorption technique since it influences the electrosorption process due to the induced electrostatic attraction. The CDI relies on the charging and discharging of porous electrodes to remove ions from water. It is well known that the adsorption of the ions in the CDI system normally depends on the voltage that thickens the EDL, which is paramount for ion adsorption (Huang *et al.*, 2013b). When a voltage is applied across the electrodes, ions in the water are attracted toward the oppositely charged electrodes, leading to their adsorption onto the electrode surface. The magnitude of the applied potential directly affects the electrostatic forces between the ions and the electrodes, influencing the CDI process. Higher applied potentials generally result in higher ion removal efficiency, enhancing the electrostatic attraction and facilitating ion adsorption. However, higher potentials also increase energy consumption and may lead to undesirable side reactions, such as water electrolysis. Therefore, optimizing the applied potential is crucial in CDI to balance ion removal efficiency and energy consumption and to ensure the overall effectiveness and efficiency of the CDI process.

Several studies investigated the influence of applied potential in CDI cells for water defluoridation. For instance, Park *et al.* (2020) investigated the impact of electric voltage on F^- removal using the rGO/HA as CDI electrode material. The maximum F^- removal capacity of rGO/HA achieved was 0.19 mg/g at 1.2 V, which was 2.4 times higher than that operated at 0.5 V. Park *et al.* (2020) reported that the increase in charging potential enhances the electrosorption capacity when the electric potential increases from 0.5 to 1.2V. However, at 1.5 V, the F^- removal capacity significantly decreased because of probably water electrolysis.

Bharath *et al.* (2021) also studied the effect of electric potential (0.8 to 1.8 V) on F^- removal capacity. The results showed the increment in electrosorption capacity as potential increases from 0.8 to 1.4 V. However, above 1.4 V, the electrosorption capacity decreases (Fig. 3a). The negative trend observed when more than 1.4 V was applied was ascribed to water electrolysis, which normally results in high energy consumption.

Li *et al.* (2019) also investigated the effect of varying applied voltage from 0.6 to 1.4 V on defluoridation. They found that increasing charging potential increases F^- removal capacity from 9.1 to 24.5 mg/g (Fig. 3b). Li *et al.* (2019) emphasized that the improved removal capacity exhibited was due to the stronger Coulomb force between the surface of the electrode and NaF and the increased EDL capacity.

Moreover, Li *et al.* (2017) also investigated the effect of applied voltage for the voltage range of 0.4 to 1.6 V towards F^- electrosorption in the CDI system. The maximum electrosorption capacity obtained was 16.8 mg/g at 1.6 V, at the flow rate of 10 mL/min and the initial concentration of 50 mg/L. Their result demonstrated the increase in electrosorption capacity as the voltage applied increases due to the increase of coulombic force as voltage rises. Dong *et al.* (2021) also studied the influence of different applied voltages on the electrosorption performance of CDI toward F^- removal. The findings demonstrated the decrease in the F^- concentration in the solution as the voltage applied increased from 0.4 to 1.2 V (Fig. 3c), resulting in improved electrosorption capacity.

The effect of applied voltage on F^- removal using the PANI-CNT composite electrode was also investigated in the 0 V to 2.4 V range by Wu *et al.* (2021). The maximum electrosorption capacity was observed at 1.6 V, attributed to the strong electrostatic force of attraction between the oppositely charged electrodes, as agreed by other studies above. However, above 1.6 V, a decreasing trend in the removal capacity was observed due to the oxidation reaction that occurred to the PANI-CNT electrode. Moreover, Gaikwad and Balomajumder (2017a) studied the defluoridation performance of CDI at different voltage ranges from 0.4 to 1.2 V and found that the best removal performance occurred at 1.2 V (Fig. 3d).

Both of these experiments show that as the applied potential increased, F^- removal capacity increased. However, the maximum F^- electrosorption capacity takes place at the voltage of 1.2 and 1.6 V; then, it can be concluded that the optimum voltage range for defluoridation with CDI should be between 1.2 to 1.6 V. Increasing the voltage to values larger than 1.6 V might result in water electrolysis and other side reactions on the electrode that might lead to high energy consumption (Jiang *et al.*, 2018; Zhang *et al.*, 2020).

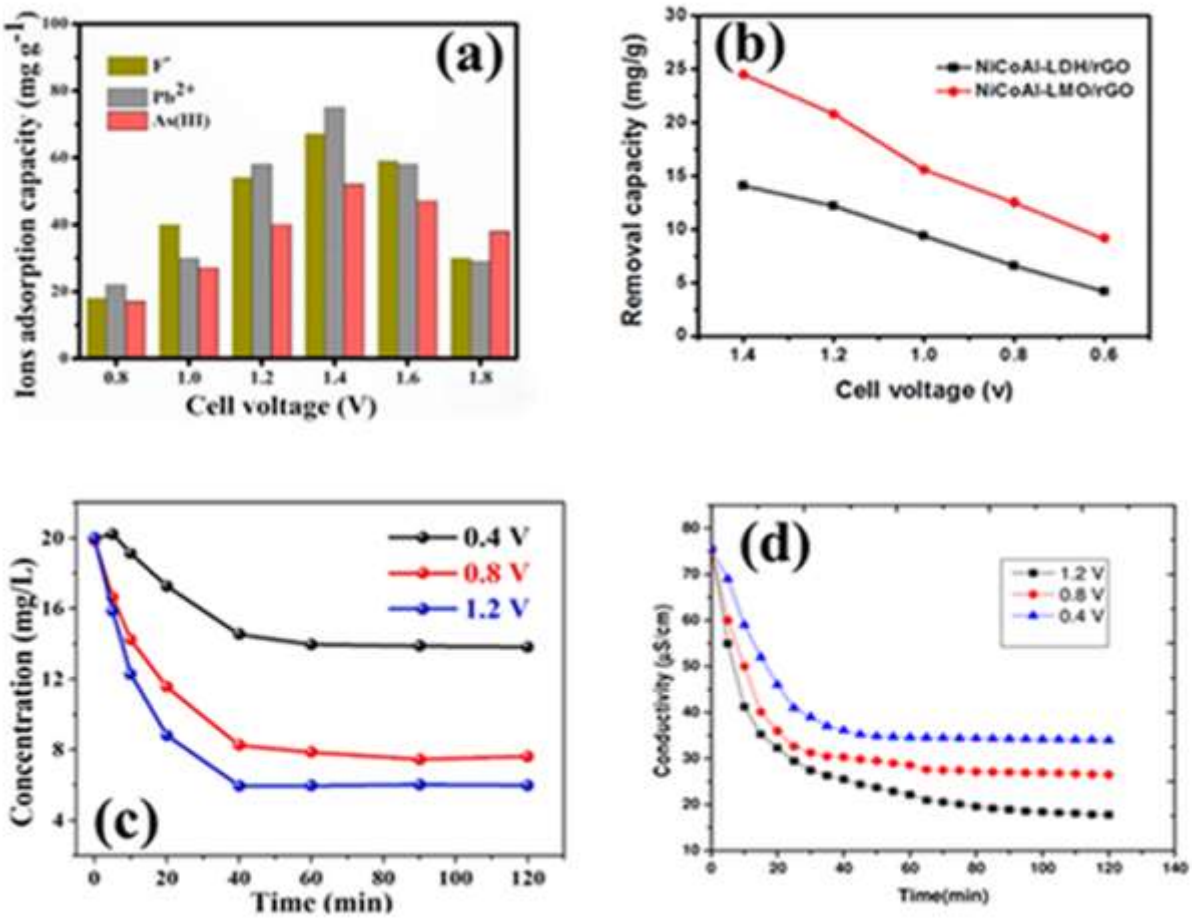

Figure 3: **(a) The effect of the applied voltage on the adsorption capacity *(Bharath et al.*, 2021), (b) Fluoride removal capacities of NiCoAl-LDH/rGO and NiCoAl-LMO/rGO in NaF solution at the initial concentration of 500 mg/L (Li *et al.*, 2019), (c) Time versus concentration at the applied voltage of 0.4, 0.8 and 1.2 V. (Dong *et al.*, 2021), (d) Conductivity versus time at different applied voltages (Gaikwad & Balomajumder, 2017a)**

2.3.2 pH of the solution

The pH of the solution in CDI plays a crucial role in determining the performance and efficiency of the CDI process. This is because the pH of the solution affects the surface charge of the electrodes, the speciation of ions in the solution, and the overall electrochemical behaviour of the system. In general, the pH of the solution in CDI should be carefully controlled to optimize the electrostatic interactions between the ions and the electrodes. Deviations from the optimal pH range can reduce ion removal efficiency, decrease capacity, and increase energy consumption. Additionally, extreme pH conditions can cause undesirable side effects, such as electrode fouling, degradation of the electrodes, and changes in the chemical composition of the treated water. Therefore, precise pH control is a critical factor in CDI processes to achieve optimal performance and ensure the long-term stability and sustainability of the system.

Several research works have reported the influence of solution pH on F^- removal in CDI systems. For instance, Bharath *et al.* (2021) investigated the effect of pH on the electrode performance for the removal of F^- at the pH range from 2 to 10. The results evidenced the increase in electrosorption capacity as the pH of the solution increased from 2 to 6.5 and decreased as the pH solution increased from 8 to 10 (Fig. 4a). The highest electrosorption capacity obtained was 74 mg/g at a pH of 6.5, then it was reduced to 39 mg/g when the pH increased to 10. Bharath *et al.* (2021) emphasized that the negative trend observed above the pH of 6.5 was attributed to the increase of hydroxyl ions in the alkaline solution, which competed with F^- on the adsorption sites to the electrode surface.

Kushwaha *et al.* (2020) also studied the effect of pH on F^- removal through the CDI process. The pH range varied from 2.5 to 10 while other CDI operating parameters were kept constant. At a pH of 8, the maximum removal efficiency of 98.49% was achieved. Wu *et al.* (2016) investigated the effect of solution pH on the removal of F^- for the pH range of 3.2 to 11.32, initial concentration of 10 ppm, and applied potential of 1.5 V. Their findings revealed an increase in electrosorption capacity with increasing pH values, with a peak at pH 9.05, however above the 9.05 pH the electrosorption capacity decreased (Fig. 4b). Kushwaha *et al.* (2020) highlighted that the lower electrosorption capacity observed in acidic medium and alkaline solution was due to the presence of different types of fluoride ions (F^- and HF^{2-}) and hydroxyl ions, respectively.

The effect of solution pH on the removal capacity of electrode materials for defluoridation was also studied by Wu *et al.* (2021), with different pH values ranging from 3 to 9 (Fig. 4c). The electrosorption capacity was observed to increase with pH up to 7. However, at pH 9, the removal capacity sharply decreases, which was explained by the deprotonation of the nitrogen atoms in PANI in an alkaline medium and hydroxide ions that normally compete with the F^- to the electrode active sites. All these studies conclude that defluoridation with CDI works well with solutions with neutral pH. Therefore, the electrode materials that give optimal results at neutral pH could be considered suitable defluoridation electrode materials for natural water systems.

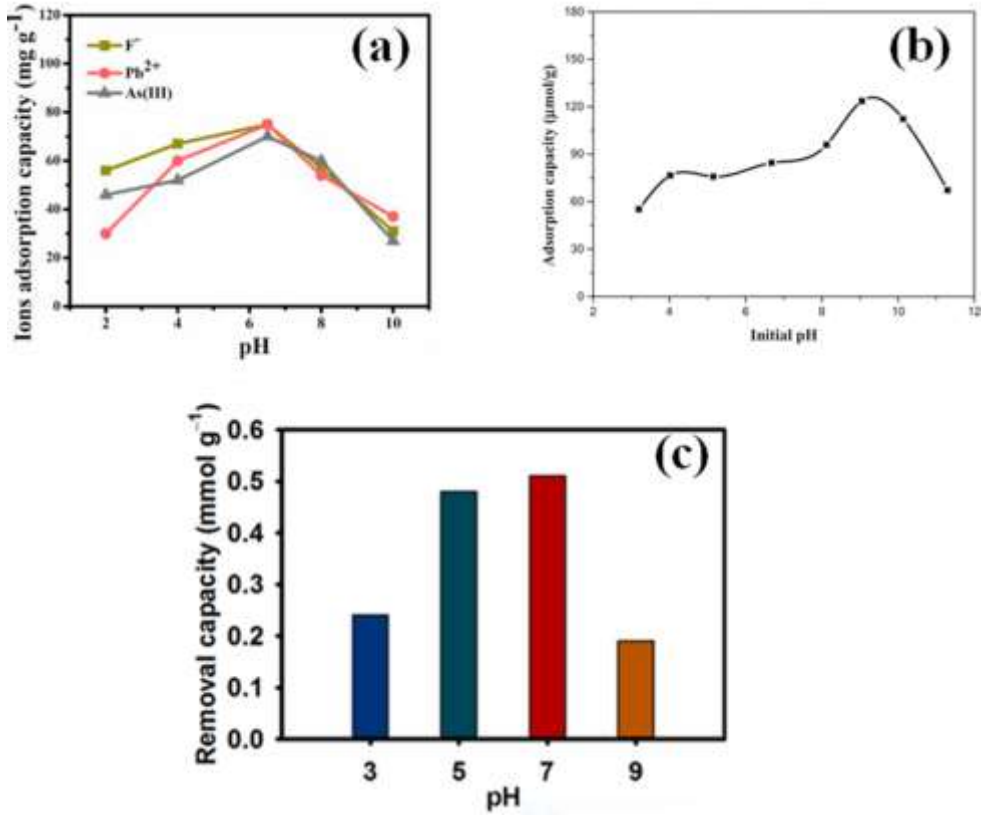

Figure 4: **(a) Operational pH versus ions adsorption capacity of Ni/MAX//pRGO asymmetric electrodes at 1.4 V (Bharath *et al.*, 2021), (b) Fluoride electrosorption by Ti-AC at various initial pH values with a starting concentration of 10 ppm (Wu *et al.*, 2016), (c) pH change with the electrochemical removal of F^- of the PANI-CNT electrode at different pH values (3, 5, 7 and 9) (Wu *et al.*, 2021)**

2.3.3 Initial fluoride concentration

The initial feedwater concentration is also a vital factor that significantly impacts the performance of CDI systems. The concentration of ions in the feedwater directly affects the efficiency and effectiveness of CDI. Higher initial concentrations of ions in the feedwater can lead to a faster saturation of the electrodes and reduced adsorption capacity, resulting in a shorter cycle time and lower removal efficiency. On the other hand, lower initial concentrations of ions may result in longer cycle times and potentially higher energy consumption to achieve the desired level of deionization. Therefore, optimizing the initial concentration of the feedwater is crucial in determining the performance of CDI systems, including their adsorption capacity, energy consumption, and overall effectiveness in producing deionized water.

This section summarized different studies that evaluated the effect of F^- initial concentration in CDI cell. Gaikwad and Balomajumder (2017b) studied the effect of different concentrations (10, 25, 50, and 100 mg/L) on the electrosorption potential of AC derived from tea waste biomass for defluoridation and Cr^- removal (Fig. 5a). The maximum F^- removal capacity

observed at 100 mg/L was 2.49 mg/L which was 3.4 times higher than the electrosorption capacity achieved for 10 mg/L. The experimental results evidenced the increase in electrosorption capacity as concentration increases which can be ascribed to the decrease in solution resistance as ionic concentration increases in the solution (Rasines *et al.*, 2012).

Similarly, Li *et al.* (2019) studied the influence of initial F^- concentration from 100 to 700 mg/L on the F^- removal capacity using NiCoAlLMO/rGO as CDI electrode materials. Their results presented the increasing trend of electrosorption capacity as NaF increases from 100 to 500 mg/ L (Fig. 5b) by keeping the voltage of 1.4 V. However, at 700 mg/L, the increase of electrosorption capacity ceased because of the saturation limit, which means that fewer active sites are available for adsorption at higher concentrations. Therefore, the feed solution's initial concentration strongly affects the electrosorption capacity, as agreed by other studies (Wang *et al.*, 2013).

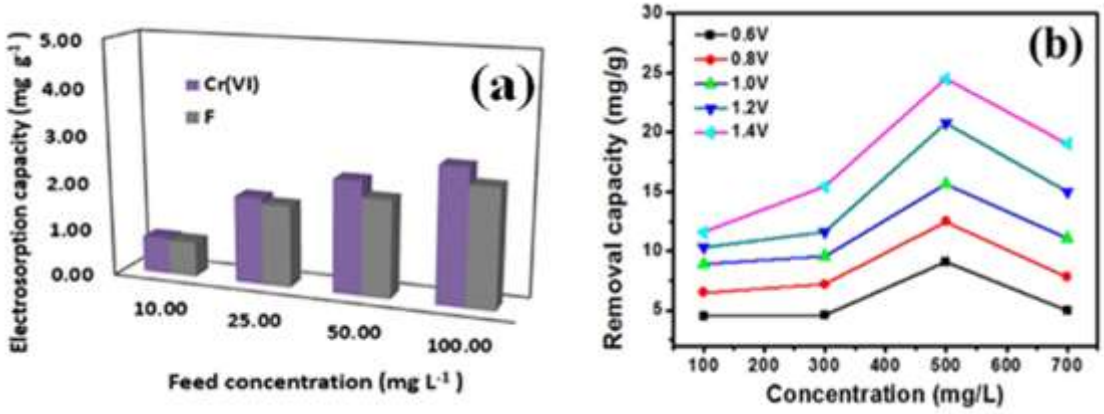

Figure 5: A plot of electrosorption capacity versus feed concentration (Gaikwad & Balomajumder, 2017b), (b) Electrosorption capacities of NiCoAl-LMO/rGO with different concentrations of NaF solution (Li *et al.*, 2019)

2.3.4 The co-existing ions

The presence of co-existing ions in CDI can significantly impact the performance of CDI systems. Natural water consists of different inorganic and organic pollutants, which could influence CDI performance. The presence of co-existing ions in water samples can compete with the target ions for adsorption sites on the electrodes, leading to reduced removal efficiency and increased energy consumption. The co-existing ions can also affect the electrical double-layer formation on the electrodes, altering the charge distribution and thus impacting the overall capacitive behavior of the system. Various studies investigated the effect of co-existing anions towards F^- removal with CDI.

For example, Tang *et al.* (2016) reported that the presence of Cl^- in the feed concentration negatively affected defluoridation. The F^- removal capacity was reported to be 1.71, 0.492, and 0.114 mg/g when feed solution of 2 mM NaF solution was mixed with 0, 5 and 20 mM of Cl^-, respectively; at a flow rate of 56 mL/min and charging voltage of 1.2 V (Fig. 6), explained that the negative trend of F^- removal capacity observed as initial Cl^- concentration increases due to the competition of Cl^- with F^- for electrosorption sites on the electrode surfaces.

Also, Dong *et al.* (2021) investigated the effect of Cl^-, SO_4^{2-}, NO_3^- and HCO_3^- towards defluoridation. The findings revealed that the presence of other ions in the mixed feed solution, in addition to F^-, affected the defluoridation removal rate in the following order: $Cl^- > SO_4^{2-} > NO_3^-$. This order was explained in terms of their differences in ion valence and hydrated radius, which were also explained by other literature (Hou & Huang, 2013; Zhao *et al.,* 2012).

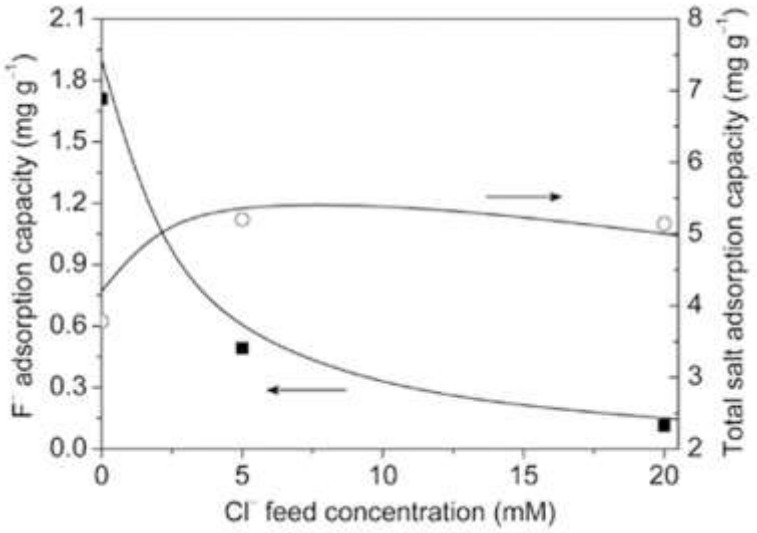

Figure 6: The effect of Cl ion initial concentration on the F adsorption capacity (Tang *et al.,* 2016)

2.3.5 Flow rate

The flow rate also plays an important role in the performance of the CDI system. The flow rate determines the speed at which water passes through the CDI cell and influences key factors such as the ion concentration gradient, ion transport kinetics, and electrochemical reactions. Therefore, finding an optimal flow rate is crucial for maximizing the performance and efficiency of CDI systems. Proper control of the flow rate in CDI can lead to improved pollutant removal efficiency, reduced energy consumption, and enhanced overall performance of the CDI technology.

Various studies studied the influence of pump flow rate in CDI cell for defluoridation. For instance, Li *et al.* (2019) evidenced the dependence of CDI defluoridation performance on the flow rate. The study varied flow rate ranges of 6, 9 and 12 mL/min (Fig. 7a) at 500 mg/L NaF initial concentration through the CDI batch mode approach. Their findings demonstrated good electrosorption capacity at the 9 mL/min flow rate due to the high electrosorption of ions. However, at a flow rate of 12 mL/min, a decrease in electrosorption capacity was seen.

Gaikwad and Balomajumder (2017a) also observed a similar trend by batch mode CDI operation in their study. The effect of different flow rates (4, 8, 12, 16 and 20 mL/min) for removing Cr (VI) and F^- was investigated. The results showed an increase in electrosorption efficiency as the flow rate increased up to 16 mL/min. However, the decrease in electrosorption capacity was observed beyond the flow rate of 16 mL/min. A similar trend was also observed by Agartan *et al.* (2019), Jande and Kim (2014), Tang *et al.* (2015) for the CDI batch mode system. They reported that ion removal performance improves with increasing flow rate and remains constant at a certain flow rate value. Because mixing happens in the recycling tank during batch mode operation, and a high flow rate (short residence time) is beneficial to the CDI system's performance when operating using the batch mode approach**.** This implies that the treated water circulation rate is also low when the flow rate is low, preventing continuous ion removal in the CDI cells. Therefore, more research may be needed to investigate further the above-observed trend for the batch mode operated CDI.

Tang *et al.* (2016) also studied the effect of flow rate by using single-pass CDI operation whereby the lower minimum F^- effluent concentration was observed at a lower flow rate (Fig. 7b) because, in single-pass CDI operation mode, sufficient contact time (greater residence time) is required for better ion electrosorption in the CDI cell (Jande & Kim, 2013; Seo *et al.*, 2010; Tang *et al.*, 2016). This means that for a given volume of the solution moving from the inlet to the outlet, more ions will be adsorbed, resulting in a lower effluent F^- concentration. However, if the flow rate is too low, dead zones in the spacer region are generated, resulting in reduced performance (Seo *et al.*, 2010).

Likewise, in the study conducted by Dong *et al.* (2021), the influence of the pump flow rate on the defluoridation process was also studied. Fluoride removal rates decrease as the flow rate increases from 2.7 to 10 mL/min in single pass operated CDI system. The maximum removal rates of F^- achieved at 2.7 mL/min.

Therefore, the effect of flow rate on CDI performance differs for the two CDI modes of operation; batch mode and single pass. A low flow rate is preferable for the single-pass operating system, and a relatively high flow rate is preferable for the batch mode system.

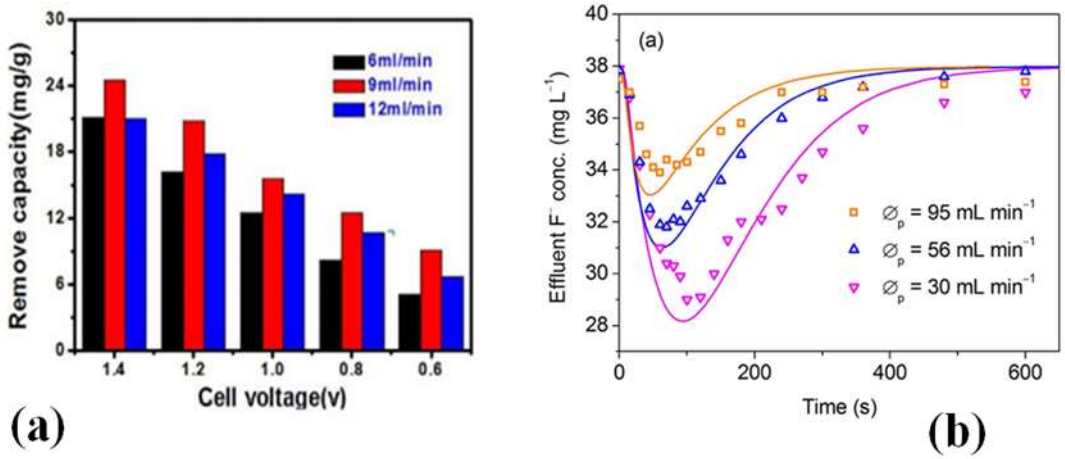

Figure 7: (a) Fluoride removal capacity of NiCoAl-LMO/rGO in NaF solution at different flow rates with an initial concentration of 500 mg/L (Li *et al.*, 2019), (b) Effect of flow rate on effluent fluoride concentration in the presence of NaCl (Tang *et al.*, 2016)

2.3.6 Other parameters

Several other parameters might affect the performance of CDI that also need to be considered during the CDI defluoridation process. These parameters include charging time, the number of electrode pairs and plate spacing. For example, it is reported that the solution concentration decreases with charging time (Jia & Zou, 2012). In addition, the best removal capacity can generally be associated with the more number of electrode pairs and plate spacing of electrodes as the smaller gap between the electrodes attributes to the stronger ion adsorption as the gap affects the electrosorption cell's volume performance (Huang *et al.*, 2013b).

2.4 Optimization of CDI parameters

The one factor at a time (OFAT) approach, commonly used by engineers and scientists, involves changing only one factor at a time while keeping the others constant (Czitrom, 1999). However, this method may not be as efficient when studying the impact of multiple factors on a response. In contrast, statistically designed experiments that vary several factors simultaneously are more effective in determining the combined effect of multiple variables and can generate mathematical models to describe process behavior. Response surface methodology (RSM) is a collection of mathematical and statistical techniques that establish functional relationships between control variables (factors) and the response of interest

(products), making it a more powerful approach for studying the effects of multiple factors on a response (Khuri & Mukhopadhyay, 2010).

Response Surface Methodology (RSM) is an important tool in the design, development, and analysis of new scientific studies and products and the improvement of existing ones. It is widely used in various fields such as industrial, clinical and biological science, food science, social science, and physical and engineering sciences. RSM offers several advantages over the traditional OFAT experiment approach. Firstly, RSM is highly resource-efficient, requiring minimal resources such as experiments, materials, and time to obtain significant information. This is especially valuable in industries where trials can be expensive and time-consuming, allowing for cost-effective and time-efficient experimentation.

Secondly, RSM provides more precise estimations of the effects of each variable. By utilizing all observations to estimate each factor's effects and interactions, RSM reduces variability and increases precision, resulting in more accurate and reliable results. Thirdly, RSM systematically estimates the interactions between variables. This allows for a comprehensive understanding of how variables interact with each other, providing insights into complex relationships and facilitating better decision-making in the design and optimization of experiments or products. Lastly, RSM enables experimental information to be obtained across a larger region of the factor space. This improves the predictability of the response in the factor space by minimizing variability and enhances the efficiency of process optimization. With RSM, the optimal solution can be sought over the entire factor space, leading to more robust and optimized outcomes (Baş & Boyacı, 2007; Czitrom, 1999).

Optimization research utilizing RSM typically involves six stages. First, identifying independent variables that have significant effects on the system is achieved through screening analyses and defining the experimental region based on the study objectives and the researcher's expertise. Second, selecting an appropriate experimental design and conducting the experiments according to the chosen design. Thirdly, statistically analyzing the obtained experimental data by fitting a polynomial function. Fourth, evaluate the fitness of the model obtained from the data analysis. Fifth, confirming the need and potential for further optimization by identifying the direction towards the optimal region. Finally, determining the optimal values for the studied variables is based on the analysis and findings from the previous stages (Bezerra *et al.,* 2008). Finally, the relationship between the response and the variables is given in Equation 1.

$$Y = f(x_1, x_2, \dots\dots, x_n) + \varepsilon \quad (1)$$

Where Y is the response, f is the unknown function of response, x_1, x_2, ..., x_n denote the independent variables, n is the number of the independent variables, while ε is the random error representing other sources of variability not accounted for by f, such measurement error. Generally, the random error is assumed to have a normal distribution with a zero mean and variance (Baş & Boyacı, 2007). In RSM, the model employed is generally a full quadratic Equation or reduced form, as shown in Equation 2 (Ranade & Thiagarajan, 2017).

$$Y = \beta_o + \sum_{i=1}^{n} \beta_i X_i + \sum_{i=1}^{n} \beta_{ii} X^2{}_i + \sum_{i=1}^{n} \sum_{j=i+1}^{n} \beta_{ij} X_i X_j + \varepsilon \quad (2)$$

Where β_o is the intercept, β_i is the linear coefficient of terms, β_{ii} is the square effect terms, β_{ij} is the interactive coefficient of terms, and X_i and X_j are the coded value of independent variables.

Response surface methodology has various designs such as Box-Behnken, Central composite, optimal, definitive screen and miscellaneous designs. Among these, the Box-Behnken design (BBD) is one of RSM most commonly used designs. Generally, the choice of experimental design depends on various factors, including the specific objectives of the experiment, the number of factors being investigated, cost and time considerations, and the availability of facilities. However, the BBD is often preferred due to its balanced and efficient nature, which allows for the estimation of main effects, quadratic effects, and two-factor interactions with relatively fewer experimental runs than other designs (Bezerra *et al.,* 2008). This makes it a popular choice for building predictive models and determining optimal conditions in a wide range of experimental processes, including electrosorption processes (Ghorbani *et al.,* 2008; Pelarti *et al.,* 2022; Su *et al.,* 2013; Vijayalakshmi *et al.,* 2001; Zhao *et al.,* 2014).

Box and Behnken (1960) introduced a technique for selecting points from a three-level factorial arrangement, known as the Box and Behnken design (BBD), which enables efficient estimation of first- and second-order coefficients for mathematical models. The BBD is constructed by considering the midpoints of the edges of the variables region and the center point. In this

design, all variable levels are adjusted at only three levels (-1, 0, +1), with evenly spaced intervals between these levels.

In various studies, Box-Behnken Design (BBD) has been utilized to optimize the process parameters of CDI, such as initial concentration, flow rate, and cell voltage, to maximize the electrosorption of ions for CDI applications. For example, Zhang *et al.* (2014) utilized BBD to investigate the effects of initial arsenic concentration, pH, and background sodium chloride concentration as independent variables on CDI performance, with arsenic removal considered as the response function. The findings demonstrated a good agreement between the predicted values of arsenic removal and the experimental data. For example, the BBD model predicted 84.2% and 100% arsenic removal rates under different experimental conditions, while the actual values reported were 82.6% and 98%, respectively.

In a study conducted by Zhao *et al.* (2014), various operating conditions for CDI were optimized using BBD based on RSM. The main experimental parameters investigated included cell voltage (ranging from 1.2 to 1.6 V), initial NaCl concentration (ranging from 200 to 1000 mg/l), and flow rate (ranging from 10 to 40 ml/min). The authors reported that the experimental data were fitted to a quadratic polynomial model with a high determination coefficient (R^2) of 0.9945 and a p-value less than 0.0001, indicating the model's reliability. Additionally, it has been reported that the analysis of variance for the quadratic model was highly significant, indicating that it can accurately predict the optimal conditions for CDI. The predicted maximum electrosorption capacity was 10.67 mg/g, obtained under the optimal conditions of a cell voltage of 1.57 V, an initial NaCl concentration of 1000 mg/l, and a flow rate of 25 ml/min. These findings were further validated through validation experiments, confirming the accuracy of the predicted optimal conditions.

In a study conducted by Zhao *et al.* (2014), BBD was utilized to optimize the operating conditions of CDI for maximizing nickel removal efficiency. The independent variables studied were initial nickel concentrations of 10, 25, and 40 mg/l, input water pH of 5, 6, and 7, and sodium chloride content of 0, 0.1, and 0.2 M. The authors reported that the optimal CDI operating conditions for achieving a nickel removal efficiency of more than 98.89% were 10 mg/l nickel initial concentration, 0.13 M electrolyte concentration (NaCl) in the inflow electrode, and a pH of 6.2.

Bao *et al.* (2021) employed BBD based on RSM to investigate the impact and interaction of three factors: weight ratio of resin to AC, the content of polyvinylidene fluoride (PVDF), and

particle size of resin in resin/carbon composite electrode on the selective separation of vanadium during the CDI process. The findings revealed that the optimal preparation conditions for the composite were as follows: weight ratio of resin to AC of 3.49, the content of PVDF of 12.15%, and resin particle size ranging from 0.075 mm to 0.06 mm. Under these conditions, the maximum vanadium electrosorption capacity was determined to be 106.89 ± 3.03 mg/g.

In a study conducted by Zhao *et al.* (2013), they utilized BBD based on RSM to investigate the impact of electrodes' potentials, the distance between electrodes' plates, and flow rates on the desalination rate of water. The findings revealed that the maximum desalination rate achieved was 59.05% under optimal conditions, including an applied potential of 1.6 V, a distance of 2 mm between the electrodes' plates, and a 21.32 ml/min flow rate. Furthermore, the analysis of variance (ANOVA) performed on the quadratic response surface model demonstrated that the regression model was statistically significant and exhibited a good fit for the experimental data. The model's reliability and accuracy were also within practical limits, aligning well with the experimental results. These findings highlight the robustness and validity of the RSM approach employed in the study, suggesting its suitability for predicting and optimizing the desalination rate of water using the chosen parameters.

The existing research on CDI has primarily focused on optimizing the CDI operational conditions. At the same time, limited information is available on optimizing the preparation conditions of composite electrodes for the removal of various pollutants in CDI using response RSM. Hence, this study utilized BBD based on RSM to optimize the ratios of trimetallic (Al, Fe, and Ti) oxides for the modification of AC to maximize the removal efficiency of F^- and investigate the interactions of the independent variables for F^- removal for the first time.

2.5 Ability of CDI for the removal of organic pollutants from water

Principally, CDI technology is the superior water treatment technology for removing ionic species from aqueous solutions based on its ability to temporarily store ions on the formed Electric double layer (EDL). However, recent studies investigated the usefulness of CDI technology for removing organic (uncharged) contaminants such as humic acid, dyes and pesticides. The findings are promising, as summarised in Table 4. For example, Senoussi and Bouhidel (2018b) used granular AC as a CDI electrode material to remove textile cationic dyes from industrial wastewater in their investigation. At an applied voltage of 2 V and a flow rate of 10 mL/min, the maximum removal efficiency and electrosorption capacity of 98% and 1.75

mg/g was achieved, respectively. Also, Liu *et al.* (2016) studied the removal of inorganic ions (bromide) over natural organic matter (Humic acid) by the CDI process whereby AC was used as electrode materials. The findings showed that CDI could simultaneously remove inorganic and organic contaminants from water. Additionally, the study findings found that the removal efficiency of organic matter was influenced by the presence of inorganic ions in the mixed solution. Organic matter in water competed with the inorganic ions for adsorption sites on the surface of the CDI electrode and reduced the desalination efficiency. Furthermore, Lester (2019) examined the impact of trace organic compounds (TOrCs) (bisphenol A, carbamazepine, estrone and pentoxifylline) in the water on the removal efficiency of salt during CDI. Their study also investigated the potential of the CDI method for the removal of TOrCs. The authors reported a removal efficiency of over 90% for bisphenol A, placing it at the forefront in terms of trace organic contaminants removal, followed by estrone, carbamazepine, and pentoxifylline. Additionally, their results revealed that the salt removal efficiency by CDI is affected by the presence of different TOrCs. The TOrCs reduced salt removal by approximately 20% compared to experiments with salt alone. Based on that, we anticipate that CDI is a potential water treatment technology for the removal of both inorganic and organic pollutants. To the authors' knowledge, no study investigated the application of CDI technology for removing PQ pesticides from water. Therefore, this study aims to evaluate the usefulness of the CDI technology for the removal of PQ pesticides from water.

Table 4: Electrode materials for the removal of organic contaminants in aqueous solution and its electrosorption capacity

Electrode materials	Organic pollutant	volume of the solution (mL)	Initial concentration (mg/L)	EC (mg/g)	RE (%)	Applied voltage (V)	Flow rate (mL/min)	References
Granular activated carbon (AC)	Astrazon Red FBL (AR) cationic dye	20	25	1.75	98	2	20	Senoussi and Bouhidel (2018a)
Activated carbon cloth (AC)	Humic acid (HA)	75	10	*-	23	0.6	0.8	Liu *et al.* (2016)
activated carbon (AC)	TOrCs (Bisphenol A)	100	60	300	90	1.4	100	Lester Yaal (2019)

*- data not found, RE removal efficiency, EC is the electrosorption capacity

2.6 Availability of the installed commercial/industrial CDI water plants

Capacitive deionization technology requires lower energy consumption than the existing technologies, potentially 30% to 60% less (Welgemoed, 2005). This opens the possibility of utilizing green energy sources such as solar or wind power to power remote CDI units. This makes it a sustainable option for water treatment in communities without access to electrical power and where the available water quality is non-potable. This is especially significant as many existing large-scale water treatment technologies rely on fossil fuels for energy, effectively trading potable water for increased CO_2 emissions, contributing to global warming and the depletion of freshwater resources.

Several companies around the world, such as Voltea in Sassenheim, Netherlands, Idropan in Australia, Reticle in California, United States, Idropan dell'Orto Depuratori S.r.l in Milan, Italy, AquaEWP, Pionetics Linx, and O_2 & B in Korea, have been involved in manufacturing and supplying commercial CDI systems for water purification (Atkinson, 2021; Jande *et al.*, 2014; Nkuna, 2017; Wimalasiri *et al.*, 2018). These companies have installed CDI systems in various locations globally, including Tanzania, where O_2 & B Company from Korea has implemented CDI water treatment systems for water hardness removal in Mbande, Dodoma, and defluoridation in Lemanda and Ngongongare, Arusha. However, limited information is available about the capacity and performance of these CDI systems in Tanzania. As CDI technology is still relatively new compared to membrane processes, long-term operational data for large-scale systems is lacking. This makes it challenging to predict electrode lifetime and potential fouling due to biological or chemical factors. Additionally, there is limited data on the contribution of purified water to the overall water supply in these areas. As a result, researchers must collaborate closely with these companies to monitor and evaluate the long-term performance of installed CDI systems and gather operational data to understand better the technology's effectiveness and sustainability in real-world applications.

CHAPTER THREE

MATERIALS AND METHODS

3.1 Materials

All chemicals were of analytical grade and used as received. Aluminium nitrate nonahydrate, iron nitrate nonahydrate, titanium oxysulfate, and polytetrafluoroethylene (PTFE, 60 wt% dispersion in water), the herbicide Paraquat (PQ, molecular formula: $[(C_6H_7N)_2]Cl_2$, 99.3%, Mw = 257.16 g mol^{-1}), were purchased from Sigma-Aldrich. Cyclohexanediaminetetraacetic acid and 99.9% ethanol were purchased from Chem Lab, Belgium. Carbon black (TIMICA SUPPER C65) and polyvinylidene fluoride (PVDF) were purchased from MTI Corporation, USA. The AC was purchased from Finar Chemicals, India. Sodium hydroxide (NaOH), hydrochloric acid, glacial acetic acid, and sodium fluoride (NaF) were purchased from Merck Company, India.

The activities and procedures used in synthesizing the metal oxides modified AC composites, development of electrodes, electrochemical characterization and evaluation of their CDI performance are summarized in the flow chart Fig. 8.

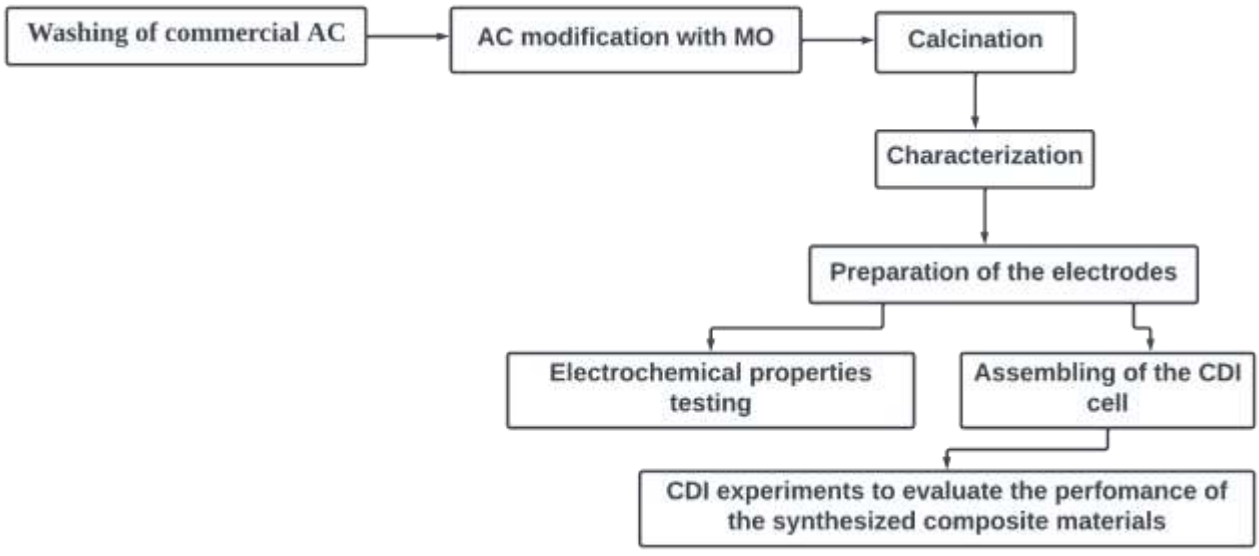

Figure 8: Flow chart of the activities involved in this study

3.2 Preparation of AC–$Al_xFe_yTi_z$ composites and statistical analysis

To evaluate the optimum conditions for the preparation of trimetallic oxide-modified AC composites and investigate the effects of the trimetallic oxide mass ratios on AC, response surface methodology (RSM) based on Box- Behnken design (BBD) was adopted for achieving

optimization. The RSM is a statistical and mathematical tool for designing experiments, improving and optimizing the experimental conditions to minimize trial and error, and evaluating the significance of process variables even under complex interactions (Aydar, 2018; Kumari & Gupta, 2019; Mourabet *et al.*, 2017). This study used RSM to investigate the interaction effects of Al, Fe, and Ti on defluoridation by the trimetallic oxide-modified AC composites as CDI electrode materials.

Design-Expert Version 12.0.3 software (Stat-Ease, Inc., Minneapolis, USA) was employed to design the experiments and optimize the factors at three levels, considering the RE% as a response. The three levels were coded as −1, 0, and +1 for low, central, and high values, respectively. The Al, Fe, and Ti salts amounts were calculated according to the independent variable ratios presented in Table 5. A total of fifteen (15) runs were designed to investigate the effects of the independent variables on the removal efficiency of F^- and CDI experiments were conducted using the synthesized materials, as summarized in Table 6.

The process of RSM involves a progression of five key stages: first, the development of statistically designed experiments; next, the creation of an empirical model; followed by a statistical assessment of the model; then, the application of the desirability function for numerical optimization; and ultimately, the verification and validation of the model.The experimental run was randomized to diminish the error and effect of uncontrolled factors (Behera *et al.*, 2018). Finally, the observed responses were used to generate an empirical model, which conforms to the experimental variables using a quadratic Equation 2.

The regression coefficients of second-order polynomial models were determined using Design-Expert software based on experimental results from fifteen (15) runs. The accuracy of the fitted model was assessed using the coefficient of R-squared. In contrast, the significance of model terms was determined using the probability value (P-value) at a 95% confidence level. Contour and 3D surface plots were developed to visualize the interaction of two independent variables while keeping the third variable at the central value. The surface plots provided valuable information about the system's behavior as processing parameters varied within the design space. The composite preparation conditions were optimized using a desirability function in Design-Expert software to maximize the F^- removal efficiency. Using the generated models, the best operating conditions that met the defined goals were identified within the design space. From the set of suggested solutions, one was chosen for the purpose of model validation. To evaluate the precision of the model, three repeated experimental runs were performed, and the results were juxtaposed with the projected values.

Table 5: Level of various independent variables at coded values of response surface methodology experimental design

Symbol	Independent variables	Coded levels		
		-1	0	+1
Al	Aluminium oxide ratio	1	2.5	4
Fe	Iron oxide ratio	1	2.5	4
Ti	Titanium oxide ratio	1	2.5	4

Table 6: Experimental design conditions of AC modified with trimetallic oxide for each experimental run

Run	Ratio of Al oxide (g)	Ratio of Fe oxide (g)	Ratio of Ti oxide (g)
1	1	1	2.5
2	4	1	2.5
3	1	4	2.5
4	4	4	2.5
5	1	2.5	1
6	4	2.5	1
7	1	2.5	4
8	4	2.5	4
9	2.5	1	1
10	2.5	4	1
11	2.5	1	4
12	2.5	4	4
13	2.5	2.5	2.5
14	2.5	2.5	2.5
15	2.5	2.5	2.5

3.3 Modification of AC with metal oxides

Activated carbon was composited with metal oxides (Al_2O_3, Fe_2O_3 and TiO_2) using a single step co-precipitation method at room temperature ranging from 23°C to 27°C, as demonstrated in Figure 9. The commercial AC was first rinsed with deionized water to remove impurities. Then, it was washed with 0.01 mol/L of HCl solution to remove salts precipitated in its pores and repeatedly washed with deionized water to remove the acid, centrifuged, oven-dried at 100°C overnight, and stored in a tight container for further use.

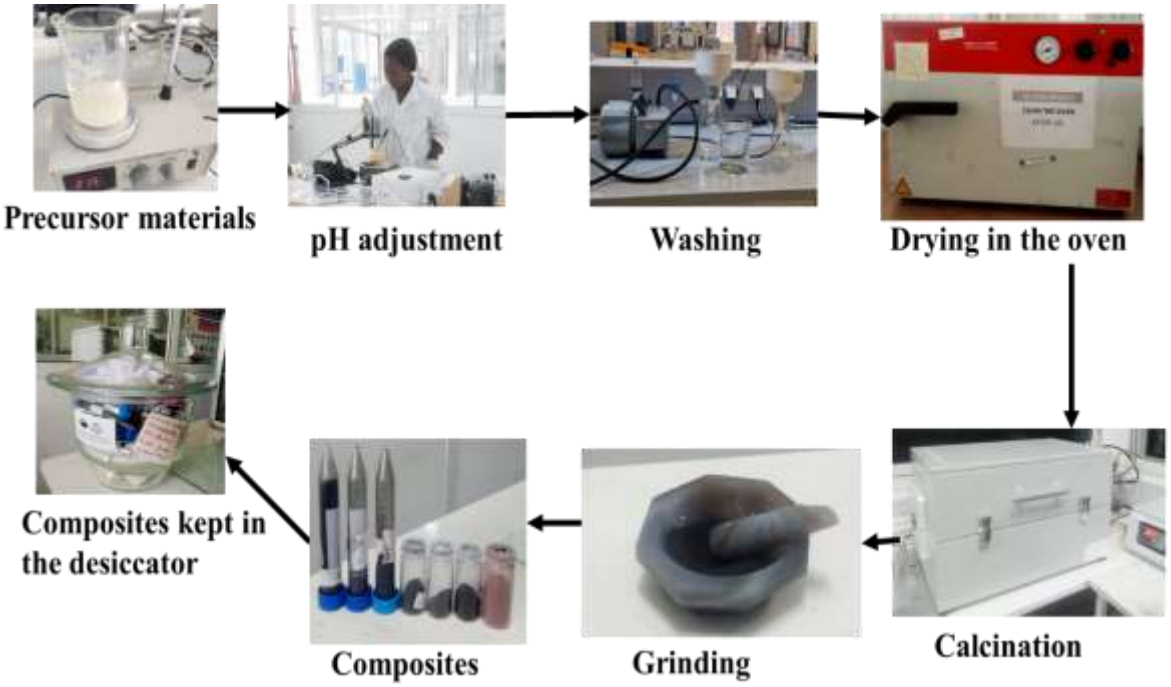

Figure 9: Schematic diagram for the synthesis of the AC composited with metal oxides

3.3.1 Synthesis of the composites of AC with monometallic oxides

The activated carbon composited with Al_2O_3 at different mass ratios was prepared by co-precipitation. Precursor materials, AC and $Al(NO_3)_3 \cdot 9H_2O$ in the various mass ratios of 1:0.25, 1:0.5, 1:1, 1:2, 1:3, 1:4 (AC: Al_2O_3) were dissolved in 1000 mL of distilled water in a beaker and homogeneously mixed by magnetic stirring. The 6 M of NaOH was added drop wise in the beaker containing the above precursor until the pH reached 8.5-8.6. Beaker was allowed to stand for 2 hrs after the complete addition of sodium hydroxide. Then the suspension was centrifuged, the supernatant was decanted, and the precipitates were re-suspended with double-distilled water. This washing process was repeated several times to remove impurities. The precipitates were kept for drying overnight at 100°C and ground into powder form with the help of mortar and pestle. The final compound was calcined in the tube furnace at 350°C for 2 hrs at a heating ramp rate of 5°C/min. After cooling, the samples were kept in the tight container standby for further use and named AC/xAl_2O_3, where x is the mass ratio of Al_2O_3. AC-Fe_2O_3 and AC-TiO_2 composites were synthesized using a similar process, wherein AC was mixed with iron nitrate nonahydrate and titanium oxysulfate, respectively. The ratio of AC and metal oxides in the composites was maintained at 1:1.

3.3.2 Synthesis of the composites of AC with bimetallic oxides

Similar preparation procedures presented in Section 3.3.1 were adopted to synthesize AC-Al_2O_3/Fe_2O_3, AC- Al_2O_3/TiO_2 and AC- Fe_2O_3/TiO_2 bimetallic oxides composites. In brief, the two precursor salts were mixed with AC in 1000 mL of deionized (DI). The ratio of AC and the two metal oxides were kept to 1:1. The precursor solution was stirred for 30 min, following drop wise addition of 6 M NaOH under continuous stirring until the pH reached 8.5-8.6. The resulting suspension was left to stand for 2 h at room temperature (23 to 27°C). After aging, the product was collected by centrifugation, washed several times with distilled water, and dried in a vacuum oven at 100°C for 12 h. The dried product was ground manually to a fine powder calcined in the tube furnace at 350°C for 2 h at a heating ramp rate of 5°C/min. After cooling, the samples were stored in a tight container at room temperature for further use.

3.3.3 Preparation of AC–$Al_xFe_yTi_z$ trimetallic oxides composites

The composites of AC and Al, Fe, and Ti oxides at different ratios were synthesized by a simple co-precipitation method at 23–2°C. Specifically, a precursor solution was prepared by dissolving AC in suitable amounts of aluminium nitrate, iron nitrate, and titanium sulfate salts in 500 mL of DI as per the mass ratio provided in Table 6. The precursor solution was stirred for 30 min, following drop wise addition of 6 M NaOH under continuous stirring until the pH reached 8.5; the resulting suspension was left to stand for 2 h at room temperature (23 to 27°C). After aging, the product was collected by centrifugation, washed several times with distilled water, and dried in a vacuum oven at 100°C for 12 h. The dried product was ground manually to a fine powder to produce an AC–$Al_xFe_yTi_z$ material and stored at room temperature, where x, y, and z are the Al, Fe, and Ti oxides mass ratios, respectively.

3.4 Characterization of the composites of AC with metal oxides

Scanning electron microscopy (SEM) (an FEI XL40 ESEM equipped with two EDAX sapphire Si (Li) energy-dispersive X-ray spectroscopy (EDS) detectors with up-to-date software) was used to analyze the morphologies of the materials. Transmission electron microscopy (TEM) studies were conducted with a JEM-2100 MULTIPURPOSE 200 kV analytical electron microscope equipped with an Oxford SDD detector for a TEM: XMaxN 80T EDS model to examine the microstructures of the samples. Specific surface area and pore volume were determined with a nitrogen absorption apparatus (Micromeritics ASAP 2460) by the Brunauer-Emmett-Teller (BET) method at 77 K from N_2 absorption-adsorption isotherms in the relative pressure range (P/Po) of 0.01–1.0, whereas the pore size distribution was calculated by using

the Barrett-Joyner-Halenda (BJH) method. A Fourier transform infrared (FTIR) spectrometer equipped with Spectrum 10^{tm} software for data generation and analysis was used to characterize the functional groups on the material surfaces. X-ray powder diffraction (XRD) (Bruker D8 Advance powder diffractometer with a Cu tube X-ray source with $\lambda = 1.54056$ nm operating at 40 kV, 40 mA, and LynxEye XE energy-dispersive strip detector) was used to characterize crystal structure changes of the prepared samples. The wettability of the electrode samples was measured by a contact angle analyzer (contact angle goniometer; L2004A-0389). Zeta potential measurements were carried out using a Malvern Zeta sizer Nano ZS instrument (Product No. DTS1070, Malvern Instruments). The powder particles were dispersed in deionized water and sonicated for 20 min before analysis. Then, NaCl was added to each sample so that a NaCl concentration of 1 mM was reached.

3.5 Electrochemical measurements

The electrochemical tests adopted a three-electrode system: saturated Ag/AgCl (KCl) as the reference electrode, a platinum wire (Pt) as the counter electrode, and the prepared material as the working electrode. Powder samples (80 wt%), conductive carbon black (10 wt%) and Poly(tetrafluoroethylene) (PTFE, 10 wt%) were uniformly dispersed in a small amount of ethanol according to their mass ratio. The dispersion was stirred for 1 h at 400 rpm, and then the sample was gently coated into a 1 cm × 1 cm carbon foam to form the working electrode. Finally, the prepared electrode was dried overnight in an 80°C oven and weighed for standby use. Cyclic voltammetry was conducted using a potentiostat/galvanostat (PGSTAT204, AUT50663 Metrohm) electrochemical station in 0.1 M NaF electrolyte at room temperature. The voltage windows were −1 to 0 V for AC, and 0 to +1 V for the composite versus reference electrode, and the potential scan rates were set as 5, 10, 20, 50, 100, and 200 mV s^{-1}. The CV measurements were also compared in 6 M KOH electrolyte at room temperature. The mass of the active electrode material was 5 mg, comprising 80 wt% active material, 10 wt% conductive carbon black, and 10 wt% PVDF binder. Each sample was gently pressed into a 1 cm × 1 cm nickel foam to form the working electrode. The voltage windows were −1 to 0 V for AC, and 0 to +5 V for the composite versus reference electrode, and the potential scan rates were set as 5, 10, 20, 50, 100, and 200 mV $s^{-1.}$ Electrochemical impedance spectroscopy (EIS) analysis was conducted to investigate the resistivity of the electrodes and the conductivity at the electrode/electrolyte interface. For this purpose, an ac voltage with amplitude of 5 mV in a frequency range of 0.01 Hz−100 kHz was applied using the FRA32 module attached to

PGSTAT204 in an open circuit. The specific capacitance C (F/g) is evaluated using Equation (3) (Yasin *et al.*, 2021).

$$C = \frac{\int Idv}{2\Delta VmR} \tag{3}$$

where I (A) is the current read by the equipment, ∫Idv is the area of the closed CV curve, ΔV is the voltage difference for the potential window, R is the potential scan rate (V/s), and m is the mass of the active material deposited on the electrode (g).

Moreover, the potential of zero charge (E_{PZC}) data is determined from a series of EIS measurements at different potentials in 5 mM NaCl solution at a frequency of 0.01 Hz using Equation (4). The value of E_{PZC} was obtained from the minimum value of the capacitance plot (as a function of the potential).

$$C = \left|\frac{1}{2\pi f Z''}\right| \tag{4}$$

where f (Hz) is the scanning frequency, and Z'' (Ω) is the imaginary part of the impedance.

3.6 Fabrication of CDI electrodes

The active material (AC or its composites), conductive carbon black, and PTFE binder were mixed in ethanol in a mass ratio of 80:10:10 until a dough-like paste was formed. Next, the paste was pressed to the required thickness, cut into pieces of 4 cm × 4 cm, and dried at 60 to 70°C overnight in a vacuum oven before testing to remove the remaining solvents. Finally, electrodes with total masses of approximately 0.5–0.6 g were assembled in a CDI cell to study their effectiveness in removing F^- and PQ pesticides. The fabrication process of electrodes was presented in Fig. 10.

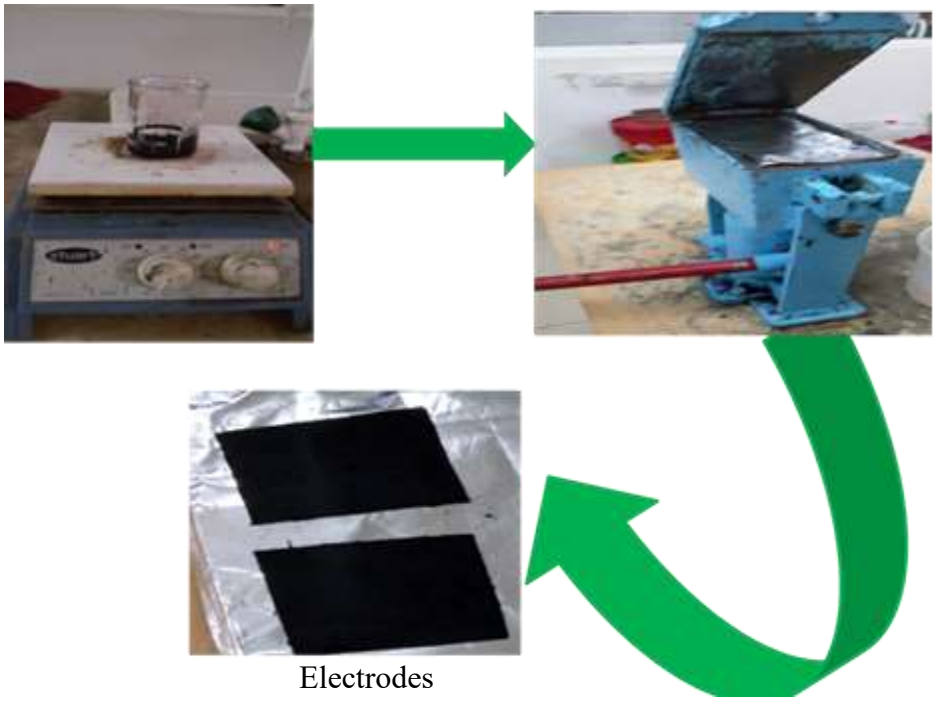

Figure 10: Schematic diagram of the fabrication of the CDI electrodes

3.7 Defluoridation and PQ removal from water with capacitive deionization

To evaluate the performance of the synthesized composites in removing F^- and PQ herbicides from water, electrosorption experiments were conducted in a laboratory-scale CDI reactor, shown in Fig. 12. The device is a flow-by CDI type that includes a computer, an electrochemical potentiostat workstation (with IviumSoft electrochemistry software), a pH meter probe, a CDI cell with a pair of electrodes, a solution tank, and a peristaltic pump. Pairs of electrodes were placed on a stainless-steel sheet current collector and separated by a plastic mesh to ensure electrolyte flow and prevent short circuits. Rubber gaskets were added to seal the cell, and all components were covered with plexiglass and tightened with screws.

A standard stock F^- solution of 1000 mg/L was prepared by dissolving 2.21 g NaF in 1000 mL DI water. The working solution for the experiments was prepared by diluting an appropriate volume of the stock solution. To investigate the effectiveness of the trimetallic oxide-loaded AC for F^- removal from water containing multiple ions, natural water was collected from Mandokey River at Ngarenanyuki, Arusha, Tanzania. In defluoridation experiments, 30 mL feed solution with 5 mg/L F^- concentration was circulated in the CDI cell at a flow rate of 15 mL/min using the peristaltic pump (MasterflexLive™, L/S® series). Moreover, a potential of 1.2 V was applied to the electrode terminals of the CDI cell using a potentiostat/galvanostat (Vertex.1A.EIS 1A/10 V/1MHz EIS, Ivium Technologies, the Netherlands). After charging for 2 h, the solution in the feed tank was removed, and the equilibrium F^- concentration in the solution was measured using an ion-selective electrode coupled with a Mettler Toledo Seven

Compact pH/Ion S220 meter. The total ionic strength buffer (TISAB II) was prepared by mixing glacial acetic acid (57.0 ml), NaCl (58.0 g) and cyclohexanediaminetetraacetic acid (CDTA (4 g)) in 500 ml of distilled water to prepare TISAB II. Solution pH was adjusted to 5.3–5.5 by adding about 150 ml of 6 M NaOH, and distilled water was then added to make it 1000 mL. The saturated electrodes were regenerated by applying a negative voltage of −1.6 V for 30 min to release the adsorbed ions into the solution.

A 1000 mg/L PQ stock solution was prepared and stored in a refrigerator at 4 to 5°C. This solution was used for one month without any indication of PQ degradation. In the CDI operation, a peristaltic pump was used to supply 40 mL of PQ solution with varying concentrations (5 to 20 mg/L) to the CDI cell. The feed solution was circulated and returned to the feed tank at different flow rates (5,10, 15, and 20 mL/min). Electric potentials of 0.6, 0.9, and 1.2 V were applied to the CDI cell at electrode terminals using a potentiostat/galvanostat to evaluate PQ herbicide electrosorption. A control experiment was conducted for comparison without application of voltage to the CDI cell. The effect of charging time on PQ removal was also investigated by performing electrosorption of PQ by varying time from 1, 2, 3 to 4 h. The PQ concentration in the solution was measured using a UV-VIS spectrophotometer (UV 6715 spectrophotometer, 1322 JENWA, UK) with UV absorbance detection based on Lambert–Beer's law at 259 nm (Fig. 11). To regenerate the saturated electrodes, a negative voltage of −1.2 V was applied for 60 min to release the adsorbed ions. The effectiveness of the prepared composites in PQ removal was studied by using natural tap water obtained from the Nelson Mandela African Institution of Science and Technology (NM-AIST) laboratory in Arusha, Tanzania. Then PQ was added to the tap water to create a natural water sample with a 20 mg/L PQ concentration. The removal efficiency (RE, %) and electrosorption capacity (r, mg/g) were determined using Equations (5) and (6), respectively (Dong *et al.,* 2021).

$$RE = \frac{C_0 - C_e}{C_0} \times 100\% \quad (5)$$

$$EC = \frac{(C_o - C_e)}{m} V \quad (6)$$

where C_o and C_e represent the initial and equilibrium F^- /PQ concentrations (mg/L), respectively.

The energy consumption (E) is calculated using Equation (7) (Vafakhah *et al.*, 2020).

$$E = \frac{V \int_0^t I dt}{Qt} \quad (7)$$

where *E* is the energy consumption in kWh/m^3, V is the applied voltage, I is the current, Q is the assigned flow rate, and t is the charging time.

The ion desorption amount at time t is evaluated using Equation (6) (Wang *et al.*, 2018).

$$Q_{des} = C_t \times V \quad (8)$$

where Q_{Des} is the F^-/PQ desorption amount at time t and C_t and V represent the ion concentration in the solution and the solution volume, respectively.

The desorption ratio was determined from Equation (7) (Wang *et al.*, 2018) below:

$$R = \frac{Q_{Des}}{Q_{Abs}} \times 100\% \quad (9)$$

where R is the desorption ratio, Q_{Abs} and Q_{Des} represent the adsorption and desorption amounts of F^-/PQ, respectively.

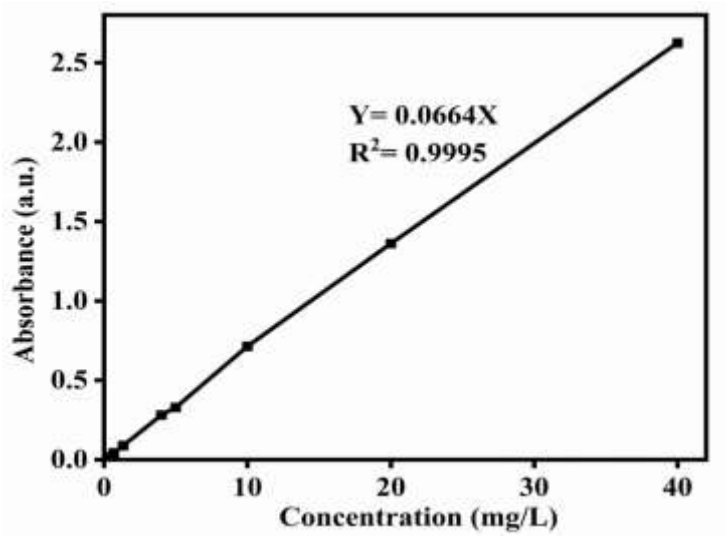

Figure 11: Calibration curve of absorbance as a function of PQ concentration at 259 nm

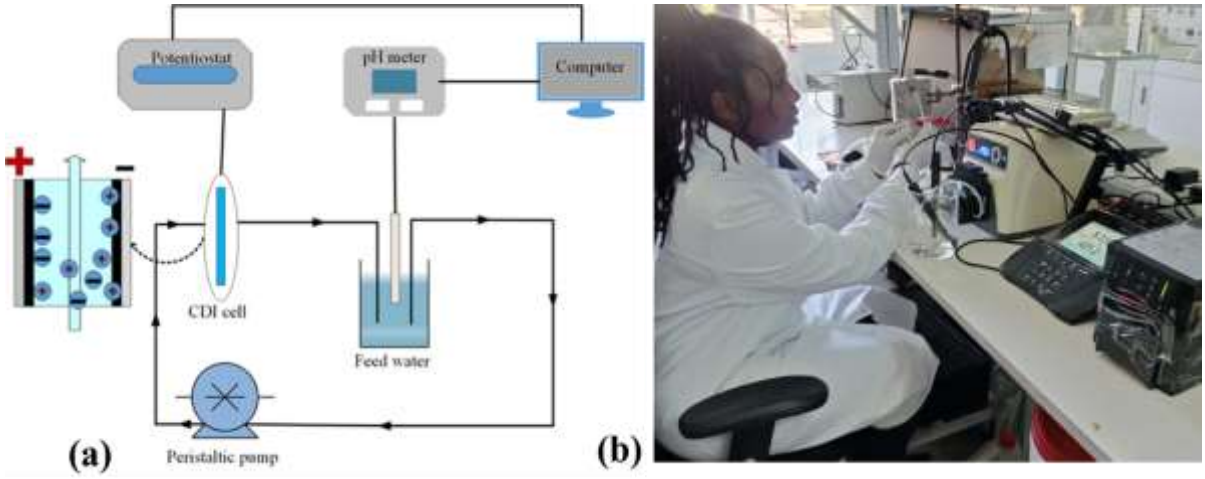

Figure 12: **(a) Schematic diagram of the CDI experiment set up (b) Image of the laboratory CDI experimental setup**

CHAPTER FOUR

RESULTS AND DISCUSSION

4.1 Structure and surface morphology of AC modified with metal oxides composites

The SEM images of the surface morphologies depicting the structural characteristics of AC and its composites are presented in Fig. 12-15. The surface SEM images in Fig. 12 illustrate the differences in the morphology of AC and AC modified with varying mass ratios of Al_2O_3 (b-g). The pristine AC surface (Fig. 13a) displayed a honeycomb-like structure of pores. However, after the modification with Al_2O_3, the pores became coated with Al_2O_3 nanoparticles distributed across the surface. As the mass ratio of Al_2O_3 increased beyond the optimal ratio of 1:1, the pores in the composite materials became blocked by the excess Al_2O_3 nanoparticles, as demonstrated in Fig. 13 (e-g). Figure 14(a) and (b) display the EDS analysis of AC before and after modification with Al_2O_3 (1:1), respectively. Figure 13(a) reveals that the primary elements in the pristine AC sample were C and O. However, after compositing with Al_2O_3, EDS mapping (Fig. 13b) shows three main elements (C, O, and Al), while Fig. 13(c) demonstrates the uniform dispersion of Al particles on the AC surface.

The SEM images of AC composited with trimetallic oxides (AC–$Al_4Fe_{2.5}Ti_4$) were presented in Fig. 15(a, b) at two different magnifications, which showed a rough surface and uniform distribution of the particles of the composite. Figure 14 (c) shows a TEM image of the AC–$Al_4Fe_{2.5}Ti_4$ composite material. It confirms that the Al, Fe and Ti oxides are successfully loaded on the AC surface, as evidenced by the EDS results in Fig. 14(d) and its corresponding elemental mapping images in Fig. 15.

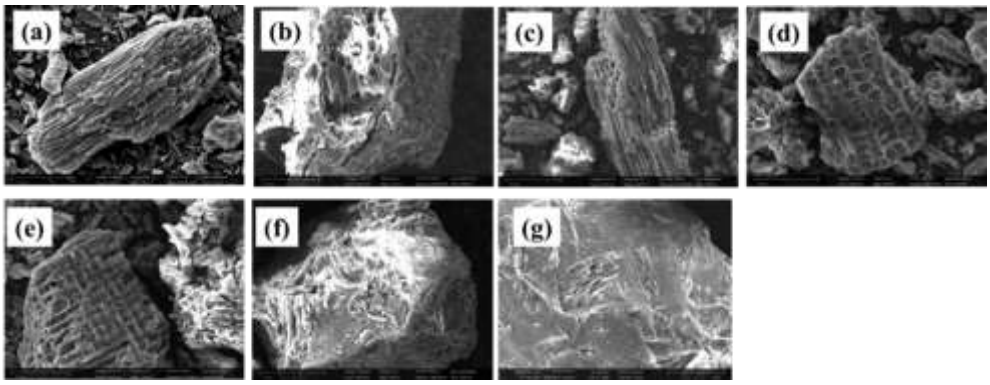

Figure 13: Scanning electron microscopy image of (a) pristine AC (b) AC/Al_2O_3-1:0.25 (c) AC/Al_2O_3-1:0.5 (d) AC/Al_2O_3-1:1 (e) AC/Al_2O_3-1:2 (f) AC/Al_2O_3-1:3 (g) AC/Al_2O_3-1:4

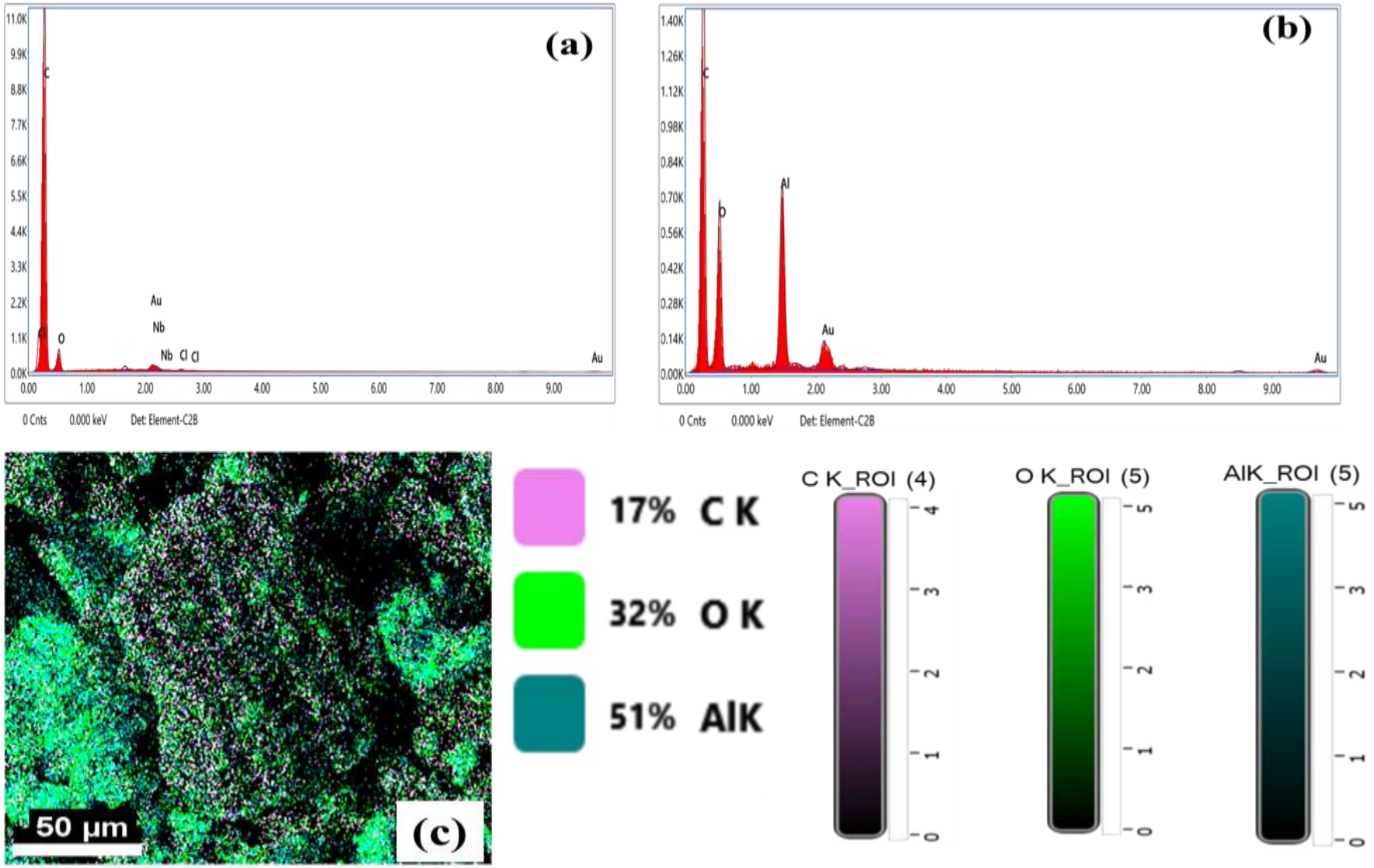

Figure 14: EDS of (a) Pristine AC, (b) AC/Al_2O_3-1:1, and (c) elemental mapping of C, O, and Al for AC/Al_2O_3-1:1 composite

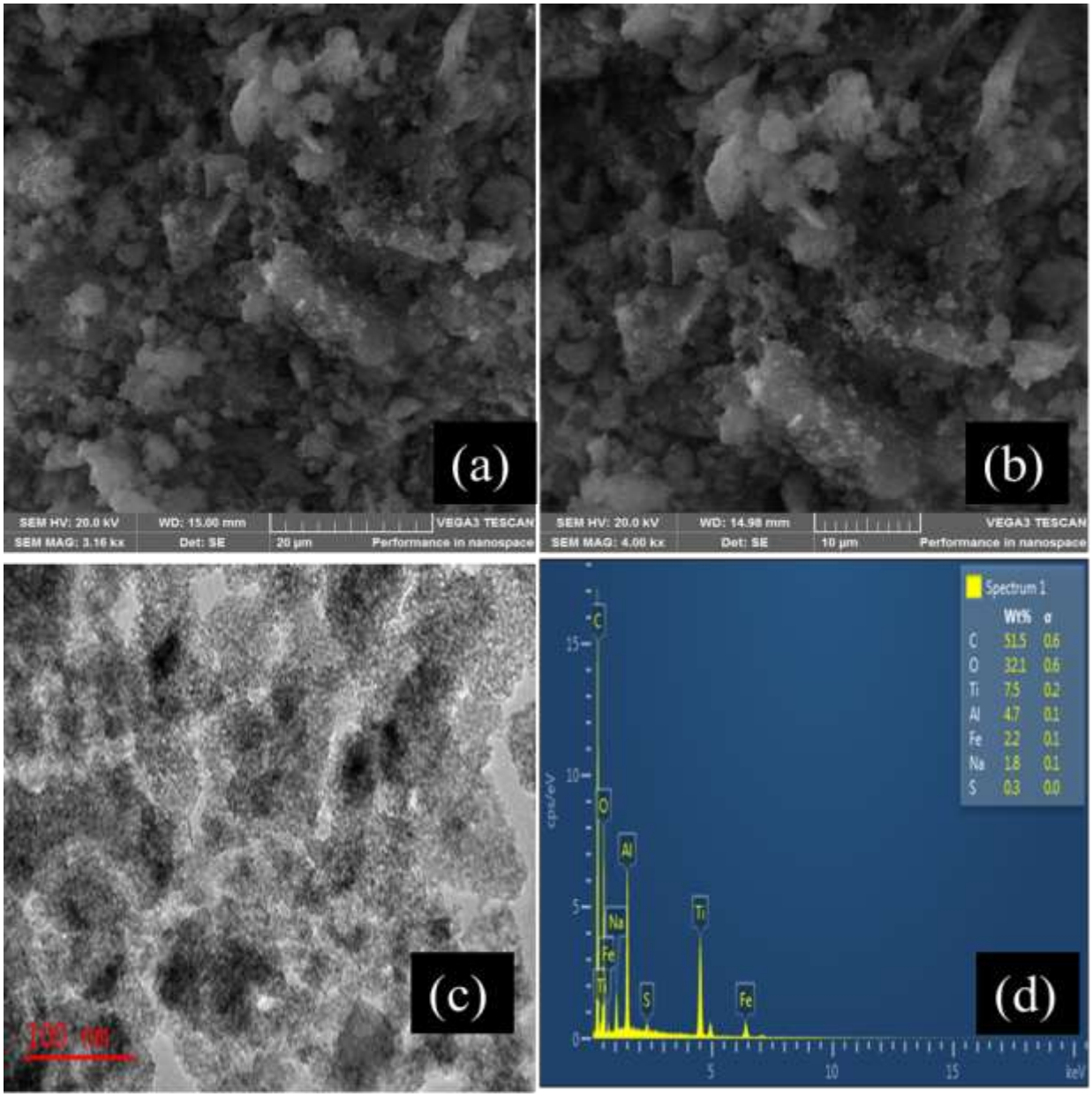

Figure 15: Scanning electron microscopy images of (a, b) AC–$Al_4Fe_{2.5}Ti_4$ at different magnifications, (c) TEM of AC–$Al_4Fe_{2.5}Ti_4$, (d) EDS of AC–$Al_4Fe_{2.5}Ti_4$

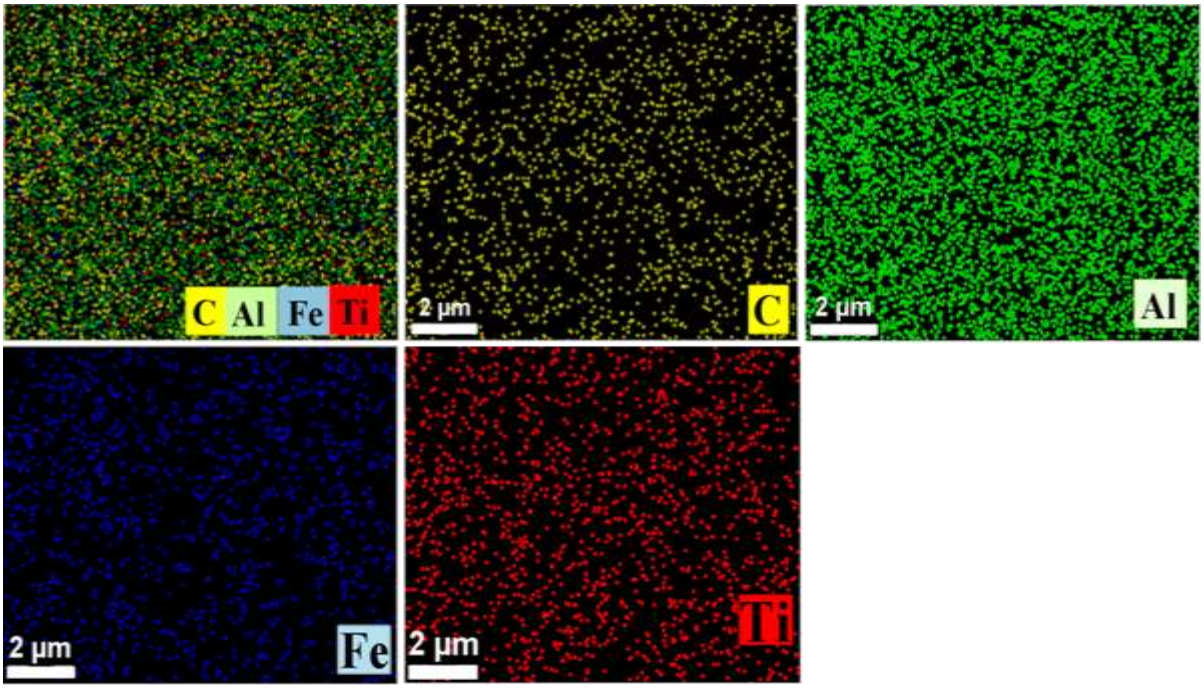

Figure 16: Elemental mapping of C, Al, Ti and Fe elements for AC–$Al_4Fe_{2.5}Ti_4$ composite

4.2 Textural characteristics of AC modified with MO composites

4.2.1 Surface area and pore structure

Determining surface area, pore size, and pore volume distributions in a porous system gives an insight into its physical structure. The surface area, pore size, and pore volume of AC and its composites (AC–$Al_4Fe_{2.5}Ti_4$, AC–$Al_1Fe_{2.5}Ti_1$, and AC–$Al_4Fe_{2.5}Ti_1$) were determined and the results are presented in Table 7. From Table 7, there is a noticeable decrease in the specific surface area after modification. This might be due to the introduced functional groups which block available pores accounting for the decrease of the specific surface areas. Further, the porous structure of the AC and its composite were characterized by N_2 adsorption/desorption isotherm (Fig. 16a) and the corresponding pore size distribution curve (Fig. 16b) determined by the BJH method. As shown in Fig. 16a, both AC and its composite exhibit a typical type-IV isotherm with a hysteresis loop at a high relative pressure range (P/Po > 0.4), showing that the materials are abundant with mesopores (Alfredy *et al.,* 2019). The presence of mesopores favors the electrosorption capacity and the RE% of the electrode materials, as previously reported by Liu *et al.* (2013). The plot for pore size distribution (Fig. 16b) shows that more pores were distributed at 3.5 nm, which is consistent with the isotherm and shows that the composite contains pores in the mesopores region. Mesopores serve as an ion reservoir in the electrode and are important for the transportation of ions.

Table 7: Surface characteristics of AC and its composites

Electrode material	Surface area (m^2/g)	Pore size (nm)	Pore volume (cm^3/g)
AC	695.0	3.4	0.23
AC–$Al_4Fe_{2.5}Ti_4$	491.4	3.5	0.54
AC–$Al_1Fe_{2.5}Ti_1$	572.8	3.5	0.39
AC–$Al_4Fe_{2.5}Ti_1$	383.2	3.5	0.36

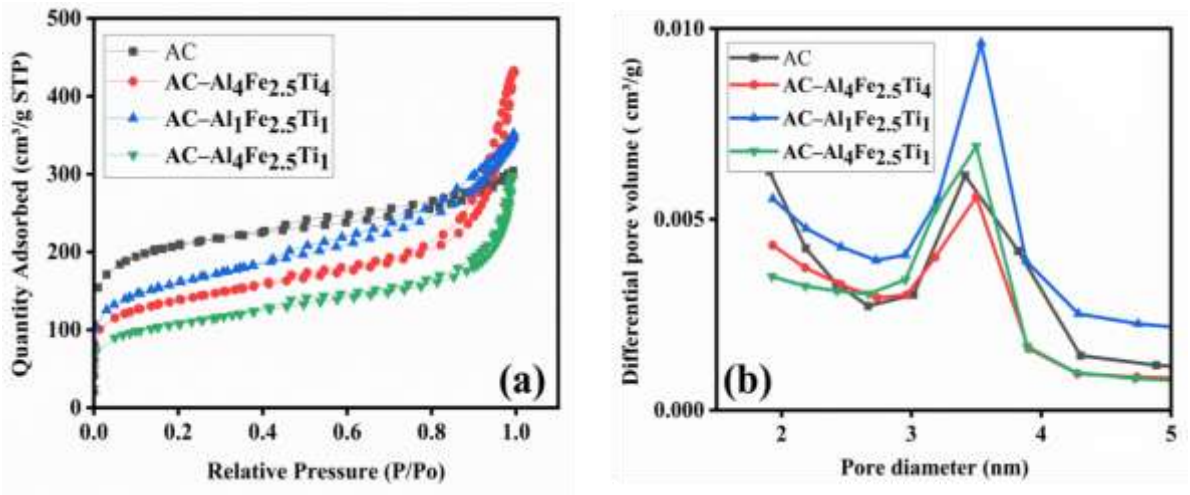

Figure 17: N_2 adsorption-desorption isotherms and BJH plot of the pore size distribution of AC and its composites

4.2.2 X-ray diffraction analysis

X-ray diffraction patterns of pristine AC and its composites are presented in Fig. 17 to 19. Figure 18 shows the XRD patterns of AC before and after compositing with different ratios of Al_2O_3. The results indicate that all the samples had a poorly crystalline nature. Although there was a slight change in the peak intensity, the Al_2O_3-modified AC samples had almost identical XRD patterns. The broad characteristic peaks observed in all the samples, both unmodified and modified materials, at approximately 26° and 42°, 2θ, correspond to the (002) and (100) crystal planes of graphite, respectively [Joint Committee on Powder Diffraction Standards (JCPDS) card no. 41-1487]. These broad diffraction peaks suggest a disordered amorphous framework of the AC used. Additionally, a new characteristic peak was observed at around 66°, 2θ in all the modified samples, indicating the presence of Al_2O_3 particles that were consistent with the (JCPDS) card no. 10-0425 (Barta *et al.*, 2014; Nayar *et al.*, 2014).

Figure 19 demonstrated the XRD patterns of AC composited with single metal oxides (AC/Al_2O_3, AC/Fe_2O_3 and AC/TiO_2), bimetallic oxides ($AC\text{-}Al_2O_3/Fe_2O_3$, $AC\text{-}Al_2O_3/TiO_2$, and $AC\text{-}Fe_2O_3/TiO_2$), and trimetallic oxide ($AC\text{-}Al_2O_3/Fe_2O_3/TiO_2$). Sample AC/Fe_2O_3 (Fig. 18a) presented significant peaks at about 24.2, 33.2, 35.7, 41, 49.6 54, 57.6, 62.6 and 54°corresponds to reflection from (012), (104), (110), (113), (024) (116) (018) (214) and (300) miller planes of the composite (JCPDS no.74-0748) (Qayoom *et al.,* 2020). The clear peak observed in the prepared sample explains that the sample has good crystallization. The most intense peak of the XRD pattern of prepared material was at 33.2° corresponding to the (104) plane, confirming the successful loading of Fe_2O_3 on the AC surface. The XRD pattern of AC/Al_2O_3 and AC/TiO_2 prepared samples showed poor crystallinity, with broad peaks at 26.6° and 25.2° confirming the presence of Al_2O_3 and TiO_2 respectively (No. 21–1272) (Sirengo *et al.,* 2019). The structure of $AC\text{-}Al_2O_3/Fe_2O_3/TiO_2$ shows sharp and intense diffraction peaks (Fig. 18b). The diffraction patterns observed at 23.9, 25.2, 33 35.6, 37.8 49.4, 47.9, 40.8, 62.8 54.2, 55.06 64.1, 68.3 70.2, and 75°. The diffraction peaks of $AC\text{-}Al_2O_3/Fe_2O_3/TiO_2$ indicated orthorhombic structure (JCPDS data file no. 76-1157) as previously observed by Mukherjee *et al.* (2019).

The XRD pattern of $AC\text{-}Al_2O_3/Fe_2O_3$ and $AC\text{-}Al_2O_3/TiO_2$ is also given in Fig. 18(b). The X-ray diffraction patterns confirmed the amorphous nature of the materials. However, the XRD pattern obtained for the $AC\text{-}Fe_2O_3/TiO_2$ (Fig. 18b) showed nine peaks at the angle 2θ values in the range 24.1°-64°. The clear peaks observed explain the crystalline nature of the prepared composite.

Figure 20 shows the XRD patterns of the AC and $AC–Al_4Fe_{2.5}Ti_4$ materials. The spectrum of AC shows two major broad peaks at approximately 2θ = 24° and 43.3°, which can be indexed as the (002) and (100) crystal planes of graphite, respectively (Lin *et al.,* 2018; Wang *et al.,* 2020). The asymmetric and broad peaks observed suggest that AC is turbostratic in nature (Kumar *et al.,* 2018). However, no peaks are observed in the XRD spectrum of $AC–Al_4Fe_{2.5}Ti_4$ across the range of 2θ = 10–90°, indicating that the developed composite material is amorphous, as previously observed by Solanki *et al.* (2019) and Zhang *et al.* (2017). Amorphous materials are reported to be good adsorbents owing to their high surface area and more active sites (Cai *et al.,* 2015). In general, it's important to note that, low crystallinity corresponds to low lattice energy, thus providing an advantage to electrode materials due to the facile de-intercalation process. This advantage could potentially contribute to the observed good performances in CDI (Kadam *et al.,* 2018).

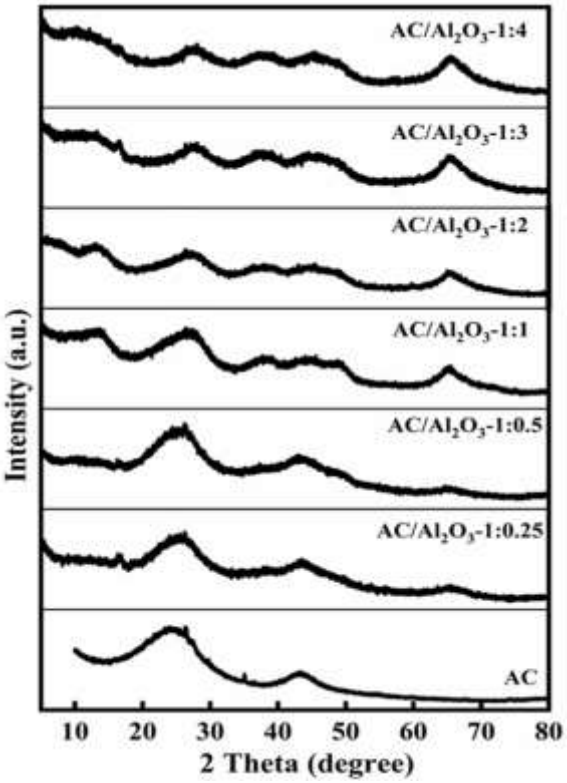

Figure 18: X-ray diffraction patterns of pristine AC and Al_2O_3 doped AC composites

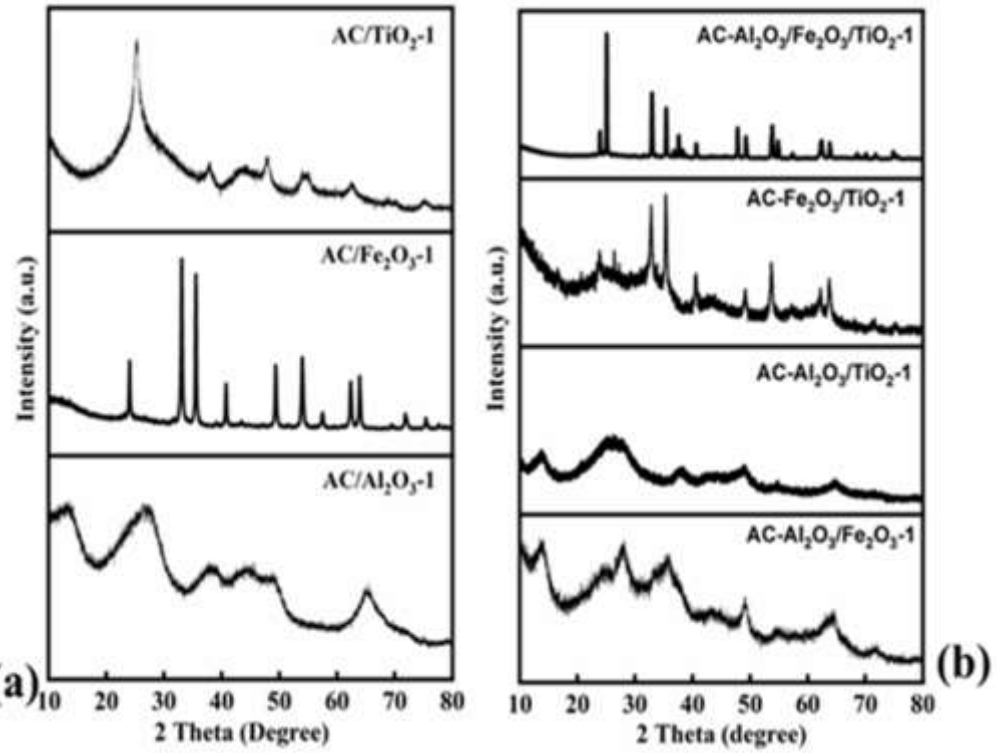

Figure 19: X-ray diffraction patterns of (a) AC composited with single metal oxides (Al_2O_3, Fe_2O_3 and TiO_2) (b) AC composited with bimetallic oxides and tri-metallic oxide

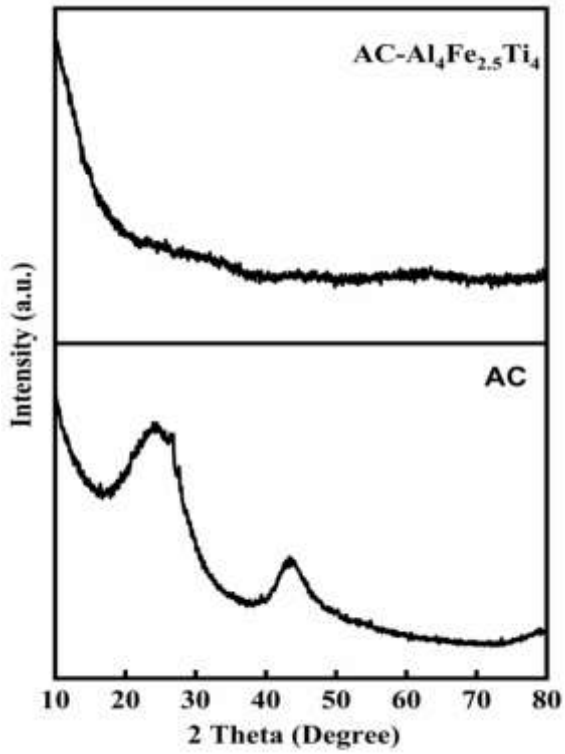

Figure 20: X-ray diffraction patterns of AC and AC–$Al_4Fe_{2.5}Ti_4$

4.2.3 Fourier-transform infrared spectroscopy analysis of AC and its composites

The FTIR spectroscopy is a useful technique for characterizing composite materials and determining the presence of functional groups (Kazeem *et al.,* 2018). The FTIR measurements were performed to identify the main functional groups of pristine AC and the metal oxides modified AC, and the results are presented in Fig. 20-22. The spectra of the FTIR analyses for the pristine AC and the Al_2O_3-modified AC at different Al_2O_3 ratios are presented in Fig. 21. The broad characteristic peaks at 1100 cm^{-1} and 1600 cm^{-1} for the pristine AC can be ascribed to infra-red vibration of C–O and bending of the H–O–H bond, respectively (Romanos *et al.,* 2013). The Al-modified samples, presented several prominent peaks when compared to pristine AC. The peak at around 450 cm^{-1}, corresponds to Al-O bonds and is indicative of the alumina presence. A peak at 1040 cm^{-1} is associated with the symmetric stretching vibrations of the Al–O–H bonds and further confirms the presence of alumina (Ganiyu *et al.,* 2016). Hydroxyl group (O-H) vibrational mode associated with the peak at 2350 $cm^{-1}$was observed in almost all samples, while the broad bands between 3200 and 3400 cm^{-1} present in all AC- Al_2O_3-modified carbon samples and almost unnoticeable in pristine AC were attributed to the O-H stretching mode (Benítez-Guerrero *et al.,* 2014; Saikia & Parthasarathy, 2010; Saravanan & Subramanian, 2005). The presence of Al-O and Al-O-H bands after modification confirm the successful loading of aluminium oxide on the AC surface and are further corroborated by the EDS results presented in Fig. 13(b).

Furthermore, the spectra of the FTIR analyses of AC composited with trimetallic oxides (AC–$Al_4Fe_{2.5}Ti_4$) were compared with that of pristine AC as shown in Fig. 22. The peaks of pristine AC observed at approximately 625, 1296, 1622, 2000, 2093, 2166, 2330, and 3743 cm^{-1} depict the presence of C–H, C–O, C=O, C≡C, O=C=O, and O–H bonds, respectively (Mojoudi *et al.*, 2019; Yang *et al.*, 2022). After compositing with Al, Fe, and Ti oxides, new peaks are observed at around 447–1102, 1211–1545, 1959, 2102–2166, and 3367–3745 cm^{-1}. These correspond to metal−oxygen (M−O; M represents Al, Fe, and Ti), C–O, C–H, C=C=O, and O–H bonds (Al-Hayali *et al.*, 2017; Homogen, 2018; Li *et al.*, 2019; T. Zhang *et al.*, 2017). The new functional group peaks arising after modification demonstrate the successful loading of the metal oxides on the AC surface, as confirmed by the EDS results presented in Fig. 14(d).

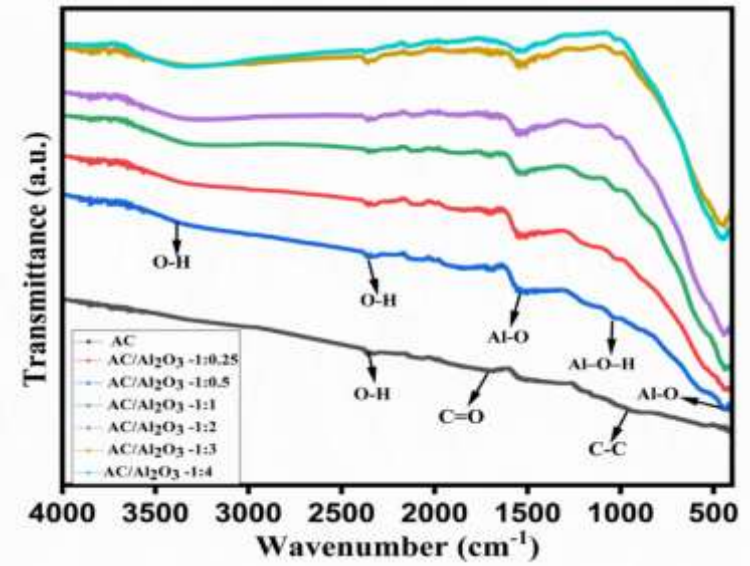

Figure 21: Fourier-transform infrared spectroscopy spectra of the pure and Al-modified AC electrode materials

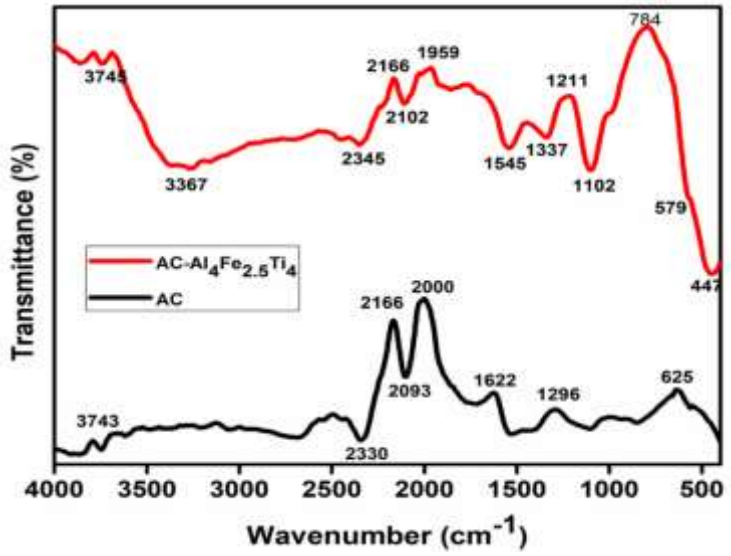

Figure 22: Fourier-transform infrared spectroscopy Spectra of AC and AC–$Al_4Fe_{2.5}Ti_4$

4.3 Wettability analysis of the samples

The wettability of the pristine AC and its composites were analyzed by a water contact angle analyzer, and the results were presented in Fig. 22 and 23. The contact angle measurements of AC and AC–$Al_4Fe_{2.5}Ti_4$ electrode surfaces at different contact times were compared, and the results are shown in Fig. 23. When the angle is below and above 90°, a material is hydrophilic and hydrophobic, respectively (Ma *et al.*, 2019). Additionally, a small contact angle implies high hydrophilicity of the material. The initial contact angle on the AC electrode surface (121.7°) is greater than that of the AC–$Al_4Fe_{2.5}Ti_4$ electrode surface (56.6°). The contact angle of the AC–$Al_4Fe_{2.5}Ti_4$ decreases to 15°, whereas that of pristine AC decreases to 108° within a time frame of 25 s.

Additionally, water contact angle measurements for AC/Al_2O_3-1:1 electrode surface were compared with that of pristine carbon, and the results are shown in Fig. 24. The initial contact angle on the AC electrode surface (121.9°) is greater than that of the AC/Al_2O_3-1:1 (68.9°) electrode surface. This suggests that the modified electrode has better wettability than the pristine one, which can benefit F^- and PQ removal experiments owing to the advantage of ion transportation (Che *et al.*, 2019).

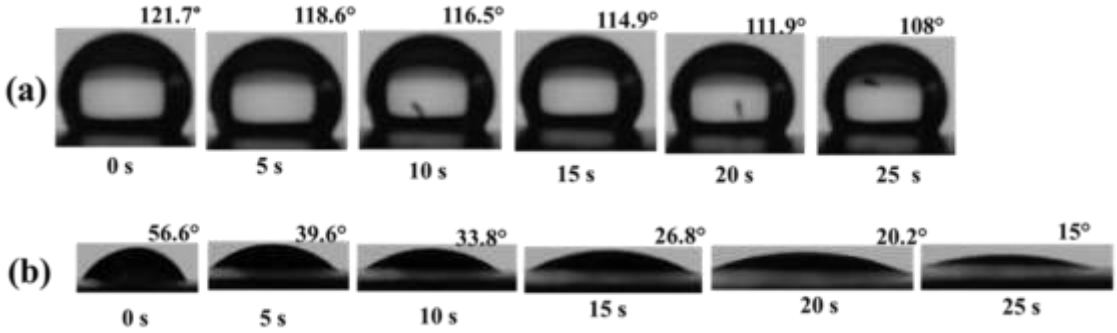

Figure 23: Photographs of water drops on (a) AC and (b) AC–$Al_4Fe_{2.5}Ti_4$ electrodes at different durations

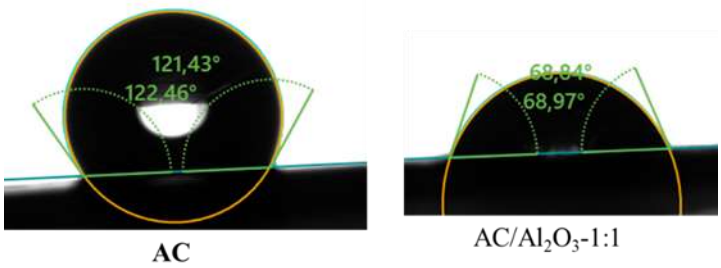

Figure 24: Photographs of water drops on (a) AC and (b) AC/Al_2O_3-1:1electrodes

4.4 Surface charge studies

4.4.1 Zeta potential measurements

In general, the effectiveness of CDI electrode materials is also affected by their surface charge. For this reason, to understand the surface charge characteristics of pristine and metal oxides modified AC, the zeta potential measurements were carried out using a Malvern Zeta sizer Nano ZS instrument. The results were presented in Fig. 25. The pristine AC surface has a negatively charged surface as evidenced by the Zeta potential of -23.9 mVat pH (5.7); however, after modification with Al_2O_3, the Zeta potential shifted to the positive value of +23.2 mV, which indicates the presence of positive groups on the composite surface at the pH of 7.01. On the other hand, when AC was modified with Fe_2O_3 and TiO_2, the Zeta potential shifted into more negative values of -32.8 mV at pH (9.4) and -46.6 mV at pH (9.8), which demonstrates the presence of negative groups on their surfaces. Moreover, AC demonstrated a positive shift of zeta potential from -23.9mV to -5.85 mV for AC-Al_2O_3/Fe_2O_3 at pH (8.2) and 1.67 mV for AC- AC-Al_2O_3/Fe_2O_3/TiO_2 at pH (7.2) respectively.

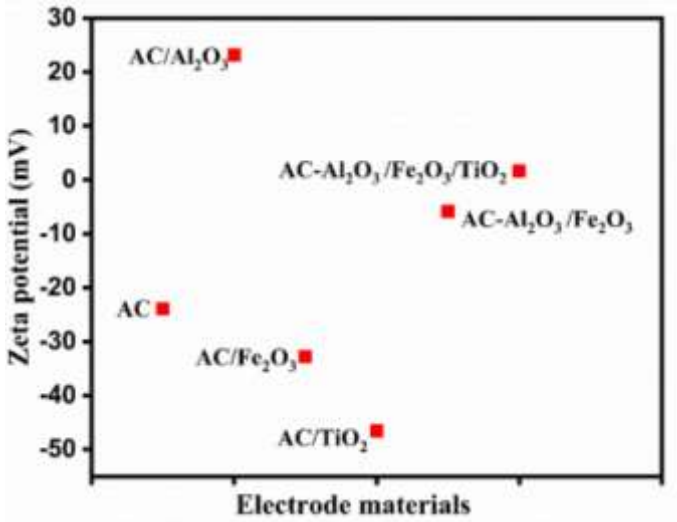

Figure 25: Zeta potential values of AC and its metal oxides modified composites

4.4.2 The potential of zero charge measurement

The potential of zero charges (E_{PZC}) values of the AC and AC–differential capacitance minimum measurements analyzed $Al_4Fe_{2.5}Ti_4$ electrodes, and the results are shown in Fig. 26. The potential of zero charges is the potential at which a material has minimum capacitance or adsorbed ions at the electrode–electrolyte interface (Landon *et al.*, 2017). The E_{PZC} of the pristine AC electrode is approximately 0.23 V, whereas the E_{PZC} of the modified AC (AC–$Al_4Fe_{2.5}Ti_4$) electrode is negatively shifted to approximately −0.61 V versus Ag/AgCl. This

indicates that positively charged groups are grafted on the AC–$Al_4Fe_{2.5}Ti_4$ electrode surface after chemical modification (Zhang *et al.*, 2019). Therefore, if this positively charged electrode material is used as the anode, CDI cell performance, such as RE%, cycle stability, and electrosorption capacity, can be improved.

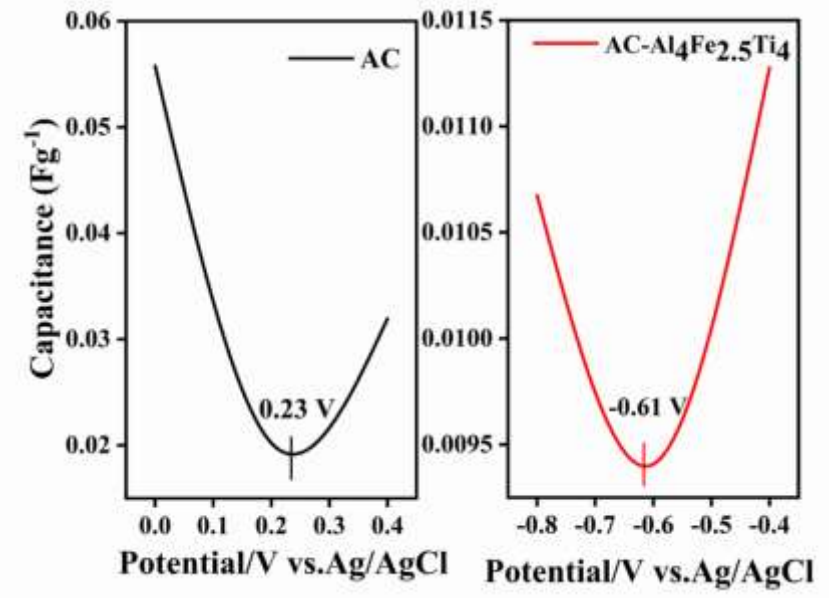

Figure 26: Normalized differential capacitance curves of AC and AC–$Al_4Fe_{2.5}Ti_4$ electrodes

4.5 Electrochemical characteristics of materials

Electrochemical testing is a critical step in the evaluation of CDI electrode materials. Such testing is typically performed using a three-electrode system, where the CDI electrode material serves as the working electrode, and an external reference electrode and the counter electrode are used to measure the electrochemical response of the material. The testing can provide valuable information such as the material's electrical conductivity, electrochemical stability, and charge storage capacity. These factors are crucial in determining the suitability of the CDI electrode material for use in water purification systems.

Cyclic Voltammetry (CV) measurements were performed in 6 M KOH using a three-electrode cell system at scanning rates ranging from 5 – 200 mV/s (Fig. 27). The CV curves of pristine AC in Fig. 26(a) exhibit quasi-rectangular shapes, showing improved electrical double-layer properties and a non-Faradaic reaction (Angeles *et al.*, 2022; Su *et al.*, 2018). The cyclic voltammetry curves of AC–$Al_4Fe_{2.5}Ti_4$ (Fig. 26(b)) show well-defined redox peaks, signifying the contribution of a Faradaic reaction even at high scan rates. The metal oxide-modified AC (AC–$Al_4Fe_{2.5}Ti_4$), has a maximum specific capacitance of 826 F/g, which is significantly higher than that of pristine AC, 53 F/g, at 5 mV/s. The synergistic effects of the metal oxides

in the composite material cause a significant difference in the specific capacitance. Figure 26(c) shows the voltammograms of AC and AC–$Al_4Fe_{2.5}Ti_4$ composite at 5 mV/s in different voltage windows. The AC electrode functions well at negative potentials, whereas the composite performs well at positive potentials. The operational voltage differences between the composite and carbon electrodes are (0.0–0.5 V) and (−1.0–0.0 V), respectively, indicating a practical match for both voltage windows. Therefore, for practical supercapacitor applications only and based on the voltage windows of AC (1.0) and composite (0.5) in KOH electrolyte, asymmetric supercapacitor (AC–$Al_4Fe_{2.5}Ti_4$/AC) assembled with solid-state electrolytes is expected to perform in a wide potential window of 1.5 as demonstrated by (Zhai *et al.,* 2022). These potential windows are considered to enable high Coulombic efficiency, which is typically a function of the oxidation of the electrode without oxidatively breaking down the electrolyte, resulting in a high specific capacitance (Kirubasankar *et al.,* 2018; Wang *et al.,* 2019).

Nyquist plots of the AC and AC–$Al_4Fe_{2.5}Ti_4$ electrodes in the frequency range of 100 kHz–0.01 Hz are shown in Fig. 28, which are used for evaluating the electrode–electrolyte interface for charge transport and electrolyte diffusion. Figure 27(a) shows a Nyquist plot has two significant parts: a semicircle in the high-frequency region representing the charge transfer resistance at the electrode–electrolyte interface region and an almost vertical line in the low-frequency zone (Su *et al.,* 2018). Smaller semicircles in AC-$Al_4Fe_{2.5}Ti_4$ indicate small charge transfer resistance. Thus, the impedance analysis suggests that AC–$Al_4Fe_{2.5}Ti_4$ possesses lower charge transfer and ion transport resistance than AC, which may be attributed to the intimate contact at the electrolyte–electrode interface (Guo *et al.,* 2017). The intercept in the real part (Z') yields the electrolyte's total resistance and the electrode's intrinsic resistance, referred to as the equivalent series resistance. AC and AC–$Al_4Fe_{2.5}Ti_4$ show equivalent series resistances of approximately 0.32 and 0.38 Ω, respectively (Fig. 27b). The pristine AC shows a nearly perpendicular line to the imaginary axis in the low-frequency region, confirming an electric double-layer capacitance mechanism (Tajik *et al.,* 2017), which is very close to ideal capacitive characteristics. In comparison, AC–$Al_4Fe_{2.5}Ti_4$ presents an inclined line, which may be due to pseudocapacitance properties (Guo *et al.,* 2018).

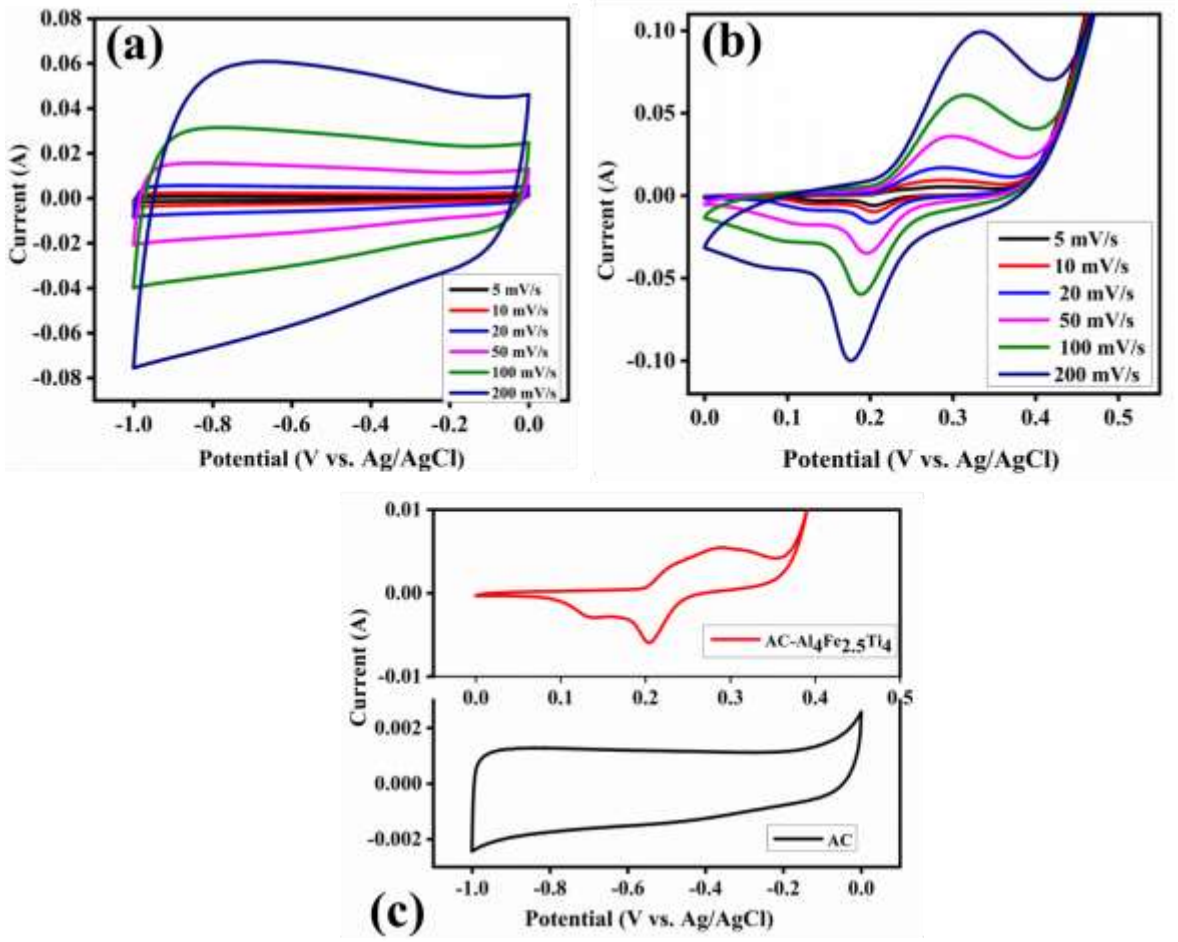

Figure 27: Cyclic voltammograms of (a) AC and (b) AC–$Al_4Fe_{2.5}Ti_4$ electrodes at different scan rates and (c) AC–$Al_4Fe_{2.5}Ti_4$ and AC at 5 mV/s

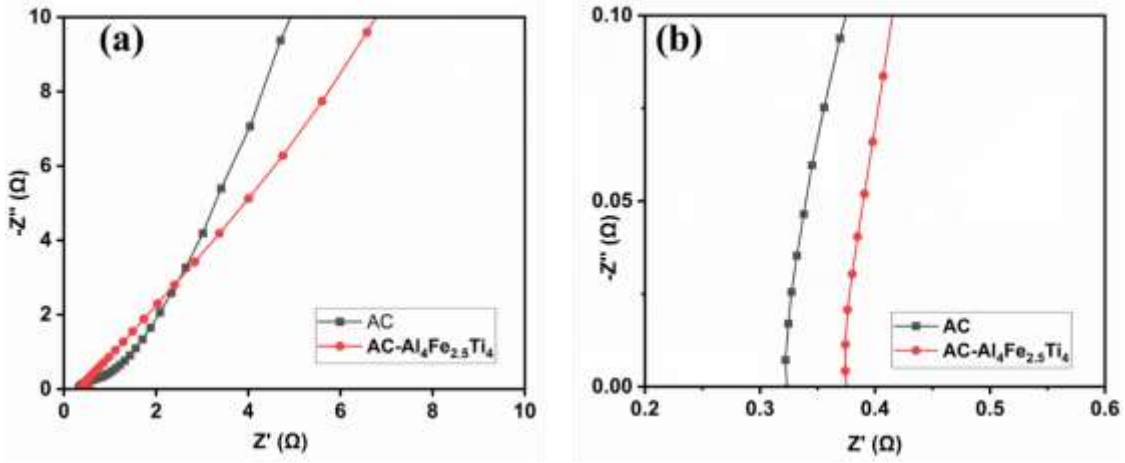

Figure 28: Nyquist profiles of AC and AC–$Al_4Fe_{2.5}Ti_4$ electrodes and (b) their magnified view in high-frequency range

Since defluoridation practically normally has been conducted in neutral media, then, CV measurements of AC and AC–$Al_4Fe_{2.5}Ti_4$ electrodes were also performed in 0.1 M NaF using a three-electrode cell system at scanning rates ranging from 5 – 200 mV/s (Fig. 29). All CV curves for pristine AC show a quasi-rectangular shape, showing improved electrical double-

layer properties and a non-Faradaic reaction (Angeles *et al.,* 2022; Su *et al.,* 2018). However, the closed area under the CV curve is larger for AC–$Al_4Fe_{2.5}Ti_4$ electrode than AC, indicating its high capacitive performances (Wang *et al.,* 2021). The metal oxide-modified AC (AC–$Al_4Fe_{2.5}Ti_4$) has a maximum specific capacitance of about 428 F/g, significantly higher than that of pristine AC, 139 F/g, at 5 mV/s. The synergistic effects of the metal oxides in the composite material cause a significant difference in the specific capacitance. In addition, Fig. 28(c) shows the specific capacitances of the AC and AC–$Al_4Fe_{2.5}Ti_4$ electrodes in 0.1 M NaF electrolyte at different scan rates. It can be seen that specific capacitance decreased as the scan rate increased. This can be explained by the fact that at higher scan rates, compared to lower scan rates, the diffusional mass transport between the electrodes and electrolytes decreased due to Ohmic loss amplification (Bharath *et al.,* 2020). The AC electrode functions well at negative potentials, whereas the composite performs well at positive potentials. The operational voltage differences between the composite and carbon electrodes are (0.0 – +1 V) and (−1.0–0.0 V), respectively, indicating a practical match for both voltage windows.

Nyquist plots of the AC and AC–$Al_4Fe_{2.5}Ti_4$ electrodes in the frequency range of 100 kHz–0.01 Hz are shown in Fig. 30, which are used for evaluating the electrode–electrolyte interface for charge transport and electrolyte diffusion. Figure 29(a) shows a Nyquist plot has two significant parts: a semicircle in the high-frequency region representing the charge transfer resistance at the electrode–electrolyte interface region and an almost vertical line in the low-frequency zone (Su *et al.,* 2018). The intercept in the real part (Z') yields the total resistance of the electrolyte and the intrinsic resistance of the electrode, referred to as the equivalent series resistance. AC and AC–$Al_4Fe_{2.5}Ti_4$ show equivalent series resistances of approximately 1.75 and 1.82 Ω, respectively (Fig. 29b), demonstrating that the pristine AC electrode possesses a lower internal resistance than the AC–$Al_4Fe_{2.5}Ti_4$ electrode. As reported in other studies, the composite showed slightly higher equivalent series resistance than AC may be because of the poor electronic conductivity of metal oxides (Barroso-Bogeat *et al.,* 2014; Sinha *et al.,* 2020).

Hence, due to the strong connection between supercapacitor behavior and CDI performance, the increased specific capacitance of AC–$Al_4Fe_{2.5}Ti_4$, along with its lower internal resistance, qualifies it as a suitable electrode materials for effective defluoridation by CDI process.

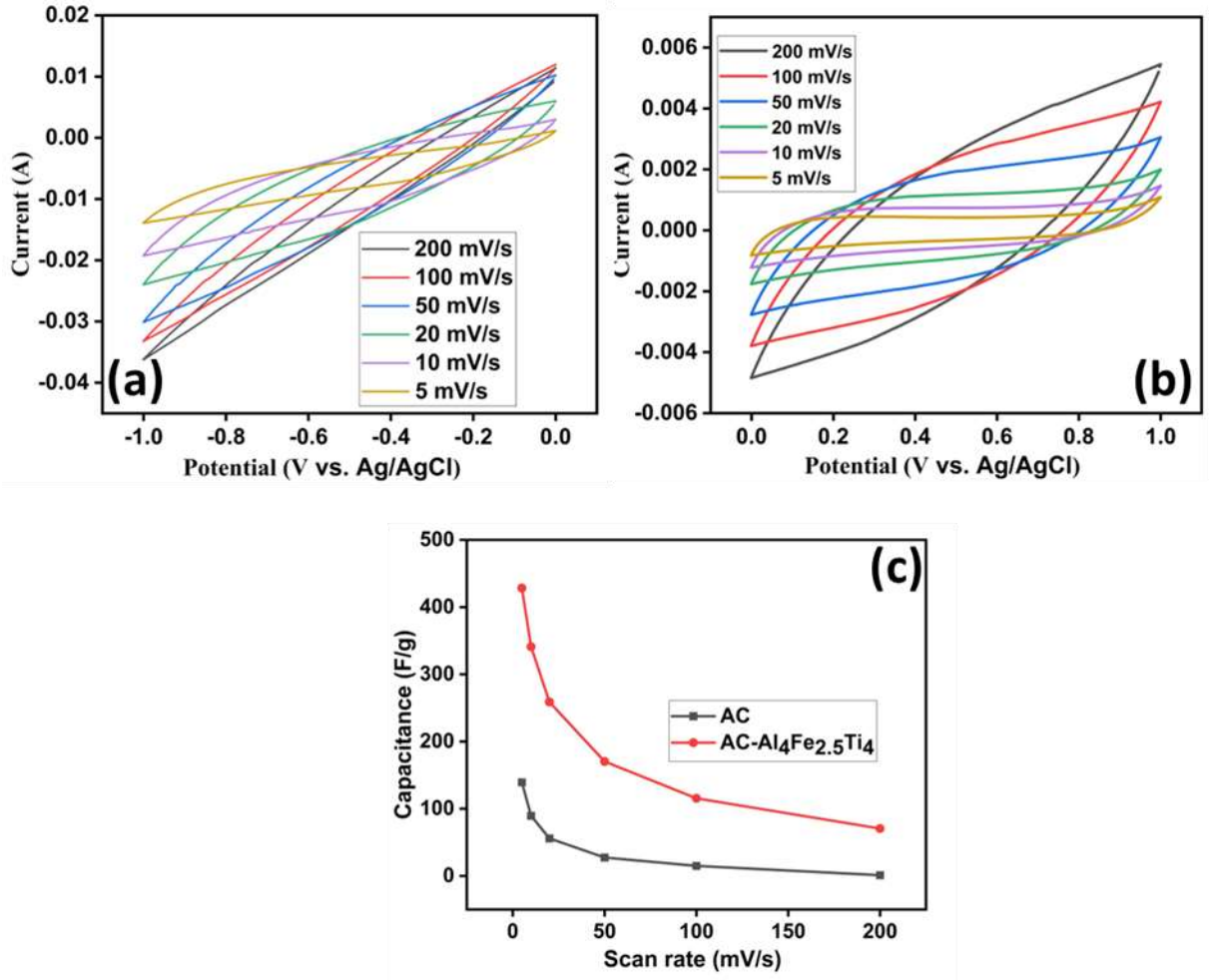

Figure 29: **Cyclic voltammograms of (a) AC and (b) AC–$Al_4Fe_{2.5}Ti_4$ electrodes at different scan rates and (c) Specific capacitance of AC and $Al_4Fe_{2.5}Ti_4$ at 5 mV/s with respect to scan rates in CV measurement**

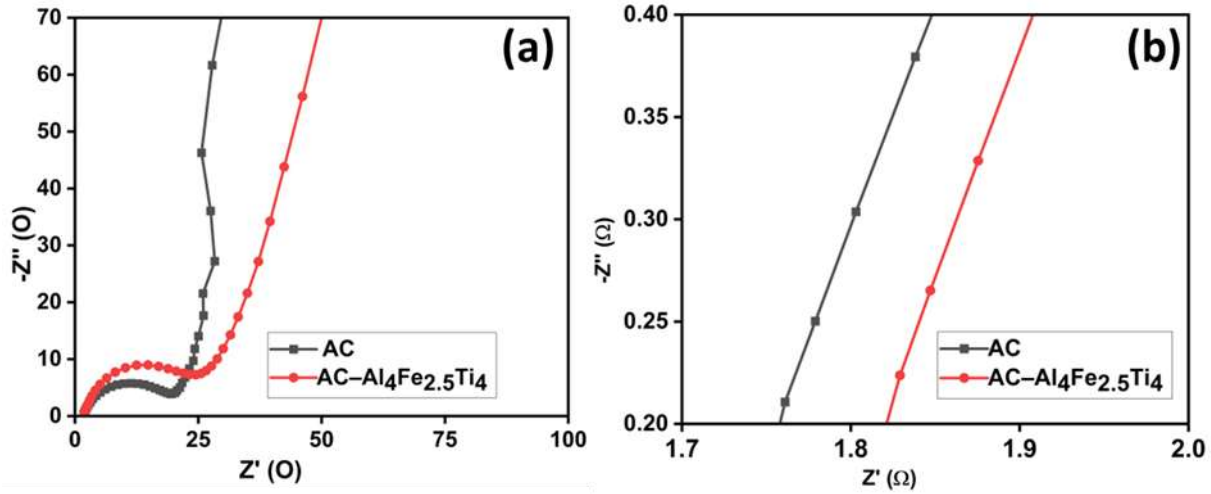

Figure 30: **Nyquist profiles of AC and AC–$Al_4Fe_{2.5}Ti_4$ electrodes and (b) their magnified view in high-frequency range**

4.6 Defluoridation with capacitive deionization

The water defluoridation experiments were conducted as described in Section 3.7. The CDI experiments were performed in a symmetric cell at an applied potential of 1.2 V in a NaF

solution containing 5 mg/L of F^-. To determine the optimal electrode material for defluoridation, which was further tested in CDI performances, 15 runs according to the Design-Expert software formulated experiments (Table 6) were carried out. The results were presented in Table 8.

Table 8: Equilibrium concentrations of F^- after electrosorption experiments

Composites of AC and Al, Fe, and Ti oxides with different mass ratios	Electrosorption equilibrium F^- concentration (mg/L)
AC–$Al_1Fe_1Ti_{2.5}$	3.25
AC–$Al_4Fe_1Ti_{2.5}$	1.48
AC–$Al_1Fe_4Ti_{2.5}$	2.6
AC–$Al_4Fe_4Ti_{2.5}$	1.28
AC–$Al_1Fe_{2.5}Ti_1$	2.65
AC–$Al_4Fe_{2.5}Ti_1$	1.32
AC–$Al_1Fe_{2.5}Ti_4$	3.0
AC–$Al_4Fe_{2.5}Ti_4$	1.05
AC–$Al_{2.5}Fe_1Ti_1$	1.75
AC–$Al_{2.5}Fe_4Ti_1$	1.3
AC–$Al_{2.5}Fe_1Ti_4$	2.05
AC–$Al_{2.5}Fe_4Ti_4$	1.85
AC–$Al_{2.5}Fe_{2.5}Ti_{2.5}$	1.8

Table 8 shows that AC–$Al_4Fe_1Ti_{2.5}$, AC–$Al_4Fe_{2.5}Ti_1$, AC–$Al_{2.5}Fe_4Ti_1$, AC-$Al_4Fe_4Ti_{2.5}$, and AC–$Al_4Fe_{2.5}Ti_4$ decrease the F^- concentration from 5 mg/L to 1.48, 1.32, 1.3, 1.28, and 1.05 mg/L, respectively. These values are below the WHO permissible limit of 1.5 mg/L for drinking water quality. Based on these results, the least electrosorption equilibrium F^- concentration was achieved at AC–$Al_4Fe_{2.5}Ti_4$ composite, which was further investigated to study the influence of other CDI parameters towards F^- removal.

4.6.1 Performance of AC–$Al_4Fe_{2.5}Ti_4$ composite in real water for defluoridation

To investigate the performance of the AC–$Al_4Fe_{2.5}Ti_4$ electrode for F^- removal, a defluoridation test was conducted by using natural water sample collected from the Mandokey River in Ngarenanyuki, Arusha. The water quality of the collected sample was analyzed, and the results are presented in Table 9. From Table 9, it can be seen that the F^- concentration exceeds the WHO standard for drinking water (1.5 mg/L) (WHO, 2017).

Table 9: Water quality from Mandokey River, Ngarenanyuki, Tanzania

Parameters	Concentration (mg/L)	WHO standards (mg/L)
Na^+	82.50	200
K^+	11.35	Not Specific
Ca^{2+}	3.29	70
Mg^{2+}	1.60	50
Cl^-	7.63	200
$SO4^{2-}$	15.6	500
HCO_3^-	228.2	Not Specific
$CO3^{2-}$	4.28	Not Specific
NH_3^-	0.08	0.5
Fe	0.01	0.3
Mn^{2+}	0.004	0.1
NO_3^-	2.80	50
PO_4^{3-}	0.18	1.0
F^-	**5.15**	**1.5**

After CDI testing with AC–$Al_4Fe_{2.5}Ti_4$ composite electrode, the F^- concentration was reduced from 5.15 to 1.18 mg/L (RE of 77%); which is below the WHO drinking water standard of 1.5 mg/L. However, the pristine AC reduced the F^- concentration to 4.5 mg/L (RE of 13%), which is significantly higher than the permissible value.

Moreover, the energy consumed to treat real water with F^- was calculated and found to be approximately 0.037 kWh/m^3.This value is lower than the values of other relevant water treatment technologies, as summarized in Table 10. Therefore, a CDI system with AC–$Al_4Fe_{2.5}Ti_4$ composite electrodes could be considered a promising F^- removal method applicable to real water.

Table 10: Energy consumed by the method used in this study for the treatment of real F^-contaminated water compared with those of other relevant water treatment technologies

Technologies	Energy consumption (kWh/m^3)	References
Electrocoagulation	0.47	Tezcan Un *et al.* (2013)
Electrodialysis	0.064	Lahnid *et al.* (2008)
Nanofiltration	0.4	Elazhar *et al.* (2009)
Combined electrocoagulation and electroflotation	1.2	Zuo *et al.* (2008)
Capacitive deionization	0.037	This study

4.6.2 Electrosorption–regeneration process

The regeneration performance is an important factor for evaluating further applications of electrode materials. Therefore, the regeneration and recyclability of the electrodes were evaluated by performing ten electrosorption/desorption cycles for 15 h. Figure 31 presents the results of the stability tests of AC–$Al_4Fe_{2.5}Ti_4$ conducted in a 5 mg/L F^- (NaF) solution at 1.2 V during charging for 1 h and discharging at −1.6 V for 30 min. In the latter, the spent electrode was regenerated. Figure 30 shows that the F^- desorption percentage for the first cycle is 95%, which after ten cycles of reuse becomes 93.8 %. These findings indicate that the F^- electrosorption on AC–$Al_4Fe_{2.5}Ti_4$ is reversible to a significant extent and that the spent AC–$Al_4Fe_{2.5}Ti_4$ electrode can be regenerated and reused. Therefore, AC–$Al_4Fe_{2.5}Ti_4$ can offer repeated applications for removing F^- from water. Moreover, note that the AC–$Al_4Fe_{2.5}Ti_4$ regeneration process did not use any chemicals; instead, it can produce current for energy recovery. Therefore, removing F^- ions using AC–$Al_4Fe_{2.5}Ti_4$ is an environmentally benign method.

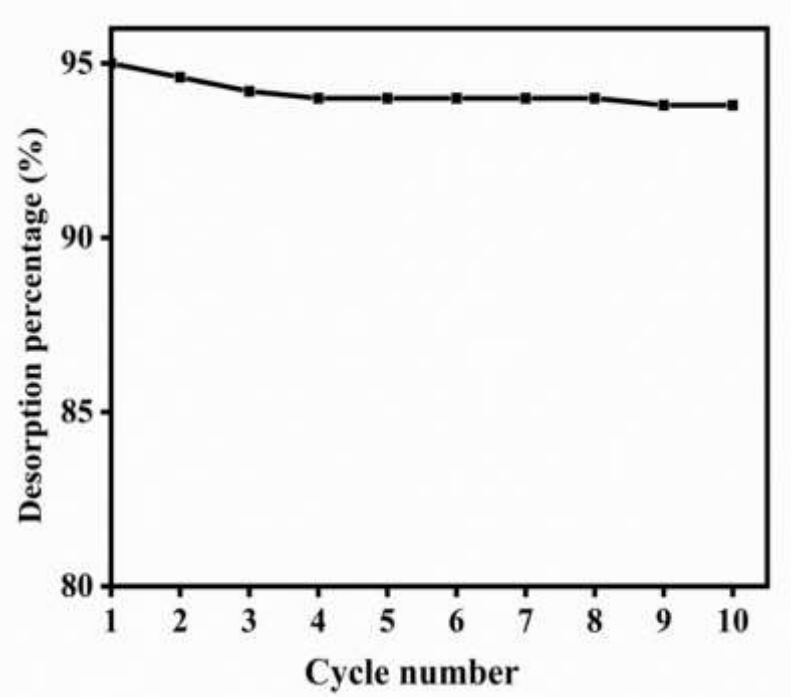

Figure 31: Reusability studies on AC–$Al_4Fe_{2.5}Ti_4$ electrode at electrosorption voltage of 1.2 V and regeneration voltage of −1.6 V using feed solution of 5 mg/L at 15 mL/min

4.6.3 pH changes

The pH of the effluent can change significantly when oxidation, reduction, or water-splitting events occur on the surface of electrodes (He *et al.,* 2016; Zhang *et al.,* 2018). In this study, the pH of the effluent was monitored throughout the experiment and presented in Fig. 32 to study if electrode reactions were occurring during the electrosorption process. According to Fig. 31 at the applied potential of 1.2 V, the pH of the effluent during the electrosorption stage was seen to slightly decrease from about 7.2 to 6.8 and 6.8 to 6.5 for AC–$Al_4Fe_{2.5}Ti_4$ and AC, respectively. This range is within the 6.5–8.2 WHO drinking acceptable water limit (WHO, 2017). Since the pH of the effluent is maintained in this range and the pH solution does not become more acidic or basic, it is implied that no Faradaic reactions, such as redox reactions and water hydrolysis, were occurring while the voltage of 1.2 V was applied to the AC and its composite.

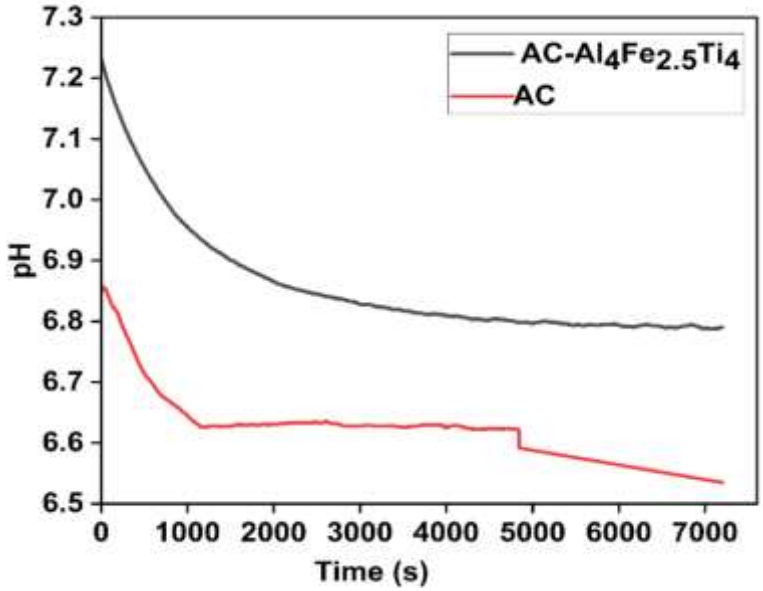

Figure 32: pH changes at an applied voltage of 1.2 V for AC and AC–$Al_4Fe_{2.5}Ti_4$ composite

4.6.4 Changes in Current

This study conducted the CDI test at a constant voltage mode. Thus, a constant potential was applied in the chronoamperometry measurements to determine the potential-dependent current profile and its stabilization over time. As a result, one may calculate the amount of energy used during the electrosorption process and understand the electrode's surface resistance from the current change profile with time shown in Fig. 33. Given that current is inversely proportional to resistance, Fig. 32 shows that the initial current of the pristine AC is higher than that of the modified AC, indicating that the surface resistance of the pristine AC is lower than that of the AC–$Al_4Fe_{2.5}Ti_4$; similar observation was previously reported by Machunda *et al.* (2009) and Trunzer *et al.* (2020). This could be explained by the presence of metal oxide on the AC surface after modification, as metal oxide has been reported to have poor electronic conductivity than AC (Barroso-Bogeat *et al.*, 2014; Sinha *et al.*, 2020).

Additionally, the current versus (vs) time curve can be used to determine the area under the curve, which together with other parameters as shown in Equation (7), will provide the energy consumed during the electrosorption process. The absolute area calculated from the current vs time curve (Fig. 32) were 15221.6 and 6567.46 coulombs for AC and AC–$Al_4Fe_{2.5}Ti_4$, respectively. By using Equation 7 and providing that other parameters of the Equation are held constant, energy consumption increases with increasing absolute area and vice versa. Since the absolute area of the pristine AC electrode is higher than that of the modified one, then pristine AC electrode consumed more energy (0.09 kWh/m^3) during defluoridation than AC–

$Al_4Fe_{2.5}Ti_4$ (0.037 kWh/m^3). Therefore, this study minimized the energy consumption of the CDI system by treating the AC with trimetallic oxides for defluoridation.

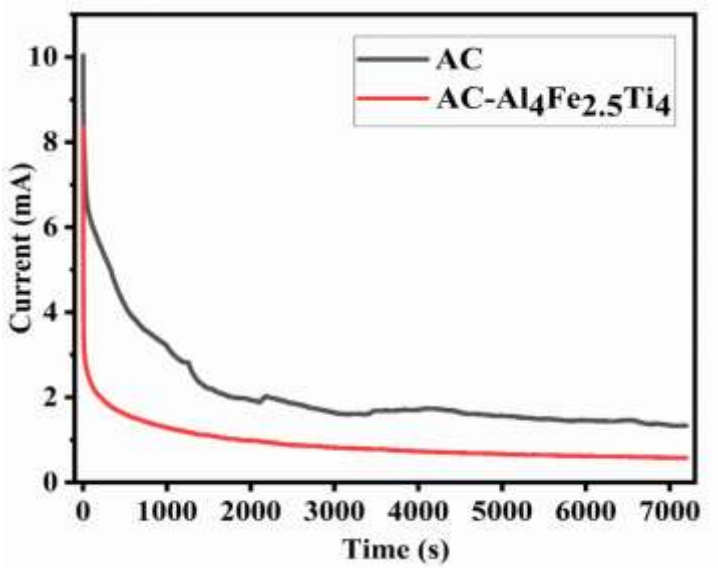

Figure 33: The current-time response obtained at an applied potential of 1.2 V on the surface of pristine AC and modified AC (AC–$Al_4Fe_{2.5}Ti_4$) in field water with 5.15 mg/L F^- at a flow rate of 15 ml/min

4.6.5 F− removal mechanism

The FTIR measurements of the AC–$Al_4Fe_{2.5}Ti_4$ electrode before and after electrosorption were conducted to understand better the F^- removal mechanism of CDI with AC loaded with the metal oxides. From Fig. 34, the intensities of the characteristic peaks of the optimized electrode material (AC–$Al_4Fe_{2.5}Ti_4$) at 3350, 2344, 1217, and 496 cm^{-1} decrease after electrosorption. In comparison, the peaks at 1632 and 1140 cm^{-1} shift, and the peak at 567 cm^{-1} disappears, indicating its involvement in F^- electrosorption, as observed by Chen *et al.* (2012). The weakened peak observed at 3350 cm^{-1} confirms that after electrosorption, F^- replaces a part of the surface hydroxyl groups to combine with Al, Fe, and Ti (ligand exchange). The location shift or disappearance of the peaks indicates the formation of new bonds or confirms the strong coordination between the metals (Al, Fe, Ti) and F^- (Yin *et al.*, 2022). Therefore, it can be deduced that ligand exchange, electrostatic force of attraction (caused by the applied voltage), and coordination/complexation jointly facilitate the F^- removal.

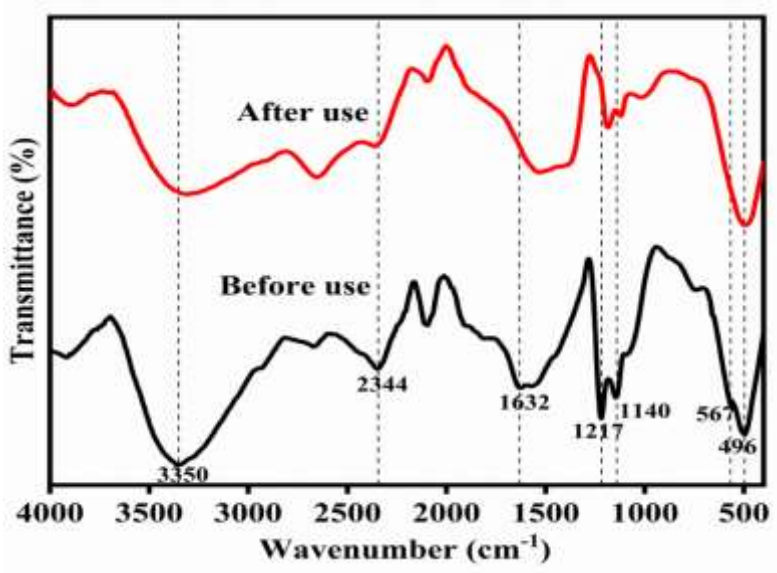

Figure 34: Fourier-transform infrared spectroscopy spectra of AC–$Al_4Fe_{2.5}Ti_4$ electrode before and after the CDI experiment

4.7 Optimization of the CDI electrode material for defluoridation

4.7.1 Model fit and statistical analysis

Table 11 shows the predicted and experimental measured responses for the 15 runs according to the Design-Expert software formulated experiments. Fluoride removal efficiency (RE) ranged from 35 to 79%, and the maximum RE value was obtained from the 8th run under the condition of A-Al = 4, B-Fe = 2.5 and C-Ti = 4. The obtained results were fitted to a second-order polynomial model, and the Design-Expert software suggested a quadratic model for the obtained response (RE), as shown in Table 11. The Equation for the final empirical model (Equation 10), using coded variables, was obtained by removing insignificant terms with p-values greater than 0.1 through a backward model selection algorithm in Design-Expert software. Nominal terms crucial to the model hierarchy were retained to capture the relationship between independent and dependent variables accurately. Therefore, A, B, C, AC and A^2 are significant terms for the RE model.

Table 11: Experimental design conditions and response of each experimental run

Run No	Independent variables			Response variable RE (%)	
	A-Al (g)	B-Fe (g)	C-Ti (g)	Experimental values	Predicted values
1	1	1	2.5	35	38.71
2	4	1	2.5	70.4	70.66
3	1	4	2.5	47.7	46.14
4	4	4	2.5	74.4	78.09
5	1	2.5	1	47	47.84
6	4	2.5	1	73.7	73.64
7	1	2.5	4	40	37.01
8	4	2.5	4	79	80.11
9	2.5	1	1	65	64.48
10	2.5	4	1	74	71.91
11	2.5	1	4	59	59.81
12	2.5	4	4	63	67.23
13	2.5	2.5	2.5	64	65.86
14	2.5	2.5	2.5	69	65.86
15	2.5	2.5	2.5	67	65.86

Table 12: Fit summary of the model

Source	Sequential p-value	Lack of Fit p-value	Adjusted R^2	Predicted R^2	
Linear	< 0.0001	0.1580	0.8302	0.7463	
2FI	0.6266	0.1320	0.8101	0.5564	
Quadratic	**0.0210**	**0.3889**	**0.9500**	**0.7829**	**Suggested**
Cubic	0.3889		0.9650		**Aliased**

$$RE(\%) = 65.86 + 15.97A + 3.71B - 2.34C + 3.07AC - 7.46A^2 \quad (10)$$

Equation (10) can be used to predict the F^- removal efficiency of the prepared composites. Generally, the negative sign typically denotes the antagonistic effects of factors, whereas the positive sign signifies the synergistic effects of the factors. Examining the coefficients and the power of the polynomial model factors, it is clear that the aluminium content has the most substantial influence on F^- removal, followed by the iron and titanium amounts.

To ensure that the polynomial model derived from the experimental data fits well, a significance test was conducted on the regression model's coefficient, lack-of-fit, and pure error. The significant factors were ranked based on their probability value (*p*-value) at a 95% confidence level. The analysis of variance (ANOVA) for the responses generated by Equation 10 is shown in Table 12. A smaller *p*-value ($p < 0.05$) indicates that the model is significant. Non-significant lack-of-fit ($p>0.05$) for the derived model implies the lack-of-fit is not substantial relative to pure error, and the model can accurately predict the variations.

The R-squared value serves as a measure of the fitted polynomial model's quality, indicating the proportion of the variability of the data accounted for in the statistical model. It is also more appropriate to use adjusted R^2 (Adj-R^2), which penalizes the statistic R^2 if unnecessary terms are added to the model (Fermoso *et al.*, 2010). In practice, R^2 should be at least 0.75, and values above 0.90 are deemed very good (Gunst, 1996; Hamada & Wu, 2000). In this study, the R^2, adjusted R^2 and predicted R^2-value for the response is close to 1, indicating the accuracy of the predicted polynomial model (Table 14). The adjusted R^2 (0.9432) is in reasonable agreement with the predicted R^2 (0.8676) (the difference is less than 0.2), evidencing a high correlation between the experimental and the predicted values. Furthermore, this suggests that the suggested regression model offers an acceptable explanation of how the independent variables and the response variable interact.

Adequate precision assesses the relationship between signal and noise ratio, and a ratio higher than four (4) is desirable. A ratio of 20.2606 is obtained in this study, indicating an adequate signal. Furthermore, this observation implies that the model has a robust signal for optimization purposes. The coefficient of variation (C.V.) provides insight into the extent of precision utilized when comparing the experiments (Gangadharan *et al.*, 2008). In this study, model repeatability is good, as evidenced by the small coefficient of variation (5.18%) presented in Table 14. The normal probability plots of the residual and experimental versus predicted values were used to determine the validity of the predicted model. The residuals are the difference between the predicted and actual values. The plots for the normal probability and the externally studentized residuals and the predicted versus actual values are demonstrated in Fig. 35. Figure 34(a) demonstrates that the residuals are generally distributed along the line of best fit, suggesting that errors are distributed properly and that the models do not contain any abnormalities. According to Fig. 34(b), it has been observed that the predicted values and experimental values within the design space are in good agreement.

Table 13: ANOVA for response surface-reduced quadratic model

Source	Sum of Squares	df	Mean Square	F-value	p-value	
Model	2441.01	5	488.20	47.51	< 0.0001	significant
A-Al	2041.60	1	2041.60	198.69	< 0.0001	
B-Fe	110.26	1	110.26	10.73	0.0096	
C-Ti	43.71	1	43.71	4.25	0.0692	
AC	37.82	1	37.82	3.68	0.0873	
A^2	207.61	1	207.61	20.20	0.0015	
Residual	92.48	9	10.28			
Lack of Fit	79.81	7	11.40	1.80	0.4028	not significant
Pure Error	12.67	2	6.33			
Cor Total	2533.48	14				

Table 14: Model fit statistics for model validation

Statistical parameters	Values of developed Model
R^2	0.9635
Adjusted R^2	0.9432
Predicted R^2	0.8676
Adeq. Precision	20.2606
Std. Dev.	3.21
Mean	61.88
C.V. %	5.18

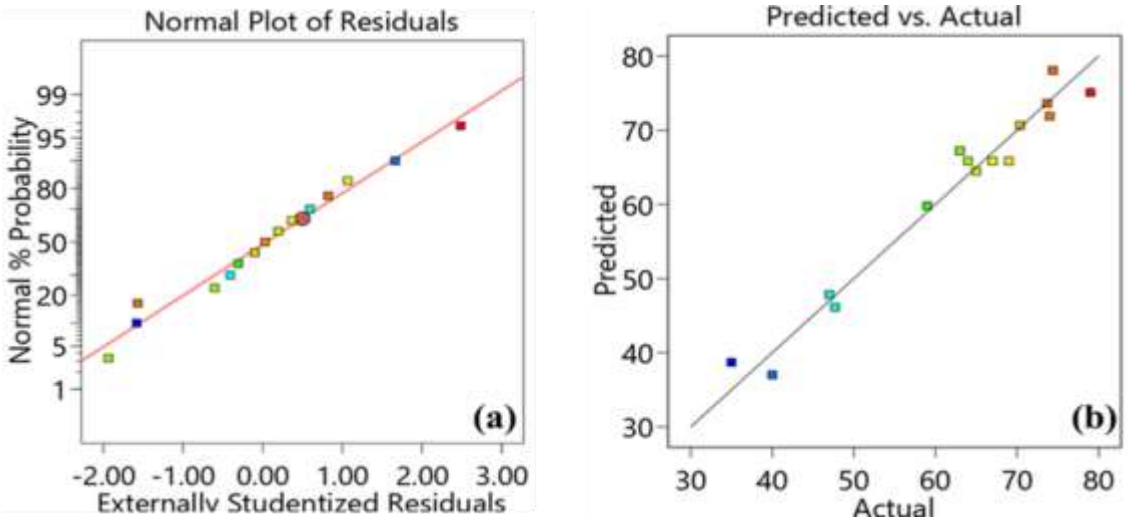

Figure 35: Normal probability plot and residual error for F^- RE% of AC–$Al_xFe_yTi_z$ (a) and predicted versus experimental F^- RE% (b)

4.7.2 Interaction between the variables and their influence on F− RE%

To examine the impacts of variable interactions on removal efficiency a three-dimensional response surface plot and its related contour were created based on a quadratic model. The interaction effects of the amount of aluminium and iron on fluoride removal efficiency are

shown in Fig. 36 (a, b). In contrast, Fig. 35(c, d) presents the interaction effect of the amount of aluminium and titanium. There is an observed increase in fluoride removal efficiency from 35 to 70.4% as the content of aluminium increases from ratio 1 to 4 while the amount of iron is kept at the lowest level. Also, a gradual increase in fluoride removal efficiency from 35 to 47.7 % was depicted when the amount of iron increased from a ratio1 to 4 while the amount of aluminium was kept at the lowest level. On the other hand, a significant increase in RE was observed when the amount of aluminium ratio increased. This was attributed to the strong affinity of F^- towards Al^{3+} as F^- has a high electronegativity and small ionic size (Chen *et al.*, 2022). Therefore, the above phenomenon is associated with a higher electrostatic attraction and more favorable F^- (hard base) interaction with hard acid Al^{3+} than Fe^{3+} (Alfarra *et al.*, 2004).

Moreover, in Fig. 35(a, b), the highest removal efficiency was achieved at the highest level of both aluminium and Titanium while the iron ratio was kept at the center. At the lowest level of titanium ratio and high aluminium ratio, removal efficiency increases from 47 to 73.7%. However, the model explains that combining the iron and titanium ratio does not significantly affect the F^- removal efficiency.

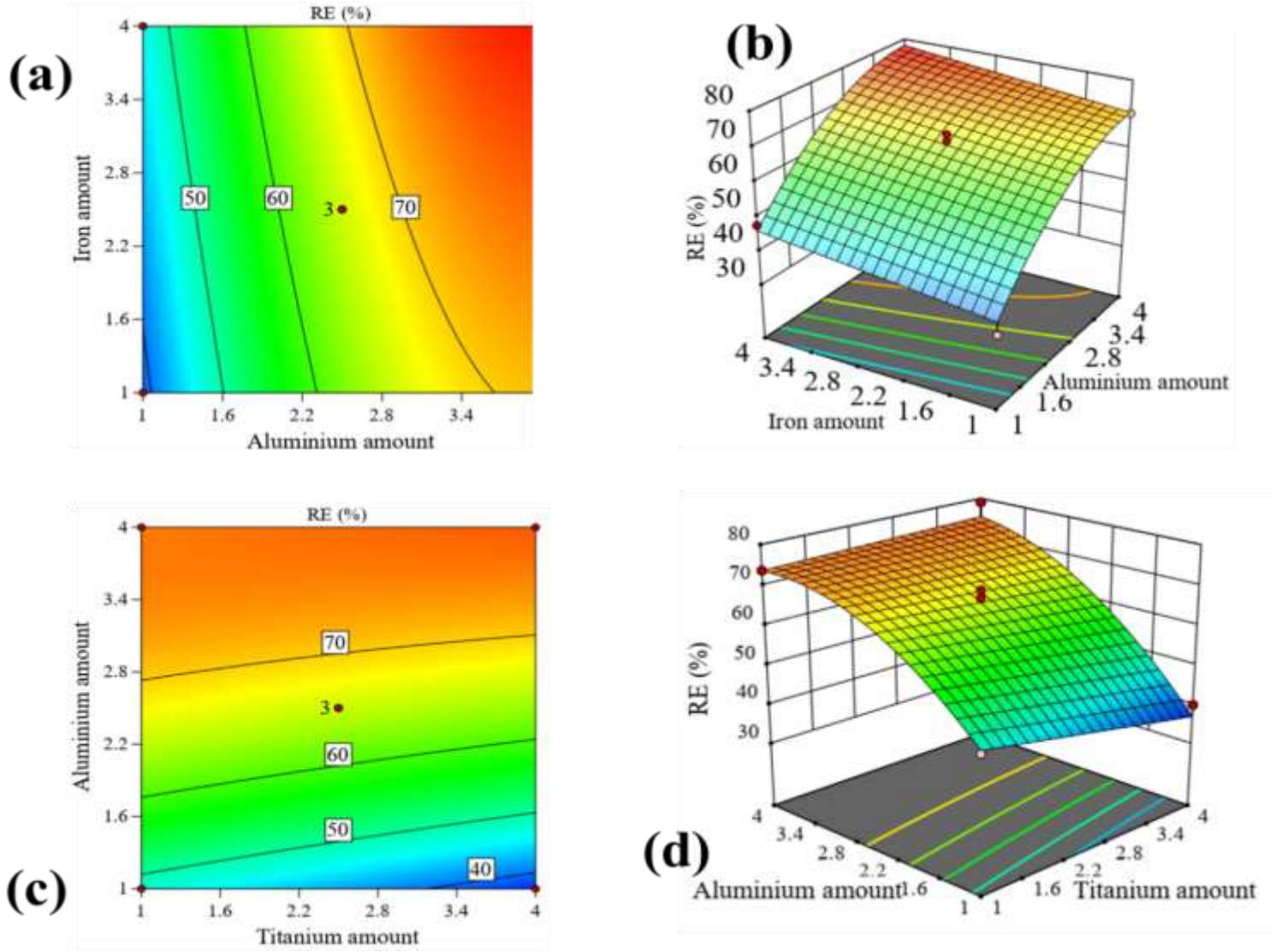

Figure 36: Contour and 3D response surface plots representing interactive effects of variables on RE: (a, b) aluminium and iron ratios, (c, d) aluminium and titanium ratios

4.7.3 Optimization using desirability functions

The optimized condition for the maximum F^- removal by the trimetallic oxide-loaded AC by the model is ratio 4:4:2.5 for Al, Fe, and Ti oxides, respectively, with the desirability of 0.993, a predicted mean of 74.38%, low and high predicted intervals of the response of 64.6 and 84.2%. Confirmatory experiments (three replicates) were conducted. The mean F^- removal efficiency was 80%, and a good agreement between the experimental and predicted values was observed because the obtained experimental response was within the acceptable response range predicted by the model.

4.8 Removal of PQ herbicide from water with capacitive deionization

Extensive studies have been carried out on CDI as a potential solution for removing inorganic pollutants from water. Nevertheless, its applicability in real-world water systems has exhibited limited practicality. Furthermore, rare studies investigated the potential of the CDI method for removing organic pollutants from water. Herein, the study investigated the use of CDI for the removal of PQ pesticide from water by using pristine AC electrodes and AC modified with metal oxide composites for the first time. Furthermore, the influence of various CDI operational factors, such as initial concentration of PQ, metal oxides mass loading, applied voltage, and treatment/charging time for PQ removal was examined in batch mode experiments.

4.8.1 The performance of commercial AC for PQ removal from synthetic water

(i) Effect of applied potential on the PQ removal

In Fig. 37, the variations in concentration and removal efficiency are portrayed in relation to the applied voltage, while maintaining a flow rate of 5 mL/min. To prevent water electrolysis and undesired faradaic reactions on the electrode, voltages above 1.2 V were not subjected to investigation (Porada *et al.,* 2013), as a result, controlling the applied voltage became a significant factor (Oladunni *et al.,* 2018). The removal efficiency increased as the applied voltage was raised from 0.8 to 1.2 V due to the stronger electrostatic forces generated by the higher potential (Jiang *et al.,* 2018). Therefore, as presented in Fig. 36, the higher PQ removal was achieved at 1.2 V with the initial concentration of 5 mg/L.

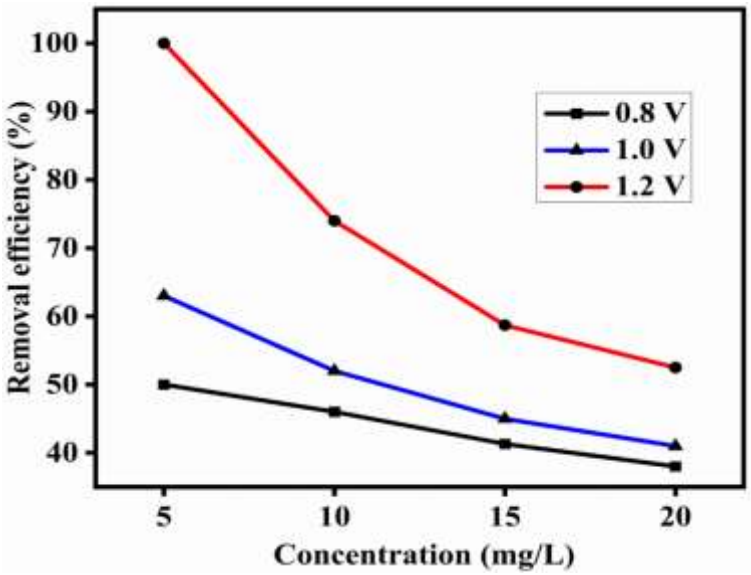

Figure 37: Removal efficiency of PQ at the different applied voltage at a flow rate of 5 mL/min

(ii) Effect of PQ initial concentration on the removal efficiency

The initial concentration of the feed solution is a critical parameter that significantly influences the functioning of the CDI system, as it can impact the effluent concentration of the outlet stream (Huyskens *et al.,* 2013). In this study, the CDI tests were conducted to study the effect of the initial concentration of PQ herbicide. The PQ concentration was varied from 5 to 20 mg/L while maintaining a constant flow rate of 5 mL/min and a voltage of 1.2 V. Figure 38(a) depicts the decrease in removal efficiencies as the initial concentration of PQ increased, aligning with the trend noted in various related studies (Jiang *et al.,* 2018). At PQ initial concentrations of 5, 10, 15, and 20 mg/L, the corresponding PQ removal efficiencies were 100%, 74%, 58.7%, and 52.5%, respectively. As the initial feed concentration increases, the reduction in removal efficiency can be ascribed to the quicker saturation of electric double layers (EDLs) at higher inlet concentrations (Hawks *et al.,* 2019; Huyskens *et al.,* 2013). Figure 37(b) illustrates that the electrosorption capacity is influenced by the initial solution concentration; as the concentration of the solution rises, the electrosorption capacity also experiences a corresponding increase. As the PQ concentration increased from 5 to 20 mg/L, the electrosorption capacity of the AC electrode experienced an approximate fourfold increase. The favorable impact of the initial concentration on the electrosorption capacity of AC electrodes can be attributed to the expansion of the diffuse double-layer capacity, primarily influenced by the concentration of the electrolyte solution (Jiang *et al.,* 2018).

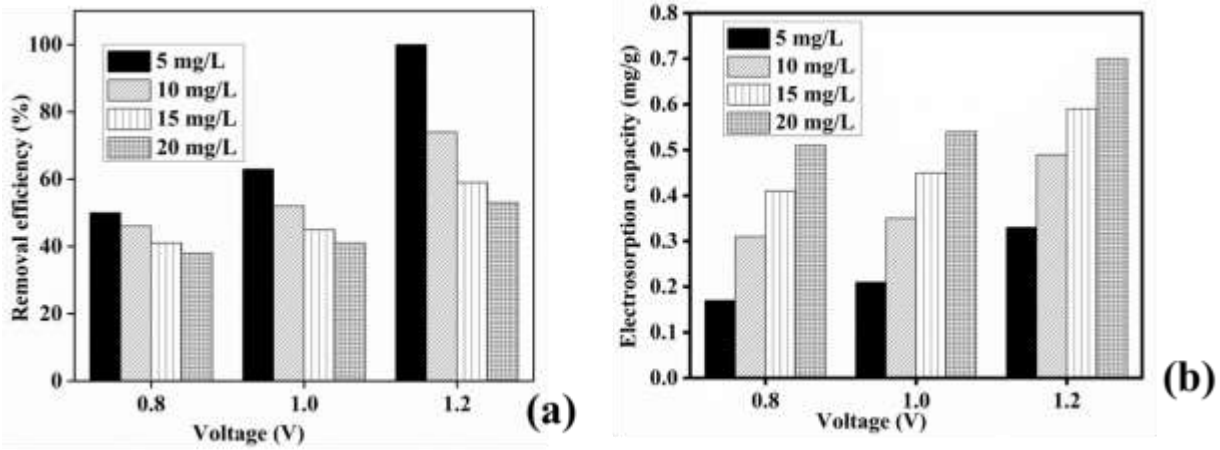

Figure 38: The removal efficiency and the electrosorption capacity of AC electrodes at various initial concentrations of PQ at different cell voltages and flow rate of 5 mL/min

(iii) Variation of PQ concentration with time

During the treatment/charging period, the concentration of ions in the solution reduces as some of the ions adsorb to the electrodes (Huang *et al.*, 2013a). The change in PQ concentration over time was investigated for two different voltage conditions, 0V and 1.2V, while maintaining a constant flow rate of 5 mL/min, with PQ initial concentration of 20 mg/L (Fig. 39). Applying a potential of 1.2 V resulted in a notable decrease in concentration within the initial 10 minutes, suggesting that PQ was rapidly electrosorbed onto the electrode surface. This phenomenon might be attributed to a substantial quantity of active sites present on the electrode surfaces, which are readily accessible for electrosorption processes. At 0 V, the PQ removal efficiency reached up to 16.5%; nonetheless, upon applying a voltage of 1.2 V, the removal efficiency significantly enhanced to 50%.

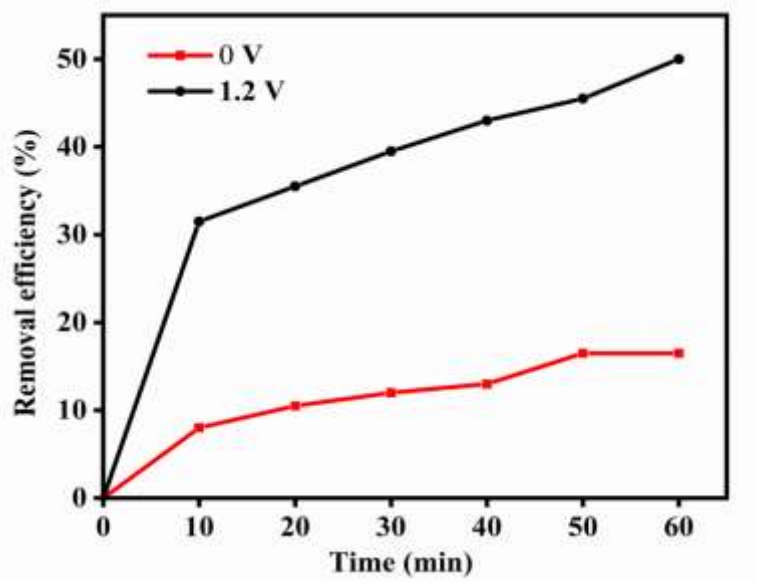

Figure 39: Paraquat herbicide removal efficiency versus time

4.8.2 The performance of AC modified with metal oxides for PQ removal

To improve the performance of AC, surface modification is important. Therefore, this study modified commercial AC with metal oxides to enhance the CDI performance for PQ pesticide removal. The Al_2O_3, Fe_2O_3 and TiO_2 were selected as modification agents in this work owning to their good cation exchange capacity, chemical stability, non-toxic nature and hydrophilicity (Cheng *et al.,* 2019; Mukherjee *et al.,* 2019; Rongchapo, 2015; Suriyaraj & Selvakumar, 2016; Wu *et al.,* 2016).

(i) The performance of AC/Al_2O_3, AC/ Fe_2O_3 and AC/ TiO_2 for PQ removal

In Fig. 40, the performance of various metal oxides loaded AC composite electrodes was compared by maintaining a metal oxide ratio of one (1) in all composites. The CDI experiments were conducted at a 1.2 V applied potential, 20 mg/L PQ initial concentration, 15 mL/min flow rate, and charging time of 1 h. The results showed that the RE of PQ was highest for the AC/Al_2O_3 composite (83%), followed by AC/Fe_2O_3 (70.5%) and AC/TiO_2 (59.5%). The higher RE observed for AC/Al_2O_3 could be attributed to the high cation exchange property of aluminium towards PQ, as previously reported by Rongchapo (2015). Based on these results, Al_2O_3 oxide was selected to investigate further the effect of metal oxides mass loading on AC for removing PQ from water. The Al_2O_3 modified AC composite with better RE (AC/Al_2O_3-1:1) was further investigated as CDI electrode material for removing PQ at different CDI controlling factors, including applied voltage, flow rate, and charging time, which was optimized to improve CDI performance.

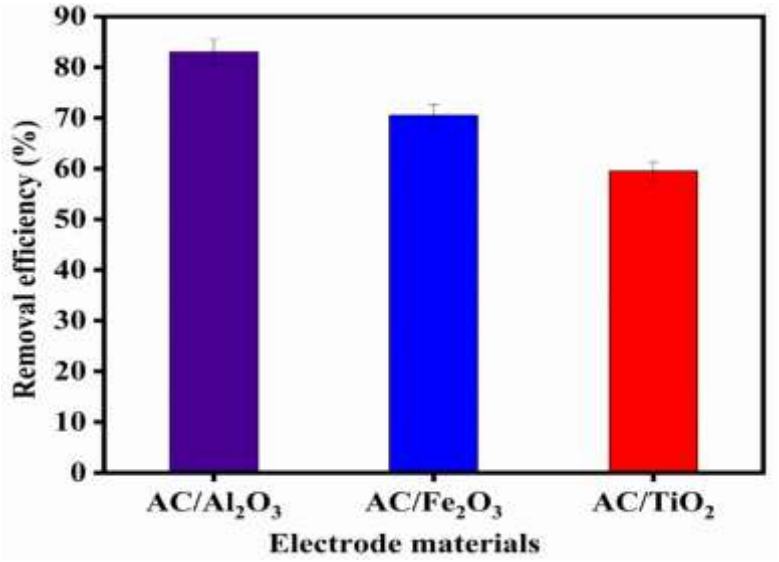

Figure 40: Paraquat herbicide removal efficiency for AC/Al_2O_3, AC/ Fe_2O_3 and AC/ TiO_2 composites

(ii) The effect of Al_2O_3 mass loading onto AC towards PQ removal efficiency

The loading of Al_2O_3 to the surface of AC has been shown to affect the electrosorption performance by modifying its chemical and textural properties. This modification leads to the formation of more surface active sites, which enriches the pore structure for better electrosorption of PQ (Kang *et al.,* 2017). Figure 41 demonstrates the Al_2O_3 mass loading effects AC surface for the PQ removal efficiency. The removal efficiency initially increases with Al_2O_3 loading, up to an equal ratio of AC/Al_2O_3, beyond which it decreases. This increase in removal efficiency at low Al_2O_3 loadings could be attributed to the enhanced surface properties of the AC, such as increased surface acidity and basicity, and the formation of new coordination sites and functional groups (Ganiyu *et al.,* 2016; Kazeem *et al.,* 2018). The decrease in removal efficiency observed when Al_2O_3 loading exceeds a 1:1 (AC/Al_2O_3) ratio may be due to excessive Al_2O_3 doping, leading to pore blockage on the AC modified carbon, which dominates the AC surface and lower the active sites as observed in the SEM results (Fig. 12 (e-g)). Therefore, a 1:1 ratio of AC/Al_2O_3 was found to be the optimum ratio and used for further parametric studies.

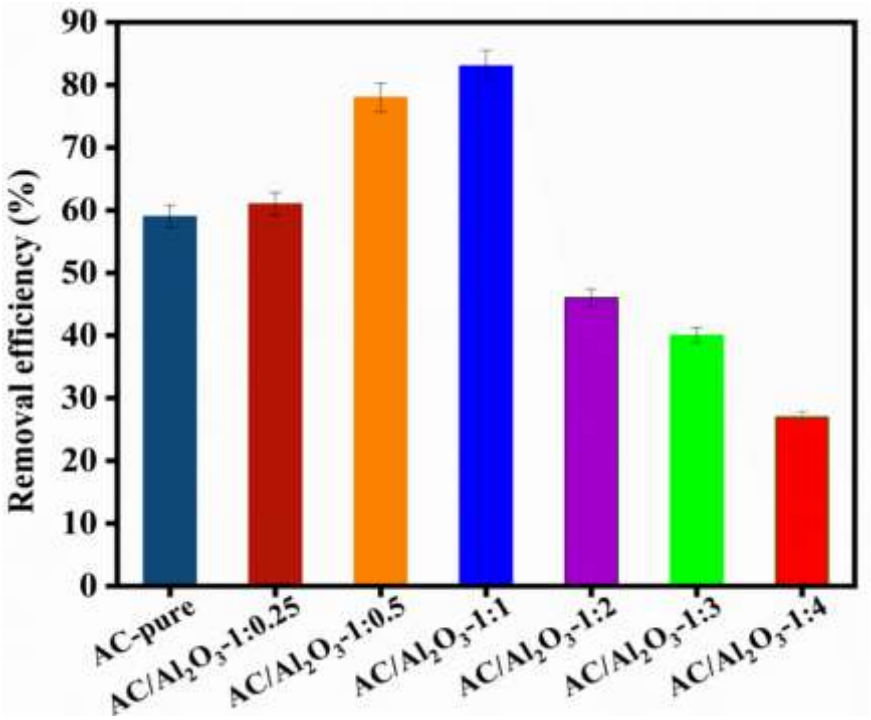

Figure 41: **Electrosorption of the unmodified AC and modified AC at different ratios of Al_2O_3 conducted at 20 mg/L PQ concentration, 1.2V applied voltage, 15 mL/min flowrate for 1 h**

(iii) Effect of applied potential

The applied voltage has a significant impact on the electrosorption efficiency in CDI. To investigate the relationship between RE and applied potential, a batch-mode experiment was conducted using AC/Al_2O_3-1:1 electrode for 20 mg/L PQ solution with three different applied voltages (0.6, 0.9, and 1.2 V), all below the voltage required for water splitting and with no potential as a control experiment. Each charging process lasted for 60 minutes. The results were presented in Fig. 42, which showed that the removal efficiency increased from 6 to 83% as the applied voltage increased from 0.0 V to 1.2 V. The removal efficiency under 1.2 V was about three times higher than that under 0.6 V. As expected, the increased voltage resulted in more ions being stored on the electrode surface due to capacitive electrosorption.

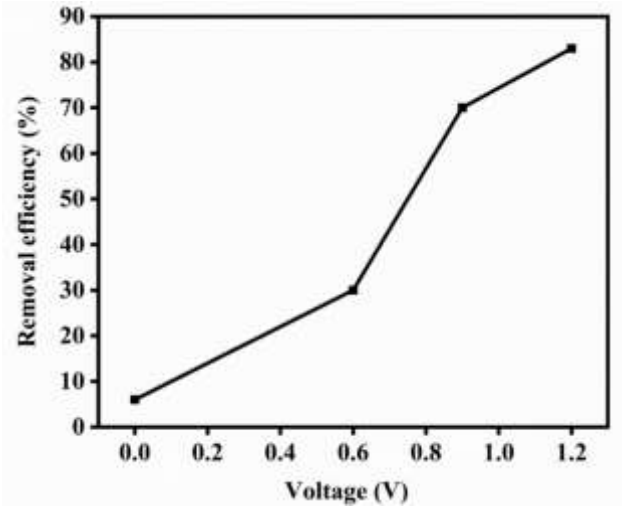

Figure 42: Effect of applied potential to PQ removal at 15mL/min, 20 mg/L initial concentration for 60 min

(iv) Effect of flow rate

Flow rate plays a critical role in determining the performance of CDI systems, impacting various factors such as ion removal efficiency, capacitance, and pressure drop. Therefore, optimizing the flow rate to achieve the desired ion removal efficiency is crucial to ensure efficient and energy-saving CDI systems. However, the optimal flow rate can vary based on the CDI system's design/size and operational conditions. In Fig. 43, the effect of flow rate on PQ removal efficiency at a constant applied voltage of 1.2 V and an initial PQ concentration of 20 mg/L is presented. The results show that the removal efficiency increases from 43 to 83% as the flow rate increases from 10 to 15 mL/min. However, when the flow rate further increased to 20 mL/min, the removal efficiency drops to 70%. Previous studies have also demonstrated that the electrode surface becomes rapidly saturated with ions as the flow rate increases beyond the optimum limit (Agartan *et al.*, 2019; Jande & Kim, 2014; Li *et al.*, 2019; Tang *et al.*, 2015).

The decrease in removal efficiency observed was due to less retention time for mass transfer inside the CDI cell (Ghorbani *et al.,* 2008; Mossad & Zou, 2012). Therefore, this study's optimal flow rate for achieving maximum removal efficiency is 15 mL/min.

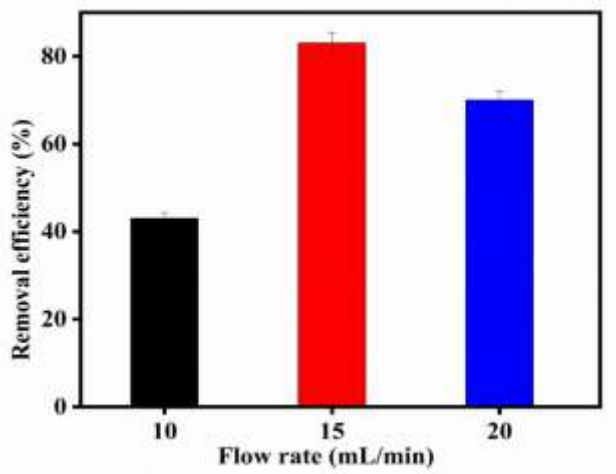

Figure 43: Effect of flow rate on PQ removal efficiency at 20 mg/L PQ initial concentration, 1.2 V applied potential for 60 min

(v) Effect of charging time

The length of the charging time is a crucial factor in the CDI process since it directly affects the number of ions that can be removed from water. However, the maximum number of ions that can be removed is determined by the electrodes' capacity, which means that overcharging can lead to reduced performance and a shorter lifespan for the electrodes. Therefore, it is necessary to find a balance between the charging time and the capacity of the electrodes toward ion removal to achieve optimal performance in the CDI process. Figure 44 illustrates the impact of charging time on the PQ herbicide removal efficiency. To evaluate this effect, CDI tests were performed at various charging times (60, 120, 180, and 240 minutes). As presented in Fig. 43, there was a gradual increase in the removal efficiency from 60 minutes to 180 minutes. This implies that the electrodes had not yet reached a saturated state by the end of the charging half cycle, and the electrodes' active mass was underutilized for PQ removal in these instances. Conversely, no significant increase in removal efficiency was observed when the charging time was extended to 240 minutes. This indicates that the electrodes had reached a saturated state, as reported in other related studies (Agartan *et al.,* 2019; Zhu *et al.,* 2019).

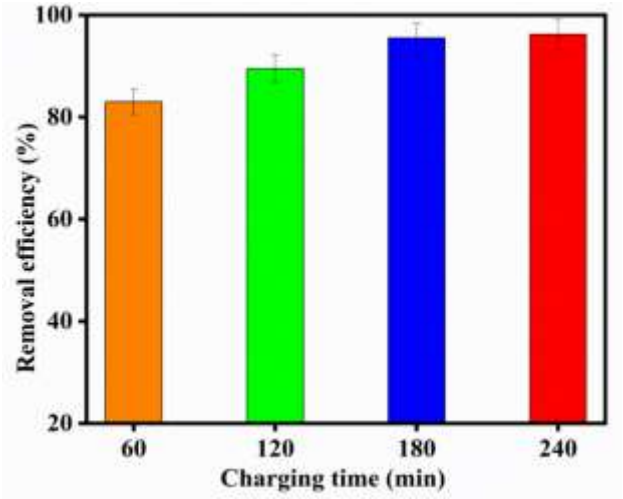

Figure 44: The influence of charging time for the PQ removal from water at 20 mg/L, 15 mL/min, and 1.2 V applied voltage

(vi) Change in pH during the electrosorption process

The pH of the effluent can change significantly due to electrode reactions like oxidation, reduction, or water-splitting during electrosorption (He *et al.*, 2016; Zhang *et al.*, 2018). Therefore, to investigate whether electrode reactions were happening during the electrosorption process, the pH of the effluent was monitored and presented in Fig. 45. The results showed that at an applied potential of 1.2 V, 15 mL/min flow rate, and 20 mg/L initial concentration, the pH of the effluent slightly decreased from about 8.2 to 7.1 for AC/Al_2O_3-1:1 and 8.2 to 6.5 for AC during the electrosorption stage. This pH range was still within the acceptable limits of drinking water set by the EPA (6.5-8.5) and WHO (6.5- 8.2) (Water & Organization, 2006). Therefore, it was concluded that no Faradaic reactions, such as redox reactions and water hydrolysis, occurred during the electrosorption process, as the pH of the solution did not become more acidic or basic and was maintained within the acceptable range.

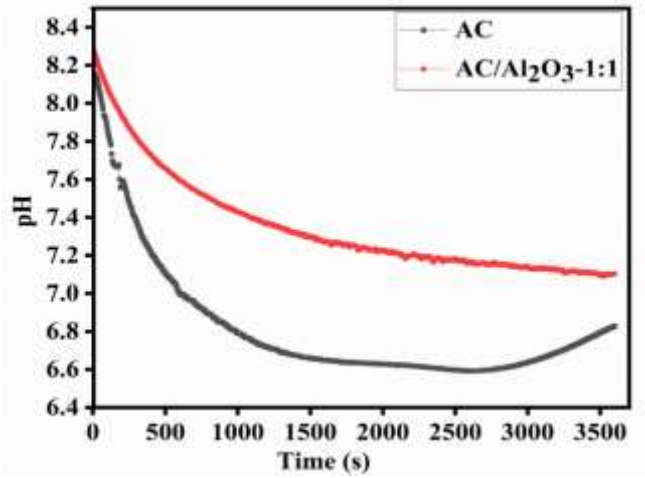

Figure 45: Changes in pH during half cycle CDI process at 15 mL/min, 1.2 V, and 20 mg/L initial concentration for AC and AC/Al_2O_3-1:1

(vii) Energy consumption during PQ removal

This study conducted the CDI test at a constant voltage mode. Thus, a constant potential of 1.2 V was applied in the chronoamperometry measurements to determine the current response to the pristine AC and AC/Al_2O_3-1:1 electrode during electrosorption and its stabilization over time. As a result, it is possible to determine the energy consumption. The energy consumed during PQ removal was calculated by using Equation 7 and found to be 0.11 and 0.055 kWh/m^3 for AC and AC/Al_2O_3-1:1 electrode, respectively. This indicates that the modified carbon minimized the energy consumption of the CDI system and enhanced PQ removal efficiency, as the energy consumed during PQ electrosorption was about two times less than the unmodified carbon.

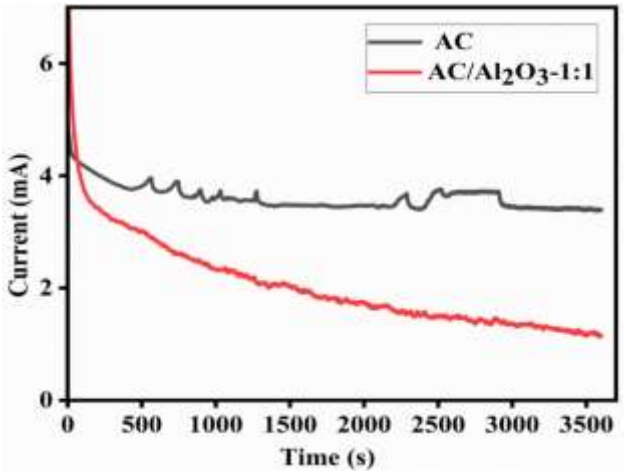

Figure 46: The current response of the AC and AC/Al_2O_3-1:1 during PQ removal from water

(viii) The performance of AC/Al_2O_3-1:1 for PQ removal from a natural water

Various organic contaminants and ions in herbicide-containing wastewater can affect the electrosorption of herbicides onto electrodes. To determine whether the synthesized electrode material (AC/Al_2O_3-1:1) is commercially viable, electrosorption experiments were conducted using tap water collected from the NM-AIST campus, spiked with 20 mg/L of PQ. The experiment was conducted with a charging time of 3 hours, a flow rate of 15 ml/min, and a solution volume of 40 ml, at an applied potential of 1.2 V. The performance of the AC/Al_2O_3-1:1 electrode material in removing PQ from both natural and simulated water (containing only paraquat) was compared, and the results were presented in Fig. 47. The results showed that in the presence of different ions and other contaminants, the removal efficiency and electrosorption capacity of the AC-Al_2O_3 electrode surface for PQ removal in tap water were 87.5% and 1.17 mg/g, respectively. The slight decrease in removal efficiency and

electrosorption capacity may be due to other impurities and ions in natural water, which compete with PQ for the available electrode surface sites (Dehghani *et al.*, 2021). The excellent removal efficiency demonstrated by the AC/Al_2O_3-1:1 composite in removing PQ from natural water indicates its potential as CDI electrode material for commercial application.

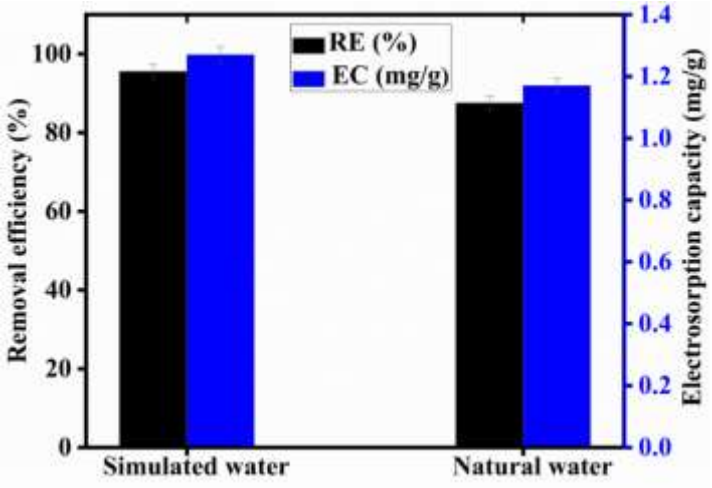

Figure 47: Effect of various ions on the adsorption of PQ by AC/Al_2O_3-1:1 composite

(ix) Electrosorption/desorption study

To evaluate the reusability of the AC/Al_2O_3-1:1 electrosorption desorption experiments conducted at 1.2 V charging for 60 min and -1.2 V discharging for 30 min for 10 cycles, 15 ml/min flow rate, 20 mg/L of the PQ solution. Desorption efficiency was calculated using Equation 9. Figure 48 shows that PQ desorption efficiency decreased from 77% to 75% after the initial reuse cycle and dropped to 73.7% after 10 cycles. This represents a 4.3% decrease in desorption efficiency after 10 cycles of electrode regeneration. The observed slight decline in desorption percentage may be attributed to the electrode's pores becoming filled with PQ molecules.

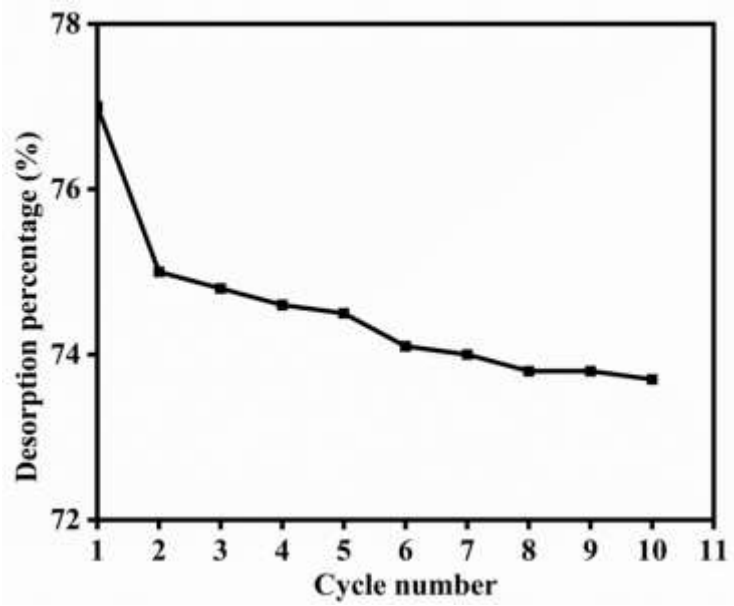

Figure 48: Reusability of AC/Al_2O_3-1:1 composite for removal PQ from water

(x) The combination effect of metal oxides on AC surface for PQ removal

Figure 49 presented the PQ removal efficiency of AC modified with bimetallic oxides (AC-Al_2O_3/Fe_2O_3, AC-Al_2O_3/TiO_2, AC/Fe_2O_3/TiO_2) and trimetallic oxide (AC/$Al_2O_3/Fe_2O_3/TiO_2$) composites. The ratio of metal oxides in all samples was maintained at 1. The results showed that the AC/$Al_2O_3/Fe_2O_3/TiO_2$ composite had the highest PQ removal efficiency of 97.9%, followed by AC-Al_2O_3/Fe_2O_3 with 87.5%, AC/Fe_2O_3/TiO_2 with 72.5%, and AC-Al_2O_3/TiO_2 with 65.5% under the same experimental conditions of 1.2 V applied potential, 15 mL/min flow rate, 20 mg/L PQ initial concentration, and 1 h charging time. The good performance of the AC/$Al_2O_3/Fe_2O_3/TiO_2$ electrode material can be attributed to the synergistic effect of the three metal oxides loaded on the AC surface, as stated in previous studies (Wang *et al.*, 2021).

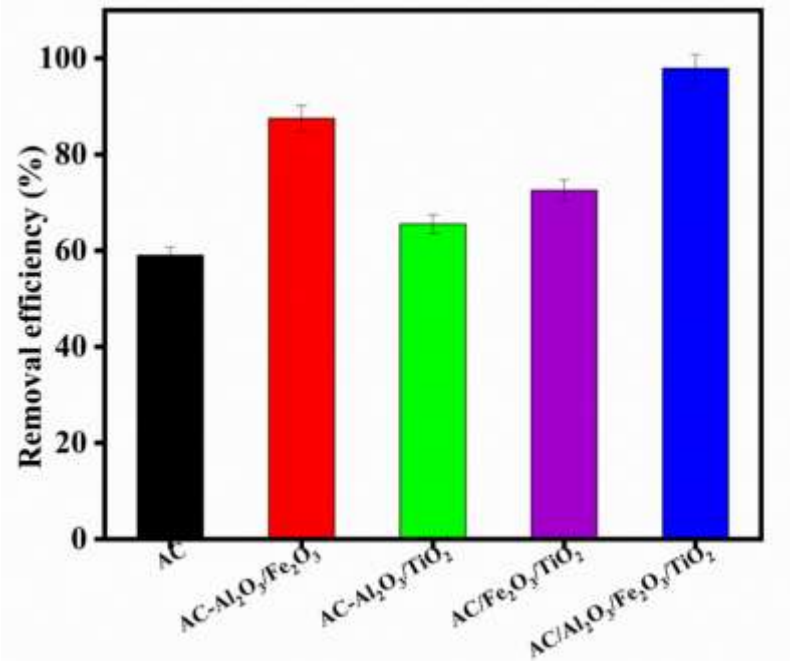

Figure 49: The performance of bimetallic and trimetallic loaded AC composites for PQ removal

(xi) Removal mechanism of paraquat herbicide

The possible PQ removal mechanisms, may include the electrostatic force of attraction, presence of oxygen-containing groups, and cation exchange mechanism (Rongchapo, 2015; Sabzehmeidani *et al.*, 2020). In this study, the electrostatic force of attraction induced by the potential applied on the electrode surface affected the PQ removal, as evidenced in Fig. 36 and Fig. 41, which confirm that the applied potential has a great contribution to the PQ removal. Additionally, the presence of oxygen-containing groups such as carboxyl (–COOH), epoxy (C–O), and hydroxyl (–OH) on the obtained composite, as evidenced by FTIR spectra (Fig. 20 and 21), may act as active binding sites for PQ removal. The cation exchange mechanism can also contribute to PQ removal. In the study conducted by Rongchapo (2015), aluminium groups have been found to have good cation exchange capacity with PQ. Thus, the high removal efficiency evidenced by the AC-Al_2O_3 composite in this study (Fig. 39) could be associated with the presence of aluminium on the AC surface. The FTIR measurements of the AC-Al_2O_3/Fe_2O_3 electrode before and after electrosorption were conducted to understand further the CDI PQ removal mechanism, and the results are presented in Fig. 49. From Fig. 50, the peaks at about 547, 1060, and 2355 cm^{-1} shifted, and the peak at 722 cm^{-1} disappeared, indicating its involvement in PQ removal. Therefore, the results indicated that cation exchange, electrostatic force of attraction, and complexation/coordination all played a role in PQ removal.

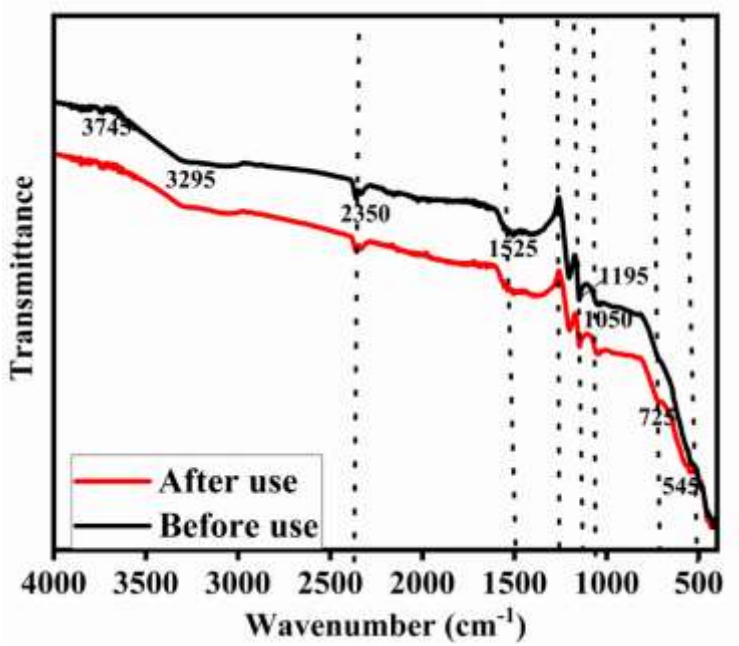

Figure 50: Fourier-transform infrared spectroscopy spectra of AC-Al_2O_3/Fe_2O_3 electrode before and after CDI experiment

CHAPTER FIVE

CONCLUSION AND RECOMMENDATIONS

5.1 Conclusion

In this study, composites of activated carbon and metal oxides (Al_2O_3, Fe_2O_3 and TiO_2) were successfully synthesized by one pot and simple co-precipitation method for fluoride (F^-) and paraquat (PQ) herbicide removal from synthetic and natural water with the green and energy saving CDI method. The surface properties of the prepared composites were determined from several characterization methods, including SEM, EDS, TEM, BET, FTIR, XRD and electrochemical measurements. The EDS and SEM analysis revealed the successful loading of metal oxide on the AC surface, which jointly enhanced the F^- and PQ herbicide removal. The textural and electrochemical characterization results showed that AC–$Al_4Fe_{2.5}Ti_4$ composite was amorphous with good wettability of 56.6° and enhanced specific capacitance of 826 F/g. Also, the EIS analysis showed that AC–$Al_4Fe_{2.5}Ti_4$ composite had lower resistance and better charge transferability than the pristine AC.

Additionally, the developed AC–$Al_xFe_yTi_z$ CDI electrode materials for water defluoridation prepared at different ratios of metal oxides demonstrated significant variations of RE values (35–79%) owing to the variations in the process parameters. The interactive effect of the process parameters on the F^- removal efficiency was determined using RSM based on BBD. A quadratic model was proposed for RE response, and the predicted values by the model were in excellent agreement with the experimental values. The RSM study revealed that the Al, Fe, and Ti loading ratio on AC plays a significant role in F^- removal. Moreover, an increase in Al loading in the synthesis process greatly influenced the enhancement of the F^- RE. Furthermore, AC–$Al_4Fe_{2.5}Ti_4$ decreased F^- concentration from natural water from an initial concentration of 5.15 to 1.18 mg/L (below the permissible limit of the WHO), showing its feasibility for real industry applications.

Additionally, the results demonstrated that CDI technology is a promising alternative method for removing different organic pollutants from water, including PQ herbicide. Also, the performance of AC/Al_2O_3-1:1 for PQ removal was compared with that of unmodified AC. The wettability of pristine AC among other properties were significantly improved by the successful loading of Al_2O_3; thereby leading to enhanced performance as evidenced by 95.5%, 1.27 mg/g, and 0.055 kWh/m^3 removal efficiency, electrosorption capacity, and energy consumption of AC/Al_2O_3-1:1 composite compared to 62%, 0.83 mg/g and 0.11 kWh/m^3 of

pure AC. The PQ removal was found to depend on the Al_2O_3 loading, applied potential, flow rate, charging time, and aluminium oxide content. The optimum CDI parameters for PQ removal were 1.2 V applied potential, 15 mL/min flow rate, 3 hrs charging time and the optimum composite of AC/Al_2O_3-1:1. Moreover, presence of other ions/pollutants had negligible interference on PQ removal as the removal efficiency and electrosorption capacity of the AC/Al_2O_3-1:1 composite in both simulated (95.5%, 1.27 mg/g) and natural water (87.5% 1.17 mg/g) was found to be comparable. The high removal efficiency and electrosorption capacity of AC/Al_2O_3-1:1 composite in natural water coupled with its high desorption efficiency shows its huge commercial applicability in PQ removal.

5.1 Recommendations

This study investigated the performance of activated carbon composited with metal oxides as electrode materials for defluoridation and removing paraquat from water with CDI technology. Based on the findings of this study, these are recommendations:

(i) Future work should consider the simultaneous removal of fluoride and paraquat herbicides with an asymmetric CDI system.

(ii) The dissolution of metals for the synthesized composites electrode materials was not analyzed it was out of scope of this study; therefore, future work should study if there were the release of the metal ions into the solution during CDI performance using Inductively Coupled Plasma Mass Spectrometry (ICP-MS) and evaluate if their concentration is below or above the recommended limit in drinking water.

(iii) In future studies, it would be beneficial to analyze further the electrode materials used for removing fluoride and paraquat pesticides before and after the electrosorption process to confirm further the removal mechanism of the fluoride and paraquat herbicides. In addition, x-ray photoelectron spectroscopy (XPS) can be utilized to understand better the removal mechanism involved in the process.

(iv) The cost analysis of the prepared CDI electrode materials and its selectivity to other non-targeted contaminants in the collected real water samples after CDI testing should be investigated in further studies.

(v) Future studies should consider developing electrode/ probe sensors for PQ herbicide detection in water sources.

(vi) Future studies should focus on developing a database that documents the presence of various pesticides in different water sources across Tanzania to raise awareness among the government, water stakeholders, and the public about the safety of the available water sources used for human consumption as well the establishment of pesticides concentrations standards in drinking water.

(vii) Because of the scarcity of resources, the CDI system was not scaled up beyond the laboratory level to the point where it could be applied at the household level (lab to market). Consequently, the developed electrode materials for defluoridation and PQ removal were not subjected to large-scale testing. Therefore, future studies should focus on exploring the commercial application of the CDI system for defluoridation and paraquat pesticide removal.

(viii) The characterization of the byproducts formed during paraquat dissociation and their potential health impacts was not evaluated in this study. To address this limitation in future studies, utilizing Gas Chromatography-Mass Spectrometry (GC-MS) equipment for characterization is recommended.

REFERENCES

Achilleos, D. S., & Hatton, T. A. (2016). Selective molecularly mediated pseudocapacitive separation of ionic species in solution. *ACS Applied Materials & Interfaces*, *8*(48), 32743-32753.

Agartan, L., Hayes-Oberst, B., Byles, B. W., Akuzum, B., Pomerantseva, E., & Caglan Kumbur, E. (2019). Influence of operating conditions and cathode parameters on desalination performance of hybrid CDI systems. *Desalination*, *452*, 1-8.

Ahmad, A., Tan, L., & Shukor, S. A. (2008). Dimethoate and atrazine retention from aqueous solution by nanofiltration membranes. *Journal of Hazardous Materials*, *151*(1), 71-77.

Al-Hayali, S. K. M., Mohammed, D. Z., Khaleel, W. A., & Al-Janabi, A. H. (2017). Aluminum oxide nanoparticles as saturable absorber for C-band passively Q-switched fiber laser. *Applied Optics*, *56*(16), 4720-4726.

Aldalbahi, A., Rahaman, M., Almoiqli, M., Hamedelniel, A., & Alrehaili, A. (2018). Single-Walled Carbon Nanotube (SWCNT) Loaded Porous Reticulated Vitreous Carbon (RVC) Electrodes Used in a Capacitive Deionization (CDI) Cell for Effective Desalination. *Nanomaterials (Basel)*, *8*(7), 1-20.

Alfarra, A., Frackowiak, E., & Béguin, F. (2004). The HSAB concept as a means to interpret the adsorption of metal ions onto activated carbons. *Applied Surface Science*, *228*(1-4), 84-92.

Alfredy, T., Jande, Y. A. C., & Pogrebnaya, T. (2019). Removal of lead ions from water by capacitive deionization electrode materials derived from chicken feathers. *Journal of Water Reuse and Desalination*, *9*(3), 282-291.

Ali, I., Alharbi, O. M., ALOthman, Z. A., Al-Mohaimeed, A. M., & Alwarthan, A. (2019). Modeling of fenuron pesticide adsorption on CNTs for mechanistic insight and removal in water. *Environmental Research*, *170*, 389-397.

Anasori, B., Lukatskaya, M. R., & Gogotsi, Y. (2017). 2D metal carbides and nitrides (MXenes) for energy storage. *Nature Reviews Materials*, *2*(2), 1-17.

Angeles, A., Park, J., Ham, K., Bong, S., & Lee, J. (2022). High-performance capacitive deionization electrodes through regulated electrodeposition of manganese oxide and

nickel-manganese oxide/hydroxide onto activated carbon. *Separation and Purification Technology*, *280*, 119873.

Atkinson, S. (2021). *Voltea Helps Secure Water Supply for Manufacturer in South Africa.* https://scholar.google.com

Aungpradit, T., Sutthivaiyakit, P., Martens, D., Sutthivaiyakit, S., & Kettrup, A. (2007). Photocatalytic degradation of triazophos in aqueous titanium dioxide suspension: Identification of intermediates and degradation pathways. *Journal of Hazardous Materials*, *146*(1-2), 204-213.

Aw, S., Briton, B. G. H., Drogui, P., Yao, K. B., & Adouby, K. (2022). Removal of fluoride in groundwater by adsorption using hydroxyapatite modified Corbula trigona shell powder. *Chemical Engineering Journal Advances*, *12*, 100386.

Aydar, A. Y. (2018). Utilization of response surface methodology in optimization of extraction of plant materials. *Statistical Approaches with Emphasis on Design of Experiments Applied to Chemical Processes*, 73690, 157-169.

Ayoob, S., Gupta, A., & Bhat, V. T. (2008). A conceptual overview on sustainable technologies for the defluoridation of drinking water. *Critical Reviews in Environmental Science and Technology*, *38*(6), 401-470.

Ayoob, S., & Gupta, A. K. (2006). Fluoride in drinking water: A review on the status and stress effects. *Critical Reviews in Environmental Science and Technology*, *36*(6), 433-487.

Bai, Z., Hu, C., Liu, H., & Qu, J. (2019). Selective adsorption of fluoride from drinking water using NiAl-layered metal oxide film electrode. *Journal of Colloid and Interface Science*, *539*, 146-151.

Bao, S., Chen, Q., Zhang, Y., & Tian, X. (2021). Optimization of preparation conditions of composite electrodes for selective adsorption of vanadium in CDI by response surface methodology. *Chemical Engineering Research and Design*, *168*, 37-45.

Bao, S., Xin, C., Zhang, Y., Chen, B., Ding, W., & Luo, Y. (2023). Application of Capacitive Deionization in Water Treatment and Energy Recovery: A Review. *Energies*, *16*(3), 1-24.

Barroso-Bogeat, A., Alexandre-Franco, M., Fernández-González, C., Macías-García, A., & Gómez-Serrano, V. (2014). Electrical conductivity of activated carbon–metal oxide nanocomposites under compression: A comparison study. *Physical Chemistry Chemical Physics*, *16*(45), 25161-25175.

Barta, J., Pospisil, M., & Cuba, V. (2014). Indirect synthesis of Al_2O_3 via radiation- or photochemical formation of its hydrated precursors. *Materials Research Bulletin*, *49*, 633-639.

Baş, D., & Boyacı, İ. H. (2007). Modeling and optimization I: Usability of response surface methodology. *Journal of Food Engineering*, *78*(3), 836-845.

Behera, S. K., Meena, H., Chakraborty, S., & Meikap, B. C. (2018). Application of response surface methodology (RSM) for optimization of leaching parameters for ash reduction from low-grade coal. *International Journal of Mining Science and Technology*, *28*(4), 621-629.

Benítez-Guerrero, M., Pérez-Maqueda, L. A., Sánchez-Jiménez, P. E., & Pascual-Cosp, J. (2014). Characterization of thermally stable gamma alumina fibres biomimicking sisal. *Microporous and Mesoporous Materials*, *185*, 167-178.

Bertrand, P. G. (2019). *Uses and Misuses of Agricultural Pesticides in Africa: Neglected Public Health Threats for Workers and Population*. https://scholar.google.com

Bezerra, M. A., Santelli, R. E., Oliveira, E. P., Villar, L. S., & Escaleira, L. A. (2008). Response surface methodology (RSM) as a tool for optimization in analytical chemistry. *Talanta*, *76*(5), 965-977.

Bharath, G., Arora, N., Hai, A., Banat, F., Savariraj, D., Taher, H., & Mangalaraja, R. (2020). Synthesis of hierarchical Mn_3O_4 nanowires on reduced graphene oxide nanoarchitecture as effective pseudocapacitive electrodes for capacitive desalination application. *Electrochimica Acta*, *337*, 135668.

Bharath, G., Hai, A., Rambabu, K., Pazhanivel, T., Hasan, S. W., & Banat, F. (2021). Designed assembly of Ni/MAX (Ti_3AlC_2) and porous graphene-based asymmetric electrodes for capacitive deionization of multivalent ions. *Chemosphere*, *266*, 129048.

Boutin, C., Héduit, A., & Helmer, J. M. (2009). *Technologies D'épuration En Vue D'une Réutilisation Des Eaux Usées Traitées* irstea]. https://scholar.google.com

Box, G. E. P., & Behnken, D. W. (1960). Some New Three Level Designs for the Study of Quantitative Variables. *Technometrics*, *2*(4), 455-475.

Bromilow, R. H. (2004). Paraquat and sustainable agriculture. *Pest Management Science: Formerly Pesticide Science*, *60*(4), 340-349.

Brown, R., Clapp, M., Dyson, J., Scott, D., Wheals, I., & Wilks, M. (2004). Paraquat in perspective. *Outlooks on Pest Management*, *15*(6), 259-267.

Cai, H. M., Chen, G. J., Peng, C. Y., Zhang, Z. Z., Dong, Y. Y., Shang, G. Z., Zhu, X H., Gao, H. J., & Wan, X. C. (2015). Removal of fluoride from drinking water using tea waste loaded with Al/Fe oxides: A novel, safe and efficient biosorbent. *Applied Surface Science*, *328*, 34-44.

Canada, H. (2011). *Guidelines for Canadian Drinking Water Quality: Guideline Technical Document: Enteric Viruses*. https://scholar.google.com

Castello, P. R., Drechsel, D. A., & Patel, M. (2007). Mitochondria are a major source of paraquat-induced reactive oxygen species production in the brain. *Journal of Biological Chemistry*, *282*(19), 14186-14193.

Chakrabortty, S., Roy, M., & Pal, P. (2013). Removal of fluoride from contaminated groundwater by cross flow nanofiltration: transport modeling and economic evaluation. *Desalination*, *313*, 115-124.

Che, N., Liu, L., Liu, Y., & Li, C. (2021). Application and influence factors of capacitive deionization method for removing inorganic contaminated ions. *Environmental Pollutants and Bioavailability*, *33*(1), 365-376.

Che, X., Wang, S., Li, C., Wang, G., Li, C., Wang, S., Li, D., & Qiu, J. (2019). Inverted Capacitive Deionization with Highly Enhanced Stability Performance Utilizing Ionic Liquid-Functionalized Carbon Electrodes. *ACS Sustainable Chemistry & Engineering*, *7*(18), 15715-15722.

Chen, J., Yang, R., Zhang, Z., & Wu, D. (2022). Removal of fluoride from water using aluminum hydroxide-loaded zeolite synthesized from coal fly ash. *Journal of Hazardous Materials*, *421*, 126817.

Chen, L., He, B. Y., He, S., Wang, T. J., Su, C. L., & Jin, Y. (2012). Fe—Ti oxide nano-adsorbent synthesized by co-precipitation for fluoride removal from drinking water and its adsorption mechanism. *Powder Technology*, *227*, 3-8.

Chen, W., He, X., Jiang, Z., Li, B., Li, X. Y., & Lin, L. (2023). A capacitive deionization and electro-oxidation hybrid system for simultaneous removal of heavy metals and organics from wastewater. *Chemical Engineering Journal*, *451*, 139071.

Chen, Y. J., Liu, C. F., Hsu, C. C., & Hu, C. C. (2019). An integrated strategy for improving the desalination performances of activated carbon-based capacitive deionization systems. *Electrochimica Acta*, *302*, 277-285.

Chen, Y., Yue, M., Huang, Z. H., & Kang, F. (2014). Electrospun carbon nanofiber networks from phenolic resin for capacitive deionization. *Chemical Engineering Journal*, *252*, 30-37.

Cheng, Y., Hao, Z., Hao, C., Deng, Y., Li, X., Li, K., & Zhao, Y. (2019). A review of modification of carbon electrode material in capacitive deionization. *RSC Advances*, *9*(42), 24401-24419.

Chuah, C. J., Lye, H. R., Ziegler, A. D., Wood, S. H., Kongpun, C., & Rajchagool, S. (2016). Fluoride: A naturally-occurring health hazard in drinking-water resources of Northern Thailand. *Science of the Total Environment*, *545*, 266-279.

Cochemé, H. M., & Murphy, M. P. (2008). Complex I is the major site of mitochondrial superoxide production by paraquat. *Journal of Biological Chemistry*, *283*(4), 1786-1798.

Costello, S., Cockburn, M., Bronstein, J., Zhang, X., & Ritz, B. (2009). Parkinson's disease and residential exposure to maneb and paraquat from agricultural applications in the central valley of California. *American Journal of Epidemiology*, *169*(8), 919-926.

Czitrom, V. (1999). One-Factor-at-a-Time versus Designed Experiments. *The American Statistician*, *53*(2), 126-131.

Dahiya, S., Singh, A., & Mishra, B. K. (2021). Capacitive deionized hybrid systems for wastewater treatment and desalination: A review on synergistic effects, mechanisms and challenges. *Chemical Engineering Journal*, 417, 128129.

Daneshvar, N., Aber, S., Khani, A., & Khataee, A. (2007). Study of imidaclopride removal from aqueous solution by adsorption onto granular activated carbon using an on-line spectrophotometric analysis system. *Journal of Hazardous materials*, *144*(1-2), 47-51.

De Souza, D., Machado, S. A., & Pires, R. C. (2006). Multiple square wave voltammetry for analytical determination of paraquat in natural water, food, and beverages using microelectrodes. *Talanta*, *69*(5), 1200-1207.

Dehghani, Z., Sedghi-Asl, M., Ghaedi, M., Sabzehmeidani, M. M., & Adhami, E. (2021). Ultrasound-assisted adsorption of paraquat herbicide from aqueous solution by graphene oxide/mesoporous silica. *Journal of Environmental Chemical Engineering*, 9(2), 105043.

Dong, Q., Yang, D., Luo, L., He, Q., Cai, F., Cheng, S., & Chen, Y. (2021). Engineering porous biochar for capacitive fluorine removal. *Separation and Purification Technology*, 257, 117932.

Elazhar, F., Tahaikt, M., Achatei, A., Elmidaoui, F., Taky, M., El Hannouni, F., Laaziz, I., Jariri, S., El Amrani, M., & Elmidaoui, A. (2009). Economical evaluation of the fluoride removal by nanofiltration. *Desalination*, *249*(1), 154-157.

Elisadiki, J., Jande, Y. A. C., Kibona, T. E., & Machunda, R. L. (2020). Highly porous biomass-based capacitive deionization electrodes for water defluoridation. *Ionics*, *26*(5), 2477-2492.

Elisadiki, J., Jande, Y. A. C., Kibona, T. E., & Machunda, R. L. (2020). Highly porous biomass-based capacitive deionization electrodes for water defluoridation. *Ionics*, 26(5), 2477-2492.

Fan, X., Parker, D. J., & Smith, M. D. (2003). Adsorption kinetics of fluoride on low cost materials. *Water Research*, *37*(20), 4929-4937.

Fermoso, J., Gil, M. V., Arias, B., Plaza, M. G., Pevida, C., Pis, J. J., & Rubiera, F. (2010). Application of response surface methodology to assess the combined effect of operating

variables on high-pressure coal gasification for H_2-rich gas production. *International Journal of Hydrogen Energy*, *35*(3), 1191-1204.

Foo, K., & Hameed, B. (2009). A short review of activated carbon assisted electrosorption process: An overview, current stage and future prospects. *Journal of Hazardous Materials*, *170*(2-3), 552-559.

Franco, D. S., Georgin, J., Lima, E. C., & Silva, L. F. (2022). Advances made in removing paraquat herbicide by adsorption technology: A review. *Journal of Water Process Engineering*, 49, 102988.

Fu, H., He, H., Usman, M., Chen, Q., Laipan, M., Yang, Y., Zhu, R., & Cai, L. (2019). Facile synthesis of Al/Fe bimetallic (oxyhydr) oxide-coated magnetite for efficient removal of fluoride from water. *Environmental Technology*, *41*(20), 2625-2636.

Gabelich, C. J., Tran, T. D., & Suffet, I. M. (2002). Electrosorption of inorganic salts from aqueous solution using carbon aerogels. *Environmental Science & Technology*, *36*(13), 3010-3019.

Gaikwad, M. S., & Balomajumder, C. (2017a). Simultaneous electrosorptive removal of chromium (VI) and fluoride ions by capacitive deionization (CDI): Multicomponent isotherm modeling and kinetic study. *Separation and Purification Technology*, *254*, 117561.

Gaikwad, M. S., & Balomajumder, C. (2017b). Tea waste biomass activated carbon electrode for simultaneous removal of Cr (VI) and fluoride by capacitive deionization. *Chemosphere*, *184*, 1141-1149.

Gaikwad, M. S., & Balomajumder, C. (2018). Removal of Cr (VI) and fluoride by membrane capacitive deionization with nanoporous and microporous Limonia acidissima (wood apple) shell activated carbon electrode. *Separation and Purification Technology*, *195*, 305-313.

Gangadharan, D., Sivaramakrishnan, S., Nampoothiri, K. M., Sukumaran, R. K., & Pandey, A. (2008). Response surface methodology for the optimization of alpha amylase production by Bacillus amyloliquefaciens. *Bioresource Technology*, *99*(11), 4597-4602.

Ganiyu, S. A., Alhooshani, K., Sulaiman, K. O., Qamaruddin, M., Bakare, I. A., Tanimu, A., & Saleh, T. A. (2016). Influence of aluminium impregnation on activated carbon for enhanced desulfurization of DBT at ambient temperature: Role of surface acidity and textural properties. *Chemical Engineering Journal*, *303*, 489-500.

Ghorbani, F., Younesi, H., Ghasempouri, S. M., Zinatizadeh, A. A., Amini, M., & Daneshi, A. (2008). Application of response surface methodology for optimization of cadmium biosorption in an aqueous solution by Saccharomyces cerevisiae. *Chemical Engineering Journal*, *145*(2), 267-275.

Gong, W. X., Qu, J. H., Liu, R. P., & Lan, H. C. (2012). Effect of aluminum fluoride complexation on fluoride removal by coagulation. *Colloids and Surfaces A: Physicochemical and Engineering Aspects*, *395*, 88-93.

Grillo, R., Pereira, A. E., Nishisaka, C. S., De Lima, R., Oehlke, K., Greiner, R., & Fraceto, L. F. (2014). Chitosan/tripolyphosphate nanoparticles loaded with paraquat herbicide: An environmentally safer alternative for weed control. *Journal of Hazardous Materials*, 278, 163-171.

Gunst, R. F. (1996). Response Surface Methodology: Process and Product Optimization Using Designed Experiments. *Technometrics*, *38*(3), 284-286.

Guo, W., Yu, C., Li, S., Yang, J., Liu, Z., Zhao, C., Huang, H., Zhang, M., Han, X., & Niu, Y. (2017). High-stacking-density, superior-roughness LDH bridged with vertically aligned graphene for high-performance asymmetric supercapacitors. *Small*, *13*(37), 1701288.

Guo, X., Zhang, W., Qian, C., Yang, H., & Fan, T. (2018). MnO_2/C composite with 3D hierarchical architecture for high-performance supercapacitor electrodes. *Ceramics International*, *44*(8), 9696-9702.

Habuda-Stanic, M., Ravancic, M. E., & Flanagan, A. (2014). A Review on Adsorption of Fluoride from Aqueous Solution. *Materials (Basel)*, *7*(9), 6317-6366.

Hamada, M., & Wu, C. F. (2000). *Experiments: Planning, Analysis and Parameter Design Optimization.* https://scholar.google.com/

Hamadi, N. K., Swaminathan, S., & Chen, X. D. (2004). Adsorption of paraquat dichloride from aqueous solution by activated carbon derived from used tires. *Journal of Hazardous Materials*, *112*(1-2), 133-141.

Hameed, R. M. A., Zouli, N., Abutaleb, A., El-Halwany, M. M., El-Newehy, M. H., & Yousef, A. (2021). Improving water desalination performance of electrospun carbon nanofibers by supporting with binary metallic carbide nanoparticles. *Ceramics International*, *48*(4), 4741-4753.

Han, B., Cheng, G., Wang, Y., & Wang, X. (2019). Structure and functionality design of novel carbon and faradaic electrode materials for high-performance capacitive deionization. *Chemical Engineering Journal*, *360*, 364-384.

Han, L., Karthikeyan, K. G., Anderson, M. A., & Gregory, K. B. (2014). Exploring the impact of pore size distribution on the performance of carbon electrodes for capacitive deionization. *Journal of Colloid and Interface Science*, *430*, 93-99.

Haq, O. U., Choi, D. S., Choi, J. H., & Lee, Y. S. (2019). Carbon electrodes with ionic functional groups for enhanced capacitive deionization performance. *Journal of Industrial and Engineering Chemistry*, *83*, 136-144.

Hawks, S. A., Ramachandran, A., Porada, S., Campbell, P. G., Suss, M. E., Biesheuvel, P., Santiago, J. G., & Stadermann, M. (2019). Performance metrics for the objective assessment of capacitive deionization systems. *Water Research*, *152*, 126-137.

He, D., Wong, C. E., Tang, W., Kovalsky, P., & Waite, T. D. (2016). Faradaic reactions in water desalination by batch-mode capacitive deionization. *Environmental Science & Technology Letters*, *3*(5), 222-226.

Homogen, M. (2018). Synthesis and physicochemical properties of magnetite nanoparticles (Fe_3O_4) as potential solid support for homogeneous catalysts. *Malaysian Journal of Analytical Sciences*, 22, 768-774.

Hou, C. H., & Huang, C. Y. (2013). A comparative study of electrosorption selectivity of ions by activated carbon electrodes in capacitive deionization. *Desalination*, *314*, 124-129.

Huang, Q., Liu, Y., Cai, T., & Xia, X. (2019). Simultaneous removal of heavy metal ions and organic pollutant by BiOBr/Ti_3C_2 nanocomposite. *Journal of Photochemistry and Photobiology A: Chemistry*, *375*, 201-208.

Huang, W., Zhang, Y., Bao, S., & Song, S. (2013a). Desalination by capacitive deionization with carbon-based materials as electrode: A review. *Surface Review and Letters*, *20*(06), 1330003.

Huang, W. E. I., Zhang, Y., Bao, S., & Song, S. (2013). Desalination by capacitive deionization with carbon-based materials as electrode: A review. *Surface Review and Letters*, 20(06), 1330003.

Huang, X., Wang, R., Jiao, T., Zou, G., Zhan, F., Yin, J., Zhang, L., Zhou, J., & Peng, Q. (2019). Facile preparation of hierarchical AgNP-loaded MXene/Fe_3O_4/polymer nanocomposites by electrospinning with enhanced catalytic performance for wastewater treatment. *ACS Omega*, *4*(1), 1897-1906.

Huyskens, C., Helsen, J., & De Haan, A. B. (2013). Capacitive deionization for water treatment: Screening of key performance parameters and comparison of performance for different ions. *Desalination*, *328*, 8-16.

Ihsanullah, I. (2020). MXenes (two-dimensional metal carbides) as emerging nanomaterials for water purification: Progress, challenges and prospects. *Chemical Engineering Journal*, 388, 124340.

Jande, Y., Asif, M., Shim, S., & Kim, W. S. (2014). Energy minimization in monoethanolamine-based CO_2 capture using capacitive deionization. *International Journal of Energy Research*, *38*(12), 1531-1540.

Jande, Y. A. C., & Kim, W. S. (2013). Desalination using capacitive deionization at constant current. *Desalination*, *329*, 29-34.

Jande, Y. A. C., & Kim, W. S. (2014). Modeling the capacitive deionization batch mode operation for desalination. *Journal of Industrial and Engineering Chemistry*, *20*(5), 3356-3360.

Jha, S., Singh, R., Damodaran, T., Mishra, V., Sharma, D., & Rai, D. (2013). Fluoride in groundwater: Toxicological exposure and remedies. *Journal of Toxicology and Environmental Health, Part B, 16*(1), 52-66.

Jia, B., & Zou, L. (2012). Graphene nanosheets reduced by a multi-step process as high-performance electrode material for capacitive deionisation. *Carbon*, *50*(6), 2315-2321.

Jiang, S., Wang, H., Xiong, G., Wang, X., & Tan, S. (2018). Removal of nitrate using activated carbon-based electrodes for capacitive deionization. *Water Supply*, *18*(6), 2028-2034.

Kadam, S., Mane, S., Tirmali, P., & Kulkarni, S. (2018). Electrochemical synthesis of flower like Mn-Co mixed metal oxides as electrode material for supercapacitor application. *Current Applied Physics*, *18*(4), 397-404.

Kang, D., Yu, X., Ge, M., Xiao, F., & Xu, H. (2017). Novel Al-doped carbon nanotubes with adsorption and coagulation promotion for organic pollutant removal. *Journal of Environmental Sciences*, *54*, 1-12.

Karthikeyan, M., & Elango, K. (2008). Removal of fluoride from aqueous solution using graphite: A kinetic and thermodynamic study. *Indian Journal of Chemical Technology*, *15*(6), 525-532.

Kazeem, T. S., Lateef, S. A., Ganiyu, S. A., Qamaruddin, M., Tanimu, A., Sulaiman, K. O., Sajid-Jillani, S. M., & Alhooshani, K. (2018). Aluminium-modified activated carbon as efficient adsorbent for cleaning of cationic dye in wastewater. *Journal of Cleaner Production*, *205*, 303-312.

Khan, Z. U., Yan, T., Han, J., Shi, L., & Zhang, D. (2019). Capacitive deionization of saline water using graphene nanosphere decorated N-doped layered mesoporous carbon frameworks. *Environmental Science: Nano*, *6*(11), 3442-3453.

Khandare, D., & Mukherjee, S. (2019). A Review of Metal oxide Nanomaterials for Fluoride decontamination from Water Environment. *Materials Today: Proceedings*, *18*, 1146-1155.

Khatibikamal, V., Torabian, A., Janpoor, F., & Hoshyaripour, G. (2010). Fluoride removal from industrial wastewater using electrocoagulation and its adsorption kinetics. *Journal of Hazardous Materials*, *179*(1-3), 276-280.

Khuri, A. I., & Mukhopadhyay, S. (2010). Response surface methodology. *Computational Statistics*, *2*(2), 128-149.

Kirubasankar, B., Murugadoss, V., Lin, J., Ding, T., Dong, M., Liu, H., Zhang, J., Li, T., Wang, N., Guo, Z., & Angaiah, S. (2018). In situ grown nickel selenide on graphene nanohybrid electrodes for high energy density asymmetric supercapacitors. *Nanoscale*, *10*(43), 20414-20425.

Kumar, E., Bhatnagar, A., Kumar, U., & Sillanpää, M. (2011). Defluoridation from aqueous solutions by nano-alumina: Characterization and sorption studies. *Journal of Hazardous Materials*, *186*(2-3), 1042-1049.

Kumar, P. S., Suganya, S., Srinivas, S., Priyadharshini, S., Karthika, M., Karishma Sri, R., Swetha, V., Naushad, M., & Lichtfouse, E. (2019). Treatment of fluoride-contaminated water. A review. *Environmental Chemistry Letters*, *17*(4), 1707-1726.

Kumar, R., Bhuvana, T., & Sharma, A. (2018). Tire Waste Derived Turbostratic Carbon as an Electrode for a Vanadium Redox Flow Battery. *Sustainable Chemistry & Engineering*, *6*(7), 8238-8246.

Kumari, M., & Gupta, S. K. (2019). Response surface methodological approach for optimizing the removal of trihalomethanes and its precursor's by surfactant modified magnetic nanoadsorbents (sMNP)-An endeavor to diminish probable cancer risk. *Scientific Reports*, *9*(1), 1-11.

Kushwaha, R., Bhaskar, D., & Mohan, S. A. D. (2020). An experimental study on some parameters for defluoridation using Capacitive Deionization with carbon electrodes. *Journal of the Indian Chemical Society*, *97*, 368-372.

Lahnid, S., Tahaikt, M., Elaroui, K., Idrissi, I., Hafsi, M., Laaziz, I., Amor, Z., Tiyal, F., & Elmidaoui, A. (2008). Economic evaluation of fluoride removal by electrodialysis. *Desalination*, *230*(1-3), 213-219.

Landon, J., Gao, X., Omosebi, A., & Liu, K. (2017). Structured and Surface-Modified Carbon Xerogel Electrodes for Capacitive Deionization. *Submicron Porous Materials*, 2017, 1-23.

Lapertot, M., Ebrahimi, S., Dazio, S., Rubinelli, A., & Pulgarin, C. (2007). Photo-Fenton and biological integrated process for degradation of a mixture of pesticides. *Journal of Photochemistry and Photobiology A: Chemistry, 186*(1), 34-40.

Lee, H. S., Lee, K. S., Yu, K., & Hong, S. Y. (2008). Expression of genes related to Parkinson's disease after paraquat treatment in Drosophila melanogaster. *Pesticide Biochemistry and Physiology, 92*(1), 19-23.

Lee, J. B., Park, K. K., Eum, H. M., & Lee, C. W. (2006). Desalination of a thermal power plant wastewater by membrane capacitive deionization. *Desalination*, *196*(1-3), 125-134.

Leite, M. P., Dos Reis, L. G. T., Robaina, N. F., Pacheco, W. F., & Cassella, R. J. (2013). Adsorption of paraquat from aqueous medium by Amberlite XAD-2 and XAD-4 resins using dodecylsulfate as counter ion. *Chemical Engineering Journal*, *215*, 691-698.

Leonard, K. C., Genthe, J. R., Sanfilippo, J. L., Zeltner, W. A., & Anderson, M. A. (2009). Synthesis and characterization of asymmetric electrochemical capacitive deionization materials using nanoporous silicon dioxide and magnesium doped aluminum oxide. *Electrochimica Acta*, *54*(22), 5286-5291.

Lester, Y., Shaulsky, E., Epsztein, R., & Zucker, I. (2020). Capacitive deionization for simultaneous removal of salt and uncharged organic contaminants from water. *Separation and Purification Technology*, 237, 116388.

Li, D., Wang, S., Wang, G., Li, C., Che, X., Wang, S., Zhang, Y., & Qiu, J. (2019). Facile Fabrication of NiCoAl-Layered Metal Oxide/Graphene Nanosheets for Efficient Capacitive Deionization Defluorination. *Applied Materials & Interfaces, 11*(34), 31200-31209.

Li, L. X., Xu, D., Li, X. Q., Liu, W. C., & Jia, Y. (2014). Excellent fluoride removal properties of porous hollow MgO microspheres. *New Journal of Chemistry*, *38*(11), 5445-5452.

Li, Y., Chen, N., Li, Z., Shao, H., & Qu, L. (2020). Frontiers of carbon materials as capacitive deionization electrodes. *Dalton Transactions*, *49*(16), 5006-5014.

Li, Y., Jiang, Y., Wang, T. J., Zhang, C., & Wang, H. (2017). Performance of fluoride electrosorption using micropore-dominant activated carbon as an electrode. *Separation and Purification Technology*, *172*, 415-421.

Li, Y., Zhang, C., Jiang, Y., Wang, T. J., & Wang, H. (2016). Effects of the hydration ratio on the electrosorption selectivity of ions during capacitive deionization. *Desalination*, *399*, 171-177.

Li, Y., Zhang, C., Jiang, Y., & Wang, T. J. (2018). Electrically enhanced adsorption and green regeneration for fluoride removal using $Ti(OH)_4$-loaded activated carbon electrodes. *Chemosphere*, *200*, 554-560.

Liang, S., Li, M., Cao, J., Zuo, K., Bian, Y., Xiao, K., & Huang, X. (2019). Integrated ultrafiltration–capacitive-deionization for enhanced antifouling performance and synchronous removal of organic matter and salts. *Separation and Purification Technology*, *226*, 146-153.

Lin, Z., Xiang, X., Peng, S., Jiang, X., & Hou, L. (2018). Facile synthesis of chitosan-based carbon with rich porous structure for supercapacitor with enhanced electrochemical performance. *Journal of Electroanalytical Chemistry*, *823*, 563-572.

Liu, D., Wang, X., Xie, Y. F., & Tang, H. L. (2016). Effect of capacitive deionization on disinfection by-product precursors. *Science of the Total Environment*, *568*, 19-25.

Liu, T., Liu, X., Graham, N., Yu, W., & Sun, K. (2020). Two-dimensional MXene incorporated graphene oxide composite membrane with enhanced water purification performance. *Journal of Membrane Science*, *593*, 117431.

Liu, Y., Li, H., Nie, C., Pan, L., & Sun, Z. (2013). Carbon nanotube and carbon nanofiber composite films grown on different graphite substrate for capacitive deionization. *Desalination and Water Treatment*, *51*(19-21), 3988-3994.

Loganathan, P., Vigneswaran, S., Kandasamy, J., & Naidu, R. (2013). Defluoridation of drinking water using adsorption processes. *Journal of Hazardous materials*, *248*, 1-19.

Loha, K. M., Lamoree, M., Weiss, J. M., & De Boer, J. (2018). Import, disposal, and health impacts of pesticides in the East Africa Rift zone: A review on management and policy analysis. *Crop Protection*, *112*, 322-331.

Ma, D., Cai, Y., Wang, Y., Xu, S., Wang, J., & Khan, M. U. (2019). Grafting the Charged Functional Groups on Carbon Nanotubes for Improving the Efficiency and Stability of Capacitive Deionization Process. *Applied Materials & Interfaces*, *11*(19), 17617-17628.

Machunda, R. L., Jeon, H., Lee, J. K., & Lee, J. (2009). Effects of acid treatment on the improvement of specific capacitance and deionization efficiency of porous carbon electrodes. *Water Science and Technology: Water Supply*, 9(2), 159-165.

Mahalakshmi, M., Arabindoo, B., Palanichamy, M., & Murugesan, V. (2007). Photocatalytic degradation of carbofuran using semiconductor oxides. *Journal of Hazardous Materials*, *143*(1-2), 240-245.

Maliyekkal, S. M., Sharma, A. K., & Philip, L. (2006). Manganese-oxide-coated alumina: A promising sorbent for defluoridation of water. *Water Research*, *40*(19), 3497-3506.

Mbabaye, G., Minja, R., Mtalo, F., Legonda, I., & Mkongo, G. (2018). Fluoride occurrence in domestic water supply sources in Tanzania: A case of Meru district Arusha region. *Tanzania Journal of Science*, *44*(3), 72-92.

Min, X., Zhu, M., He, Y., Wang, Y., Deng, H., Wang, S., Jin, L., Wang, H., Zhang, L., & Chai, L. (2020). Selective removal of Cl(-) and F(-) from complex solution via electrochemistry deionization with bismuth/reduced graphene oxide composite electrode. *Chemosphere*, *251*, 126319.

Mohapatra, M., Anand, S., Mishra, B. K., Giles, D. E., & Singh, P. (2009). Review of fluoride removal from drinking water. *Journal of Environmental Management*, *91*(1), 67-77.

Mojoudi, N., Mirghaffari, N., Soleimani, M., Shariatmadari, H., Belver, C., & Bedia, J. (2019). Phenol adsorption on high microporous activated carbons prepared from oily sludge: Equilibrium, kinetic and thermodynamic studies. *Scientific Reports*, *9*(1), 19352.

Mossad, M., & Zou, L. (2012). A study of the capacitive deionisation performance under various operational conditions. *Journal of Hazardous Materials*, *213-214*, 491-497.

Mourabet, M., El Rhilassi, A., El Boujaady, H., Bennani-Ziatni, M., & Taitai, A. (2017). Use of response surface methodology for optimization of fluoride adsorption in an aqueous solution by Brushite. *Arabian Journal of Chemistry*, *10*, S3292-S3302.

Mukherjee, A., Adak, M. K., Upadhyay, S., Khatun, J., Dhak, P., Khawas, S., Ghorai, U. K., & Dhak, D. (2019). Efficient Fluoride Removal and Dye Degradation of Contaminated Water Using Fe/Al/Ti Oxide Nanocomposite. *ACS Omega*, *4*(6), 9686-9696.

Nanseu-Njiki, C. P., Dedzo, G. K., & Ngameni, E. (2010). Study of the removal of paraquat from aqueous solution by biosorption onto Ayous (Triplochiton schleroxylon) sawdust. *Journal of Hazardous materials*, *179*(1-3), 63-71.

Nayar, P., Khanna, A., Kabiraj, D., Abhilash, S. R., Beake, B. D., Losset, Y., & Chen, B. (2014). Structural, optical and mechanical properties of amorphous and crystalline alumina thin films. *Thin Solid Films*, *568*, 19-24.

Ndiaye, P., Moulin, P., Dominguez, L., Millet, J., & Charbit, F. (2005). Removal of fluoride from electronic industrial effluentby RO membrane separation. *Desalination*, *173*(1), 25-32.

Nkuna, S. (2017). *Development of Capacitive Deionisation Electrodes: Optimization of Fabrication Methods and Composition.* https://scholar.google.com

Núñez, O., Kim, J. B., Moyano, E., Galceran, M. T., & Terabe, S. (2002). Analysis of the herbicides paraquat, diquat and difenzoquat in drinking water by micellar electrokinetic chromatography using sweeping and cation selective exhaustive injection. *Journal of Chromatography A*, *961*(1), 65-75.

Nyangi, M. J., Chebude, Y., Kilulya, K. F., & Andrew, M. (2021). Simultaneous removal of fluoride and arsenic from water by hybrid Al-Fe electrocoagulation: Process optimization through surface response method. *Separation Science and Technology*, *56*(15), 2648-2658.

Oladunni, J., Zain, J. H., Hai, A., Banat, F., Bharath, G., & Alhseinat, E. (2018). A comprehensive review on recently developed carbon based nanocomposites for capacitive deionization: From theory to practice. *Separation and Purification Technology*, *207*, 291-320.

Oren, Y. (2008). Capacitive deionization (CDI) for desalination and water treatment: Past, present and future (a review). *Desalination*, *228*(1-3), 10-29.

Park, G., Hong, S. P., Lee, C., Lee, J., & Yoon, J. (2021). Selective fluoride removal in capacitive deionization by reduced graphene oxide/hydroxyapatite composite electrode. *Journal of Colloid and Interface Science, 581*, 396-402.

Park, G., Pil-Hong, S., Lee, C., Lee, J., & Yoon, J. (2020). Selective Fluoride Removal in Capacitive Deionization by reduced Graphene Oxide/Hydroxyapatite Composite Electrode. *Journal of Colloid and Interface Science*.

Park, K. K., Lee, J. B., Park, P. Y., Yoon, S. W., Moon, J. S., Eum, H. M., & Lee, C. W. (2007). Development of a carbon sheet electrode for electrosorption desalination. *Desalination, 206*(1-3), 86-91.

Pelarti, M. M., Mirbagheri, S. A., Dehghan, K., & Alam, M. (2022). Nickel removal from aqueous solutions using flow-electrode capacitive deionization (Optimization by Response Surface Methodology). *Water Science and Technology, 86*(6), 1299-1307.

Pérez-Parada, A., Goyenola, G., De Mello, F. T., & Heinzen, H. (2018). Recent advances and open questions around pesticide dynamics and effects on freshwater fishes. *Current Opinion in Environmental Science & Health, 4*, 38-44.

Porada, S., Borchardt, L., Oschatz, M., Bryjak, M., Atchison, J., Keesman, K., Kaskel, S., Biesheuvel, P., & Presser, V. (2013). Direct prediction of the desalination performance of porous carbon electrodes for capacitive deionization. *Energy & Environmental Science, 6*(12), 3700-3712.

Porada, S., Zhao, R., Van Der Wal, A., Presser, V., & Biesheuvel, P. (2013). Review on the science and technology of water desalination by capacitive deionization. *Progress in Materials Science, 58*(8), 1388-1442.

Prasad, K. S., Amin, Y., & Selvaraj, K. (2014). Defluoridation using biomimetically synthesized nano zirconium chitosan composite: Kinetic and equilibrium studies. *Journal of Hazardous Materials, 276*, 232-240.

Qayoom, M., Shah, K. A., Pandit, A. H., Firdous, A., & Dar, G. N. (2020). Dielectric and electrical studies on iron oxide (α-Fe_2O_3) nanoparticles synthesized by modified solution combustion reaction for microwave applications. *Journal of Electroceramics, 45*(1), 7-14.

Rafique, T., Chadhar, K. M., Usmani, T. H., Memon, S. Q., Shirin, K., Kamaluddin, S., & Soomro, F. (2015). Adsorption behavior of fluoride ion on trimetal-oxide adsorbent. *Desalination and Water Treatment*, *56*(6), 1669-1680.

Ranade, S. S., & Thiagarajan, P. (2017). Selection of a design for response surface. *IOP Conference Series: Materials Science and Engineering*, *263*, 022043.

Rasines, G., Lavela, P., Macías, C., Haro, M., Ania, C., & Tirado, J. (2012). Electrochemical response of carbon aerogel electrodes in saline water. *Journal of Electroanalytical Chemistry*, *671*, 92-98.

Raul, P. K., Devi, R. R., Umlong, I. M., Banerjee, S., Singh, L., & Purkait, M. (2012). Removal of fluoride from water using iron oxide-hydroxide nanoparticles. *Journal of Nanoscience and Nanotechnology*, *12*(5), 3922-3930.

Ritter, K. S., Paul, S., Ken, H. Patricia, K., Gevan, M., & Beth, L. L. (2002). Sources, pathways, and relative risks of contaminants in surface water and groundwater: A perspective prepared for the Walkerton inquiry. *Journal of Toxicology and Environmental Health Part A*, *65*(1), 1-142.

Romanos, J., Beckner, M., Stalla, D., Tekeei, A., Suppes, G., Jalisatgi, S., Lee, M., Hawthorne, F., Robertson, J. D., Firlej, L., Kuchta, B., Wexler, C., Yu, P., & Pfeifer, P. (2013). Infrared study of boron–carbon chemical bonds in boron-doped activated carbon. *Carbon*, *54*, 208-214.

Rongchapo, W. (2015). *Removal of Paraquat and other Pollutants by Adsorption and Photocatalysis.* https://mail.google.com

Ryoo, M. W., Kim, J. H., & Seo, G. (2003). Role of titania incorporated on activated carbon cloth for capacitive deionization of NaCl solution. *Journal of Colloid and Interface Science*, *264*(2), 414-419.

Sabzehmeidani, M. M., Karimi, H., & Ghaedi, M. (2020). Enhanced visible light-active CeO_2/CuO/Ag $2CrO_4$ ternary heterostructures based on CeO_2/CuO nanofiber heterojunctions for the simultaneous degradation of a binary mixture of dyes. *New Journal of Chemistry*, *44*(13), 5033-5048.

Saikia, B. J., & Parthasarathy, G. (2010). Fourier Transform Infrared Spectroscopic Characterization of Kaolinite from Assam and Meghalaya, Northeastern India. *Journal of Modern Physics*, *01*(04), 206-210.

Saleem, M. W., & Kim, W. S. (2018). Parameter-based performance evaluation and optimization of a capacitive deionization desalination process. *Desalination*, *437*, 133-143.

Salomón, Y. L. D. O., Georgin, J., Franco, D. S., Netto, M. S., Piccilli, D. G., Foletto, E. L., Oliveira, L. F., & Dotto, G. L. (2021). High-performance removal of 2, 4-dichlorophenoxyacetic acid herbicide in water using activated carbon derived from Queen palm fruit endocarp (Syagrus romanzoffiana). *Journal of Environmental Chemical Engineering*, *9*(1), 104911.

Santos, M. S., Madeira, L. M., & Alves, A. (2014). Paraquat quantification in deposits from drinking water networks. *Analytical Methods*, *6*(11), 3791-3798.

Santos, M. S., Schaule, G., Alves, A., & Madeira, L. M. (2013). Adsorption of paraquat herbicide on deposits from drinking water networks. *Chemical Engineering Journal*, *229*, 324-333.

Saravanan, L., & Subramanian, S. (2005). Surface chemical studies on the competitive adsorption of poly(ethylene glycol) and ammonium poly(methacrylate) onto alumina. *Journal of Colloid and Interface Science*, *284*(2), 363-377.

Senoussi, H., & Bouhidel, K. E. (2018a). Feasibility and optimisation of a batch mode capacitive deionization process for textile cationic dyes removal and recovery from industrial wastewaters. *Journal of Cleaner Production*, *205*, 721-727.

Senoussi, H., & Bouhidel, K. E. (2018b). Feasibility and optimization of a batch mode capacitive deionization process for textile cationic dyes removal and recovery from industrial wastewaters. *Journal of Cleaner Production*, *205*, 721-727.

Seo, S. J., Jeon, H., Lee, J. K., Kim, G. Y., Park, D., Nojima, H., Lee, J., & Moon, S. H. (2010). Investigation on removal of hardness ions by capacitive deionization for water softening applications. *Water Research*, *44*(7), 2267-2275.

Shen, F., Chen, X., Gao, P., & Chen, G. (2003). Electrochemical removal of fluoride ions from industrial wastewater. *Chemical Engineering Science*, *58*(3-6), 987-993.

Sieliechi, J. M., & Thue, P. S. (2014). Removal of paraquat from drinking water by activated carbon prepared from waste wood. *Desalination and Water Treatment*, *55*(4), 986-998.

Sinha, P., Banerjee, S., & Kar, K. K. (2020). *Transition Metal Oxide/Activated Carbon-Based Composites as Electrode Materials for Supercapacitors. Handbook of Nanocomposite Supercapacitor Materials II: Performance.* https://scholar.google.com

Sirengo, K., Jande, Y. A. C., Kibona, T. E., Hilonga, A., Muiva, C., & King'ondu, C. K. (2019). Fish bladder-based activated carbon/Co_3O_4/TiO_2 composite electrodes for supercapacitors. *Materials Chemistry and Physics*, *232*, 49-56.

Solanki, Y. S., Agarwal, M., Gupta, S., Shukla, P., Maheshwari, K., & Midda, M. O. (2019). Application of synthesized Fe/Al/Ca based adsorbent for defluoridation of drinking Water and its significant parameters optimization using response surface methodology. *Journal of Environmental Chemical Engineering*, *7*(6), 103465.

Srimuk, P., Kaasik, F., Krüner, B., Tolosa, A., Fleischmann, S., Jäckel, N., Tekeli, M. C., Aslan, M., Suss, M. E., & Presser, V. (2016). MXene as a novel intercalation-type pseudocapacitive cathode and anode for capacitive deionization. *Journal of Materials Chemistry A*, *4*(47), 18265-18271.

Su, C., Li, W., & Wang, Y. (2013). Adsorption property of direct fast black onto acid-thermal modified sepiolite and optimization of adsorption conditions using Box-Behnken response surface methodology. *Frontiers of Environmental Science & Engineering*, *7*, 503-511.

Su, X. L., Chen, J. R., Zheng, G. P., Yang, J. H., Guan, X. X., Liu, P., & Zheng, X. C. (2018). Three-dimensional porous activated carbon derived from loofah sponge biomass for supercapacitor applications. *Applied Surface Science*, *436*, 327-336.

Su, X., & Hatton, T. A. (2017). Redox-electrodes for selective electrochemical separations. *Advances in Colloid and Interface Science*, *244*, 6-20.

Suriyaraj, S., & Selvakumar, R. (2016). Advances in nanomaterial based approaches for enhanced fluoride and nitrate removal from contaminated water. *RSC Advances*, *6*(13), 10565-10583.

Suss, M. E., Porada, S., Sun, X., Biesheuvel, P. M., Yoon, J., & Presser, V. (2015). Water desalination via capacitive deionization: What is it and what can we expect from it? *Energy & Environmental Science*, *8*(8), 2296-2319.

Szuplewska, A., Kulpińska, D., Dybko, A., Chudy, M., Jastrzębska, A. M., Olszyna, A., & Brzózka, Z. (2020). Future applications of MXenes in biotechnology, nanomedicine, and sensors. *Trends in Biotechnology*, *38*(3), 264-279.

Tajik, S., Dubal, D. P., Gomez-Romero, P., Yadegari, A., Rashidi, A., Nasernejad, B., Inamuddin, & Asiri, A. M. (2017). Nanostructured mixed transition metal oxides for high performance asymmetric supercapacitors: Facile synthetic strategy. *International Journal of Hydrogen Energy*, *42*(17), 12384-12395.

Tang, W., Kovalsky, P., Cao, B., & Waite, T. D. (2016). Investigation of fluoride removal from low-salinity groundwater by single-pass constant-voltage capacitive deionization. *Water Research*, 99, 112-121.

Tang, C., Huang, X., Wang, H., Shi, H., & Zhao, G. (2020). Mechanism investigation on the enhanced photocatalytic oxidation of nonylphenol on hydrophobic TiO_2 nanotubes. *Journal of Hazardous Materials*, *382*, 121017.

Tang, W., Kovalsky, P., He, D., & Waite, T. D. (2015). Fluoride and nitrate removal from brackish groundwaters by batch-mode capacitive deionization. *Water Research*, *84*, 342-349.

Tang, W., Liang, J., He, D., Gong, J., Tang, L., Liu, Z., Wang, D., & Zeng, G. (2019). Various cell architectures of capacitive deionization: Recent advances and future trends. *Water Research*, *150*, 225-251.

Tatjana, V., Domitille, S., & Jean-Charles, S. (2021). Paraquat-induced cholesterol biosynthesis proteins dysregulation in human brain microvascular endothelial cells. *Scientific Reports*, *11*(1), 18137.

Un, U. T., Koparal, A. S., & Ogutveren, U. B. (2013). Fluoride removal from water and wastewater with a bach cylindrical electrode using electrocoagulation. *Chemical Engineering Journal*, 223, 110-115.

Thompson, T., Fawell, J., Kunikane, S., Jackson, D., Appleyard, S., Callan, P., Bartram, J., Kingston, P., Water, S., & Organization, W. H. (2007). *Chemical safety of Drinking Water: Assessing Priorities for Risk Management*. World Health Organization.

Thongpitak, J., Pumas, P., & Pumas, C. (2020). Paraquat Degradation by Biological Manganese Oxide (BioMnO x) Catalyst Generated From Living Microalga Pediastrum duplex AARL G060. *Frontiers in Microbiology*, *11*, 575361.

Toledo-Carrillo, E., Zhang, X., Laxman, K., & Dutta, J. (2020). Asymmetric electrode capacitive deionization for energy efficient desalination. *Electrochimica Acta*, 358, 136939.

Tomar, V., Prasad, S., & Kumar, D. (2013). Adsorptive removal of fluoride from water samples using Zr–Mn composite material. *Microchemical Journal*, *111*, 116-124.

Tomlin, C. D. (2009). *The Pesticide Manual: A World Compendium*. British Crop Production Council. https://scholar.google.com/

Trunzer, T., Stummvoll, T., Porzenheim, M., Fraga-Garcia, P., & Berensmeier, S. (2020). A carbon nanotube packed bed electrode for small molecule electrosorption: An electrochemical and chromatographic approach for process description. *Applied Sciences*, 10(3), 1133.

Turner, B. D., Binning, P., & Stipp, S. (2005). Fluoride removal by calcite: Evidence for fluorite precipitation and surface adsorption. *Environmental Science & Technology*, *39*(24), 9561-9568.

Vafakhah, S., Beiramzadeh, Z., Saeedikhani, M., & Yang, H. Y. (2020). A review on free-standing electrodes for energy-effective desalination: Recent advances and perspectives in capacitive deionization. *Desalination*, *493*, 114662.

Vickers, N. J. (2017). Animal communication: When i'm calling you, will you answer too? *Current Biology*, *27*(14), R713-R715.

Vijayalakshmi, G., Shobha, B., Vanajakshi, V., Divakar, S., & Manohar, B. (2001). Response surface methodology for optimization of growth parameters for the production of carotenoids by a mutant strain of Rhodotorula gracilis. *European Food Research and Technology*, *213*, 234-239.

Wan, K., Huang, L., Yan, J., Ma, B., Huang, X., Luo, Z., Zhang, H., & Xiao, T. (2021). Removal of fluoride from industrial wastewater by using different adsorbents: A review. *Science of the Total Environment*, *773*, 145535.

Wang, C., Chen, L., Liu, S., & Zhu, L. (2018). Nitrite desorption from activated carbon fiber during capacitive deionization and membrane capacitive deionization. *Colloids and Surfaces A: Physicochemical and Engineering Aspects*, *559*, 392-400.

Wang, G., Li, D., Wang, S., Zhao, Z., Lv, S., & Qiu, J. (2021). Ternary NiFeMn layered metal oxide (LDO) compounds for capacitive deionization defluoridation: The unique role of Mn. *Separation and Purification Technology*, 254, 117667.

Wang, G., Qian, B., Dong, Q., Yang, J., Zhao, Z., & Qiu, J. (2013). Highly mesoporous activated carbon electrode for capacitive deionization. *Separation and Purification Technology*, *103*, 216-221.

Wang, S., Nam, H., Gebreegziabher, T. B., & Nam, H. (2020). Adsorption of acetic acid and hydrogen sulfide using NaOH impregnated activated carbon for indoor air purification. *Engineering Reports*, 2(1), e12083.

Wang, Y. F., Zhao, S. X., Yu, L., Zheng, X. X., Wu, Q. L., & Cao, G. Z. (2019). Design of multiple electrode structures based on nano Ni_3S_2 and carbon nanotubes for high performance supercapacitors. *Journal of Materials Chemistry A*, *7*(13), 7406-7414.

Water, S., & Organization, W. H. (2006). *Guidelines for Drinking-Water Quality [Electronic Resource]: Incorporating First Addendum. Vol. 1, Recommendations*. https://scholar.google.com

Welgemoed, T. (2005). *Capacitive Deionization Technology: Development And Evaluation of an Industrial Prototype System [University of Pretoria* Dissertation]. https://scholar.google.com

Welgemoed, T., & Schutte, C. (2005). Capacitive deionization technology™: An alternative desalination solution. *Desalination*, *183*(1-3), 327-340.

WHO. (2017). *Guidelines for Drinking-Water Quality: Fourth Edition Incorporating the First Addendum*. https://scholar.google.com

Wimalasiri, Y., Van Leeuwen, J., & Awad, J. (2018). Assessment of small-scale desalination by capacitive deionization for horticulture on the Northern Adelaide Plains. *Goyder Institute for Water Research Technical Report Series*, (01/18), 4.

Wu, J. C., Chen, S. S., Yu, T. C., Wu, K. C. W., & Hou, C. H. (2021). Effective electrochemically controlled removal of fluoride ions using electrodeposited polyaniline-carbon nanotube composite electrodes. *Separation and Purification Technology*, 254, 117561.

Wu, P., Xia, L., Dai, M., Lin, L., & Song, S. (2016). Electrosorption of fluoride on TiO_2-loaded activated carbon in water. *Colloids and Surfaces A: Physicochemical and Engineering Aspects, 502*, 66-73.

Xiao, S., & Hatton, A. T. (2017). Electrosorption at functional interfaces: From molecular-level interactions to electrochemical cell design. *Physical Chemistry Chemical Physics, 19*(35), 23570-23584.

Yang, J., Zou, L., & Choudhury, N. R. (2013). Ion-selective carbon nanotube electrodes in capacitive deionisation. *Electrochimica Acta, 91*, 11-19.

Yang, Y., Li, X., Gu, Y., Lin, H., Jie, B., Zhang, Q., & Zhang, X. (2022). Adsorption property of fluoride in water by metal organic framework: Optimization of the process by response surface methodology technique. *Surfaces and Interfaces, 28*, 101649.

Yasin, A. S., Mohamed, A. Y., Kim, D., Yoon, S., Ra, H., & Lee, K. (2021). Efficiency Enhancement of Electro-Adsorption Desalination Using Iron Oxide Nanoparticle-Incorporated Activated Carbon Nanocomposite. *Micromachines, 12*(10), 1148.

Yin, C., Huang, Q., Zhu, G., Liu, L., Li, S., Yang, X., & Wang, S. (2022). High-performance lanthanum-based metal-organic framework with ligand tuning of the microstructures for removal of fluoride from water. *Journal of Colloid and Interface Science, 607*(Pt 2), 1762-1775.

Ying, Y., Liu, Y., Wang, X., Mao, Y., Cao, W., Hu, P., & Peng, X. (2015). Two-dimensional titanium carbide for efficiently reductive removal of highly toxic chromium (VI) from water. *ACS Applied Materials & Interfaces*, *7*(3), 1795-1803.

Zhai, Y., Hou, W., Chen, Z., Zeng, Z., Wu, Y., Tian, W., Liang, X., Paoprasert, P., Wen, Z., & Hu, N. (2022). A hybrid solid electrolyte for high-energy solid-state sodium metal batteries. *Applied Physics Letters*, *120*(25), 253902.

Zhang, C., He, D., Ma, J., Tang, W., & Waite, T. D. (2018). Faradaic reactions in capacitive deionization (CDI)-problems and possibilities: A review. *Water Research*, *128*, 314-330.

Zhang, C., Li, Y., Wang, T. J., Jiang, Y., & Fok, J. (2017). Synthesis and properties of a high-capacity iron oxide adsorbent for fluoride removal from drinking water. *Applied Surface Science*, *425*, 272-281.

Zhang, C. J., & Nicolosi, V. (2019). Graphene and MXene-based transparent conductive electrodes and supercapacitors. *Energy Storage Materials*, *16*, 102-125.

Zhang, J., Tang, L., Tang, W., Zhong, Y., Luo, K., Duan, M., Xing, W., & Liang, J. (2020). Removal and recovery of phosphorus from low-strength wastewaters by flow-electrode capacitive deionization. *Separation and Purification Technology*, 237, 116322.

Zhang, T., Zhao, N., Li, J., Gong, H., An, T., Zhao, F., & Ma, H. (2017). Thermal behavior of nitrocellulose-based superthermites: Effects of nano-Fe_2O_3 with three morphologies. *RSC Advances*, *7*(38), 23583-23590.

Zhang, W., Mossad, M., Yazdi, J. S., & Zou, L. (2014). A statistical experimental investigation on arsenic removal using capacitive deionization. *Desalination and Water Treatment*, *57*(7), 3254-3260.

Zhang, Y., Wang, G., Wang, S., Wang, J., & Qiu, J. (2019). Boron-nitride-carbon nanosheets with different pore structure and surface properties for capacitive deionization. *Journal of Colloid and Interface Science*, *552*, 604-612.

Zhao, R., van Soestbergen, M., Rijnaarts, H. H., van der Wal, A., Bazant, M. Z., & Biesheuvel, P. M. (2012). Time-dependent ion selectivity in capacitive charging of porous electrodes. *Journal of Colloid and Interface Science*, *384*(1), 38-44.

Zhao, Y., Hu, X. M., Jiang, B. H., & Li, L. (2014). Optimization of the operational parameters for desalination with response surface methodology during a capacitive deionization process. *Desalination*, *336*, 64-71.

Zhao, Y., Hu, X. M., Jiang, B. H., Ye, S. F., Li, L., Tian, Z., & Wang, Y. J. (2013). Optimization of Capacitive Deionization for Salt Removal from Water with Response Surface Methodology. *Applied Mechanics and Materials*, *368-370*, 257-260.

Zhu, E., Hong, X., Ye, Z., Hui, K. S., & Hui, K. N. (2019). Influence of various experimental parameters on the capacitive removal of phosphate from aqueous solutions using LDHs/AC composite electrodes. *Separation and Purification Technology*, *215*, 454-462.

Zhu, J., Ha, E., Zhao, G., Zhou, Y., Huang, D., Yue, G., Hu, L., Sun, N., Wang, Y., Lee, L. Y. S., Xu, C., Wong, K. Y., Astruc, D., & Zhao, P. (2017). Recent advance in MXenes: A promising 2D material for catalysis, sensor and chemical adsorption. *Coordination Chemistry Reviews*, *352*, 306-327.

Zou, G., Guo, J., Peng, Q., Zhou, A., Zhang, Q., & Liu, B. (2016). Synthesis of urchin-like rutile titania carbon nanocomposites by iron-facilitated phase transformation of MXene for environmental remediation. *Journal of Materials Chemistry A*, *4*(2), 489-499.

Zuo, Q., Chen, X., Li, W., & Chen, G. (2008). Combined electrocoagulation and electroflotation for removal of fluoride from drinking water. *Journal of Hazardous Materials*, *159*(2-3), 452-457.

RESEARCH OUTPUTS

(i) Publications

Alfredy, T., Elisadiki, J., Dahbi, M., King'ondu, C. K., & Jande, Y. A. C. (2024). Electrosorption of paraquat pesticide on activated carbon modified by aluminium oxide (Al_2O_3) with capacitive deionization. *Desalination*, 572, 117116.

Alfredy, T., Elisadiki, J., Kim, Y. D., & Jande, Y. A. C. (2023). Water defluoridation using Al/Fe/Ti ternary metal oxide-loaded activated carbon by capacitive deionization. *Environmental Science: Water Research & Technology*, *9*(3), 957-972.

Alfredy, T., Elisadiki, J., & Jande, Y. A. C. (2021). Capacitive deionization for the removal of paraquat herbicide from aqueous solution. *Adsorption Science & Technology*, *2021*, 1-9.

Alfredy, T., Elisadiki, J., & Jande, Y. A. C. (2022). Capacitive deionization: a promising technology for water defluoridation: A review. *Water Supply*, *22*(1), 110-125.

(ii) Poster presentation

The performance of activated carbon composited with Al, Fe and Ti oxides for defluoridation, Tusekile Alfredy, Joyce Elisadiki, Yusufu Jande and Mouad Dahbi Presented in the 1st Workshop Bi-National Energy Initiative Morocco-Israel held on 14th to 16th March 2023 at Mohammed VI Polytechnic University Benguerir, Morocco.

Poster presentation in the 6th international conference on battery deionization & electrochemical separation held on July 2-6, 2023, Taipei, Taiwan city Topic: The performance of activated carbon composited with Al, Fe and Ti oxides for defluoridation

(iii) Oral presentation

T. Alfredy, M. Dahbi, J. Elisadiki, Y. Jande, Electrosorption of paraquat pesticide on activated carbon modified by aluminium oxide (Al_2O_3) in capacitive deionization. Presented in the six International Conference on Materials Science and Exhibition for Science (ICMES) "Health, Sustainability, and Resiliency Through Research and Innovation" held on 7th to 11th June 2023 at the hotel Oasis Atlantico Saidia Palace and Blue Pearl Oujda Berkane Saidia-Morocco.